

Air Force Institute of Technology

**AFIT Scholar**

---

Theses and Dissertations

Student Graduate Works

---

8-25-2008

## **Distribution Iteration: A Robust Alternative to Source Iteration for Solving the Discrete Ordinates Radiation Transport Equations in Slab and XY- Geometries**

Nicholas J. Prins

Follow this and additional works at: <https://scholar.afit.edu/etd>



Part of the [Nuclear Engineering Commons](#)

---

### **Recommended Citation**

Prins, Nicholas J., "Distribution Iteration: A Robust Alternative to Source Iteration for Solving the Discrete Ordinates Radiation Transport Equations in Slab and XY- Geometries" (2008). *Theses and Dissertations*. 2647.

<https://scholar.afit.edu/etd/2647>

This Dissertation is brought to you for free and open access by the Student Graduate Works at AFIT Scholar. It has been accepted for inclusion in Theses and Dissertations by an authorized administrator of AFIT Scholar. For more information, please contact [richard.mansfield@afit.edu](mailto:richard.mansfield@afit.edu).



DISTRIBUTION ITERATION: A ROBUST ALTERNATIVE TO SOURCE  
ITERATION FOR SOLVING THE DISCRETE ORDINATES RADIATION  
TRANSPORT EQUATIONS IN SLAB AND XY - GEOMETRIES

DISSERTATION

Nicholas J. Prins, Lieutenant Colonel, USA

AFIT/DS/ENP/08-S04

DEPARTMENT OF THE AIR FORCE  
AIR UNIVERSITY

***AIR FORCE INSTITUTE OF TECHNOLOGY***

---

Wright-Patterson Air Force Base, Ohio

APPROVED FOR PUBLIC RELEASE; DISTRIBUTION UNLIMITED

The views expressed in this dissertation are those of the author and do not reflect the official policy or position of the United States Air Force, Department of Defense, or the United States Government.

AFIT/DS/ENP/08-S04

DISTRIBUTION ITERATION: A ROBUST ALTERNATIVE TO SOURCE  
ITERATION FOR SOLVING THE DISCRETE ORDINATES RADIATION  
TRANSPORT EQUATIONS IN SLAB AND XY - GEOMETRIES

DISSERTATION

Presented to the Faculty

Graduate School of Engineering and Management  
Air Force Institute of Technology  
Air University  
Air Education and Training Command

in Partial Fulfillment of the Requirements for the

Degree of Doctor of Philosophy

Nicholas J. Prins, BS, MS

Lieutenant Colonel, USA

September 2008

APPROVED FOR PUBLIC RELEASE; DISTRIBUTION UNLIMITED

Distribution Iteration: A Robust Alternative to Source Iteration for Solving the Discrete  
Ordinates Radiation Transport Equations In Slab and XY - Geometries

Nicholas J. Prins, BS, MS  
Lieutenant Colonel, USA

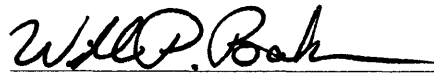
Approved:



Kirk A. Mathews (Chairman)

12 Aug 2008

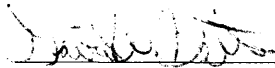
Date



William P. Baker (Member)

12 Aug 08

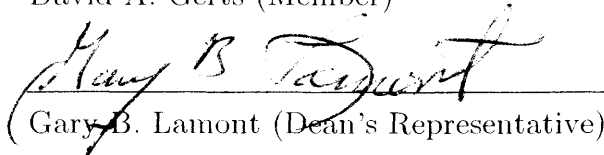
Date



David A. Gerts (Member)

13 Aug 08

Date



Gary B. Lamont (Dean's Representative)

19 Aug 08

Date

Accepted:



Marlin U. Thomas

25 Aug 08

Date

Dean, Graduate School of  
Engineering and Management

## **Abstract**

The discrete ordinates method is widely used to solve the Boltzmann transport equation for neutral particle transport for many engineering applications. Source iteration is used to solve the discrete ordinates system of equations, but can be slow to converge in highly scattering problems. Synthetic acceleration techniques have been developed to address this shortcoming; however, recent research has shown synthetic acceleration to lose effectiveness or diverge for certain problems.

LTC Wager introduced an alternative to source iteration and demonstrated it in slab geometry. Here the method is further developed, enhancing efficiency in various ways, and demonstrated in XY-geometry as well as slab geometry. It is shown to be efficient even for those problems for which diffusion-synthetic and transport-synthetic accelerations fail or are ineffective. The method has significant advantages for massively-parallel implementations.

## **Acknowledgments**

I would like to extend my gratitude to my faculty advisor, Dr. Kirk Mathews, for his support and inspiration throughout the course of my research effort. His experience and patience are deeply appreciated. I would also like to thank my research committee for both the support and time they provided to me in this endeavor.

I am also indebted to my fellow students who spent their valuable time assisting me through this processes and providing moral support. In addition, I would like to thank my Army functional area manager for the opportunity to complete this research. Last but certainly not least, special thanks go to my wife for her continued support and patience in this and all my endeavors.

Nicholas J. Prins

## Table of Contents

	Page
Abstract .....	iv
Acknowledgements .....	v
List of Figures .....	xi
List of Tables .....	xv
List of Acronyms .....	xvii
List of Variables .....	xviii
I. Introduction .....	1
A. Background.....	2
1. Source Iteration.....	2
2. Synthetic Acceleration.....	3
3. Angle Iteration .....	5
B. Motivation .....	9
C. Goal of the Research.....	10
D. Objectives .....	10
E. Scope.....	11
F. Assumptions/Limitations .....	12
G. Approach .....	13
II. Theory .....	16
A. Discrete Ordinates System of Equations.....	18



	Page
1. Local Detailed Balance.....	18
2. Global Flow Balance .....	19
3. Coupling the Local Balances .....	21
B. Choices that Define a Method .....	23
1. Angular Quadrature Sets .....	23
a. Slab Geometry .....	23
b. XY-Geometry .....	26
2. Spatial Quadratures .....	28
a. Linear Methods.....	28
b. Non-Linear Methods.....	30
3. Cell Face Flow Variables .....	30
a. Angular Flux as Cell Face Variable.....	30
b. Angular Current as Cell Face Variable .....	31
4. Coupling the Local Balances.....	31
a. Local Balance Sweeping.....	31
b. Red/Black .....	32
c. Discrete Ordinates Sweep .....	33
d. Parallel Efficiency of Reb/Black vs Sweeping.....	34
III. Slab Geometry Implementation and Testing .....	36
A. Local Detailed Balance Problem.....	36

	Page
1. Zeroth Spatial Moment methods.....	36
a. Angular Flux Formulation.....	39
b. Current Formulation .....	41
2. First Spatial Moment methods.....	42
a. Angular Flux Formulation.....	47
b. Current Formulation .....	48
B. Global Flow Balance Problem .....	50
C. Test Results In Slab Geometry.....	54
1. Preliminaries: Measuring Convergence Tolerance .....	54
2. Test Problems .....	55
3. Edge Flow Variable Representation .....	55
4. Coupling the Local Balances .....	56
IV. Implementation in XY - Geometry.....	60
A. Zeroth Spatial Moment Methods Distribution Iteration	
Derivation .....	60
1. Step Characteristic Transport Coefficients.....	64
2. Weighted Diamond Difference Transport Coefficients .....	68
B. First Spatial Moment Methods Distribution Iteration Derivation ..	70
1. Linear Characteristic Transport Coefficients .....	77
2. Linear Discontinuous Transport Coefficients .....	82

	Page
C. Partial Current Problem.....	87
1. Zeroth Spatial Moment Partial Current Problem .....	87
2. First Spatial Moment Partial Current Problem .....	92
V. Validation and Performance .....	95
A. Validation.....	95
1. Initial Checks .....	95
2. Consistency Checks.....	96
3. Source Iteration Comparison.....	103
4. Benchmarking .....	104
B. Routine Problem Comparison.....	107
1. Aspect Ratios.....	108
2. Scattering Ratios.....	111
3. Two Material Problem .....	113
VI. Challenging Problems – Comparison with DSA and TSA .....	117
A. Where DSA Loses Effectiveness.....	117
1. Weighted Diamond Difference Comparison.....	114
2. Linear Discontinuous Comparison.....	122
3. Azmy PHI Timing Analysis .....	124
B. Where TSA fails .....	130
1. Weighted Diamond Difference Comparison.....	132

	Page
2. Other Spatial Methods Comparison .....	135
VII. Additional Test Problems .....	139
A. The Checkerboard Problem .....	139
1. Spatial Method Performance.....	140
2. Edge Distribution Improvement.....	141
3. Timing Analysis .....	146
B. Scattering Ratio Horizontal Interface Problem.....	149
1. Weighted Diamond Difference Performance.....	152
2. Linear Discontinuous Performance.....	154
VIII. Conclusions and Recommendations .....	158
B. Conclusions.....	158
B. Recommendations .....	160
Appendix A. Linear Discontinuous Equations in Slab Geometry.....	162
Appendix B. Zeroth Spatial Moment Methods Current Equations in XY-geometry .....	164
Appendix C. First Spatial Moment Methods Derivation in XY-Geometry ..	169
Appendix D. First Spatial Moment Methods Current equations in XY-Geometry .....	176
Appendix E. First Spatial Moment Methods Derivation in Slab Geometry.	189
Bibliography.....	192

## List of Figures

Figure	Page
1. Figure 2.1 Flowchart describing the general distribution iteration method.....	22
2. Figure 3.1 The problem solution time versus number of cells for different cell flow coupling methods with step characteristic .....	57
3. Figure 3.2. The problem solution time versus number of cells for different cell flow coupling methods with linear discontinuous .....	58
4. Figure 4.1. Rectangular cell for implementation of the zeroth spatial moment methods.....	64
5. Figure 4.2. Setting up the partial current problem for a two cell by two cell problem showing the ordering of the partial currents.....	89
6. Figure 5.1. Problem values for the uniform universe test problem.....	97
7. Figure 5.2. Problem values for the single vacuum boundary and three reflective boundary problem .....	99
8. Figure 5.3. Problem variables for the source iteration comparison test problem.....	103
9. Figure 5.4. Problem variables for the benchmark problem.....	104

Figure	Page
10. Figure 5.5. Results of the SC comparison with a Monte Carlo solution to the benchmark problem. The plot of the partial current out the top edge is shown for both methods.....	105
11. Figure 5.6. Results of the LD comparison with a Monte Carlo solution to the benchmark problem. The plot of the partial current out the top edge is shown for both methods .....	106
12. Figure 5.7. Problem variables for the DSA aspect ratios comparison ..	108
13. Figure 5.8. Problem variables for the DSA scattering ratio comparison.....	111
14. Figure 5.9. Problem variables for the two material DSA comparison problem.....	114
15. Figure 6.1. Problem variables for the Azmy Periodic Horizontal Interface (PHI) .....	117
16. Figure 6.2. Convergence rates for the Azmy Periodic Horizontal Interface (PHI) problem with DI using WDD and $S_6$ at $\sigma = 10$ cross section for various mesh sizes.....	119
17. Figure 6.3. Convergence rates for the Azmy Periodic Horizontal Interface (PHI) problem with DI using WDD and $S_6$ cross section $\sigma = 160$ for various mesh sizes .....	120
18. Figure 6.4. Problem variables for the Chang Periodic Horizontal Interface (PHI) .....	131

Figure	Page
19. Figure 6.5. Convergence rates for the Chang Periodic Horizontal Interface (PHI) problem with DI using WDD and $S_6$ for $\sigma_1 = 10^{-4}$ and $\sigma_2$ at various cross section combinations with a scattering ratio of 0.9.....	132
20. Figure 7.1. Problem variables for the checkerboard problem .....	140
21. Figure 7.2. DI Convergence rates for different spatial methods on the checkerboard problem for a single DO sweep.....	141
22. Figure 7.3. DI Convergence rates for different spatial methods on the checkerboard problem for a three DO sweeps .....	142
23. Figure 7.4. DI Convergence rates for different spatial methods on the checkerboard problem for the adaptive DO sweep technique.....	144
24. Figure 7.5. Comparison of total convergence time for the checkerboard problem with DI using WDD for a single DO sweep and the adaptive DO sweep technique.....	147
25. Figure 7.6. Comparison of total convergence time for the checkerboard problem with DI using LD for a single DO sweep and the adaptive DO sweep technique.....	148
26. Figure 7.7. Problem variables for the scattering ratio PHI problem ....	149

Figure	Page
27. Figure 7.8. Convergence rates for different spatial methods versus iterations using $S_6$ to the scattering ratio PHI problem. Total cross section is 0.1 and scattering ratios of 1.0 and 0.0 for regions A and B respectively .....	150
28. Figure 7.9. Convergence rates for different spatial methods versus iterations using $S_6$ to the scattering ratio PHI problem. Total cross section is 1.0 and scattering ratios of 1.0 and 0.0 for regions A and B respectively .....	151
29. Figure 7.10. Convergence rates for different spatial methods versus iterations using $S_6$ to the scattering ratio PHI problem. Total cross section is 10.0 and scattering ratios of 1.0 and 0.0 for regions A and B respectively .....	152
30. Figure B.1. Rectangular cell for zeroth spatial moment methods. Cell shows problem variables used for solving the discrete ordinates equations.....	164
31. Figure D.1. Rectangular cell for first spatial moment methods. Cell shows problem variables used for solving the discrete ordinates equations.....	176



## List of Tables

Table	Page
1. Table 3.1. Iterations to convergence for current vs angular flux .....	56
2. Table 5.1. Results of the uniform universe test .....	100
3. Table 5.2. DSA aspect ratio comparison results .....	109
4. Table 5.3. DSA aspect ratio comparison results adaptive DO sweep results .....	110
5. Table 5.4. DSA scattering ratio comparison results .....	113
6. Table 5.5. DSA two material comparison results .....	115
7. Table 6.1. Published DSA with WDD results .....	121
8. Table 6.2. DI with WDD results .....	122
9. Table 6.3. Published DSA with BLN results .....	123
10. Table 6.4. DI with LD results .....	123
11. Table 6.5. WDD Iteration timing .....	125
12. Table 6.6. WDD Partial current problem timing .....	126
13. Table 6.7. WDD Discrete ordinates sweep timing .....	127
14. Table 6.8. LD iteration timing .....	128
15. Table 6.9. LD Partial current problem timing .....	128
16. Table 6.10. LD Discrete ordinates sweep timing .....	129

Table	Page
17. Table 6.11. Chang PHI Test for $c = 0.9$ , with DI AWDD using $S_4$ , and TSA DD using $S_4 / S_2$ .....	133
18. Table 6.12. Chang PHI Test for $c = 0.99$ with DI Results AWDD using $S_6$ , and TSA DD Results using $S_6 / S_2$ .....	134
19. Table 6.13. Chang PHI Test for $c = 1.0$ , DI with AWDD using $S_6$ ....	135
20. Table 6.14. Chang PHI Problem for $c=0.9$ using $S_6$ .....	136
21. Table 6.15. Chang PHI Problem for $c=0.99$ using $S_6$ .....	137
22. Table 6.16. Chang PHI Problem for $c=1.0$ using $S_6$ .....	137
23. Table 7.1. Number of DI iterations for the checkerboard problem.....	145
24. Table 7.2. Total number of DO sweeps for checkerboard problem .....	145
25. Table 7.3. AWDD results for scattering ratio PHI problem with total cross section $\sigma = 0.1$ as scattering ratio varies .....	153
26. Table 7.4. AWDD results for scattering ratio PHI problem with total cross section $\sigma = 1.0$ .....	154
27. Table 7.5. LD results for scattering ratio PHI problem with total cross section $\sigma = 1.0$ . Shading indicates strictly positive solutions .....	154
28. Table 7.6. AWDD results for scattering ratio PHI problem with total cross section $\sigma = 10.0$ .....	156

## List of Acronyms

AI:	Angle Iteration
AWDD:	Adaptive Weighted Diamond Difference
BTE:	Boltzmann transport equation
BLN:	Bi-Linear Nodal
c:	Scattering ratio
DSA:	Diffusion synthetic acceleration
DI:	Distribution Iteration
EC:	Exponential Characteristic
LBLN:	Linear Bi-Linear Nodal
LC:	Linear Characteristic
LD:	Linear Discontinuous
PHI:	Periodic Horizontal Interface
SC:	Step Characteristic
SI:	Source iteration
SRD:	Symmetric relative difference
TSA:	Transport synthetic acceleration

## List of Variables

Variable	Summary	Page
$\sigma$	Total cross section	39
$\sigma_s$	Scattering cross section	1
$n$	Angular quadrature ordinate index	39
$\mu_n$	X direction cosine for ordinate ( $n$ ) for angular quadrature set	39
$\eta_n$	Y direction cosine for ordinate ( $n$ ) for angular quadrature set	64
$\vec{\psi}^{out}, \vec{\psi}^{in}$	Array of cell edge angular flux outflow/inflow	5
$\vec{j}^{out}, \vec{j}^{in}$	Array of cell edge current outflow/inflow	36
$\vec{\psi}^A$	Array of cell average angular flux	5
$\vec{\psi}^X, \vec{\psi}^Y$	Array of cell x/y moment of angular flux	43
$\vec{S}^A$	Array of cell average scatter	5
$\vec{S}^X, \vec{S}^Y$	Array of cell x/y moment of scatter	43
$\vec{E}^A$	Array of cell average emissions	5
$\vec{E}^X, \vec{E}^Y$	Array of cell x/y moment of emissions	43
$\Sigma_S$	Scattering matrix	5
$\epsilon_n$	Cell optical thickness for ordinate $n$	39
$\epsilon_{y_n}, \epsilon_{x_n}$	Y/X cell optical thickness for ordinate $n$	64

<b>Variable</b>	<b>Summary</b>	<b>Page</b>
$\alpha_n$	Cell aspect ratio	65
$\Delta x, \Delta y$	X/Y cell thickness	39
$\mathbf{K}_{XY}$	Diagonal matrix for relation within a cell giving $X$ from $Y$	36
$D(\vec{x})$	Diagonal operator creating diagonal matrix from $\vec{x}$	36
$\mathbf{m}_{XY}$	Cell matrix for relation within a cell giving $X$ from $Y$ including all scatters	6
$J^X$	Cell face partial current, indexed with repective direction $X$	17
$\alpha_x$	Boundary condition on material edge $X$	90
$M_n(x)$	Exponential moment function	39

# Distribution Iteration: A Robust Alternative to Source Iteration for Solving the Discrete Ordinates Radiation Transport Equations In Slab and XY - Geometries

## I. Introduction

The time-independent, single energy group, linearized *Boltzmann Transport Equation* (BTE) for non-multiplying systems can be written:

$$[\bar{\Omega} \cdot \bar{\nabla} + \sigma_t(\vec{r})]\psi(\vec{r}, \bar{\Omega}) = \int d\Omega' \sigma_s(r, \bar{\Omega}' \cdot \bar{\Omega})\psi(\vec{r}, \bar{\Omega}') + q_{ext}(\vec{r}, \bar{\Omega}), \quad (1.1)$$

where  $\psi$  is the angular flux;  $\sigma_t$  is the total cross section;  $\sigma_s$  is the scattering cross section; and  $q_{ext}$  is the external source (5: 2). The BTE in this form is an integro-differential equation that is coupled in space and angle. The discrete ordinates method discretizes the BTE in space and angle and the resulting system of equations is widely used for solutions to the BTE for many engineering applications.

This research demonstrates a new method that is a robust, flexible and rapid way of solving the discrete ordinates system of equations. Various techniques have been applied to solve the discrete ordinates equations with varying degrees of success. A brief review of several techniques follows.

## A. Background

### 1. Source Iteration

One technique that is commonly used to solve the discrete ordinates system of equations is known as source iteration (SI). The BTE can be written in an operator notation:

$$\mathbf{L}\psi = \mathbf{S}\psi + E, \quad (1.2)$$

where  $\mathbf{L}\psi = [\vec{\Omega} \cdot \vec{\nabla} + \sigma_t(\vec{r})]\psi(\vec{r}, \vec{\Omega})$  is the streaming and collision operator;

$\mathbf{S}\psi = \int d\Omega' \sigma_s(r, \vec{\Omega}' \cdot \vec{\Omega})\psi(\vec{r}, \vec{\Omega}')$  is the scattering operator or (within group)

scattering source, and  $E$  is the emission source<sup>1</sup> (which includes scatter into the group from other groups in a multigroup formulation). As an iterative scheme,

SI is written (5: 2):

$$\mathbf{L}\psi^{(l+1)} = \mathbf{S}\psi^{(l)} + E. \quad (1.3)$$

The BTE is discretized in angle and space. An initial estimate of the scattering source is made. The right side of equation (1.3) is treated as the source for this method, the sum of both the scattered particles, as determined by the integral and the emission sources in the material. The discretization in angle allows the integral for the scattering source to be evaluated using a quadrature rule with the initial flux estimate for  $N$  directions to determine the source. If the initial guess for the scattering source is 0, then the  $l$ -th iteration, or estimate of

---

<sup>1</sup> My notation,  $S$  and  $E$ , rather than  $q^{scat}$  and  $q^{ext}$ ; was chosen to reserve subscripts and superscripts for other uses.

the angular flux, is due to particles that have scattered at most  $l-1$  times (5: 2). The number of scatters that must be modeled determines the speed with which SI converges.

Source iteration has been used for many years, but has several shortcomings. For problems that are dominated by scattering with little or no absorption, the SI method may take many iterations to converge and require impractical compute times. Further, in highly scattering problems, the difference between two iterations may meet the convergence tolerance before the true solution is reached. This phenomenon is known as false convergence. Techniques to speed the convergence have been studied with varying degrees of success (18: 1, 5: 1). Currently there is no technique to speed the convergence that works for all problems in two dimensions.

## 2. Synthetic Acceleration

Methods have been developed over the past 40 years to accelerate or rapidly converge SI, particularly for diffusive type problems. One technique that is commonly used is synthetic acceleration, which is at least a two stage iteration scheme. The first stage is a normal iteration from SI, with a change of the iteration subscript from equation (1.3):

$$\mathbf{L}\psi^{(l+\frac{1}{2})} = \mathbf{S}\psi^{(l)} + \mathbf{E} . \quad (1.4)$$



The intent of the second stage is to find a low order approximation to add to  $\psi^{(l+\frac{1}{2})}$  as a better approximation to the exact solution  $\psi$ . Subtracting equation (1.4) from equation (1.2) and solving for the exact solution:

$$\psi = \psi^{(l+\frac{1}{2})} + (\mathbf{L}-\mathbf{S})^{-1} \mathbf{S}(\psi^{(l+\frac{1}{2})} - \psi^{(l)}). \quad (1.5)$$

Finding  $(\mathbf{L}-\mathbf{S})^{-1}$  to a high order is as difficult as solving the original problem; therefore, a low order approximation is used where  $\mathbf{M} \approx (\mathbf{L}-\mathbf{S})^{-1}$  is easier to compute. The synthetic acceleration scheme then is:

$$\psi^{(l)} = \psi^{(l+\frac{1}{2})} + \mathbf{M}\mathbf{S}(\psi^{(l+\frac{1}{2})} - \psi^{(l)}). \quad (1.6)$$

Diffusion synthetic acceleration (DSA) and transport synthetic acceleration (TSA) are two commonly used synthetic acceleration methods. The DSA scheme uses a diffusion approximation as the low order approximation, while the TSA scheme uses a simplified transport operator, for example a smaller angular quadrature, as the low order approximation. For homogenous material problems, these techniques have been highly effective (5: 2-3).

Adams and Larsen presented a comprehensive review of these methods, as well as others, along with their strengths and limitations (2: 139). For problems with severe spatial heterogeneities, DSA in multiple dimensions has been shown to degrade significantly and TSA has been shown to diverge. Additionally, a new consistent differencing derivation is needed for each new type of problem with DSA, and TSA still has difficulties for problems that are highly scattering. As

the authors state, there is strong interest in new methods that are efficient and easy to implement.

### 3. Angle Iteration

Wager developed a new method to solve the BTE that could be a practical replacement for source iteration. His method is called Angle Iteration (AI) and uses iteration on the cell edge flux distribution to rapidly converge on a flux solution. His method does not converge falsely. His work showed promising results but was only demonstrated in slab geometry for isotropic scatter.

His method begins by treating the discretization in angle and space as a system of equations, representing the flux for all directions as a vector and the spatial relations as a matrix multiplying the flux vector. For a single cell (cell  $i$ ) in one dimension for any spatial method, the outgoing flux, the incoming flux, average flux and average source relations in his notation are:

$$\vec{\psi}_{out_i} = \mathbf{K}_{OI} \vec{\psi}_{in_i} + \mathbf{K}_{OS_i} \vec{S}_{A_i} + \mathbf{K}_{OE_i} \vec{E}_{A_i}, \quad (1.7)$$

$$\vec{\psi}_{A_i} = \mathbf{K}_{AI} \vec{\psi}_{in_i} + \mathbf{K}_{AS_i} \vec{S}_{A_i} + \mathbf{K}_{AE_i} \vec{E}_{A_i}, \quad (1.8)$$

$$\vec{S}_{A_i} = \sum_{S_i} \vec{\psi}_{A_i}. \quad (1.9)$$

In these equations,  $\mathbf{K}_{OI}$ ,  $\mathbf{K}_{OSA}$ ,  $\mathbf{K}_{OEA}$ ,  $\mathbf{K}_{AI}$ ,  $\mathbf{K}_{ASA}$ , and  $\mathbf{K}_{AEA}$ , are diagonal matrices of transport coefficients. Each element is the quantity of flux (out or average in the cell) constituted by the uncollided (first-flight) streaming of a unit quantity of flux, scattering source or emission source. Only the first flight flux is included in each  $\mathbf{K}$ ; the flux of scattered particles is included as the

first flight of the (previously) scattered source particles ( $\bar{S}$ ). The quantities  $\bar{S}_{A_i}$  and  $\bar{E}_{A_i}$  are the variables that represent the average scatter and average emissions in a cell. Also,  $\Sigma_S$  represents the scattering cross sections with the appropriate quadrature weights to calculate the scattering source from the cell average angular flux (16: 2-26).

Equations (1.9) and (1.8) can be substituted into equation (1.7) to solve for the vector of cell face fluxes out of a cell in terms of the vector of incoming fluxes and the vector of emission in the cell:

$$\begin{aligned} \bar{\psi}_{out_i} = & (\mathbf{K}_{OI_i} + \mathbf{K}_{OS_i} \Sigma_{S_i} (\mathbf{I} - \mathbf{K}_{AS_i} \Sigma_{S_i})^{-1} \mathbf{K}_{AI_i}) \bar{\psi}_{in_i} + \\ & (\mathbf{K}_{OE_i} + \mathbf{K}_{OS_i} \Sigma_{S_i} (\mathbf{I} - \mathbf{K}_{AS_i} \Sigma_{S_i})^{-1} \mathbf{K}_{AE_i}) \bar{E}_{A_i}. \end{aligned} \quad (1.10)$$

The factor  $(\mathbf{I} - \mathbf{K}_{AS_i} \Sigma_{S_i})^{-1}$  in the above equation is the sum of an infinite geometric series as long as  $\|\mathbf{K}_{AS_i} \Sigma_{S_i}\| < 1$ . Further, each term in the sum models a scattering event within a cell. The factor  $(\mathbf{I} - \mathbf{K}_{AS_i} \Sigma_{S_i})^{-1}$  therefore models all numbers of scatters that a particle can have before leaving the cell (16: 2-55). I call this *infinite within-cell scatters*. This is different than SI which models each scattering event separately and hence has difficulties with dominantly scattering problems. Equation (1.10) can be given in a compact notation which represents the matrices in the outer parentheses as a single matrix:

$$\bar{\psi}_{out_i} = \mathbf{m}_{OI_i} \bar{\psi}_{in_i} + \mathbf{m}_{OE_i} \bar{E}_{A_i}. \quad (1.11)$$

While this relation does model infinite within cell scatters (15: 2-31), it accounts for contributions to the flux from other cells in the slab only indirectly, through

$\vec{\psi}_{in_i}$ . Scattering among cells is addressed by representing equation (1.11) as a coupled system of equations across all the cells:

$$\vec{\Psi}_{out} = \mathbf{M}_{OI} \vec{\Psi}_{in} + \mathbf{M}_{OE} \vec{E}_A. \quad (1.12)$$

Further, the incoming flux in a cell is the outgoing flux from adjacent cells, (except at exterior boundaries) hence:

$$\vec{\Psi}_{in} = \mathbf{P} \vec{\Psi}_{out}, \quad (1.13)$$

where  $\mathbf{P}$  is the permutation matrix that reorders the outgoing flux vector appropriately. Substituting equation (1.13) into equation (1.12) yields (after some algebra):

$$\vec{\Psi}_{out} = (\mathbf{P}_m (\mathbf{I} - \mathbf{M}_{OI} \mathbf{P}))^{-1} \mathbf{M}_{OE} \vec{E}_A, \quad (1.14)$$

where  $\mathbf{P}_m$  is a permutation matrix that reorders the matrix to be of minimum bandwidth. This system of equations fully couples angle and space to get a flux solution, but is impractical to solve for fine angular and spatial resolution because it is the full set of simultaneous discrete ordinates equations (16: 2-44). Wager's AI method makes use of the strengths of both equations (1.11) and (1.14).

In the AI method, the outgoing, within cell flux is solved using equation (1.11). The flux solution is then collapsed into two directions. The collapsing is done by summing (integrating) the fluxes in a given hemisphere over the hemisphere. The collapsed flux is used to solve equation (1.14) for two directions across the spatial grid for what he called the global problem. The new flux solution from the global problem is apportioned back into the original cell

representation using the original flux distribution (16: 2-73). This initial distribution is normalized to create flux weights. A flux weight for a direction is the flux moving in that direction divided by the sum of all the flux moving along the same hemisphere. A similar flux weight can be defined for the opposite direction, as well as the average flux in a cell, and the scattered and emission source in a cell. This process of collapsing, solving and apportioning gives a better estimate for the cell edge flux and can be used to solve for an updated cell edge flux (15: 2-66-69). The updated cell edge flux can be collapsed with new flux weights and the process repeated. This process describes one iteration. The iterative process is continued until a convergence tolerance is met (16: 2-73).

The AI method has been tested using two positive spatial methods: step characteristic (SC) and exponential characteristic (EC). In both cases, it was shown to be reliable and to rapidly converge across a broad range of cross sections and a full range of scattering ratios for these positive spatial methods (16: 6-1).

Despite the success of the AI method, there are several issues to address: angular quadrature choices, cell particle flow variable representation, and coupling of the scattering among cells. These issues will be developed and addressed in the next two chapters.

Additionally, the AI method was demonstrated for spatial quadratures that only required the calculation of a zeroth spatial moment of the flux in a cell.

The higher spatial moments for the nonlinear EC method were found through a root solving routine. Implementation of linear first spatial moment methods was not yet derived. In addition, the effect of using non-positive linear spatial methods in the AI method needed to be examined.

The AI method was demonstrated in slab geometry. An extension to multiple dimensions required addressing two issues: how to incorporate the flux scattering from the orthogonal directions; and how to efficiently communicate cell information about cell emissions and absorptions across the spatial mesh. For one dimension, the global problem resulted in a penta-diagonal matrix which can be solved efficiently. A similar coupled global problem in two dimensions needed to include the scattering terms as well.

## **B. Motivation**

Despite the challenges that needed to be addressed for the AI method, the results demonstrated in slab geometry showed promise that a flexible, robust method could be developed and demonstrated in multiple dimensions. Further, Wager's tests in slab geometry suggested that this new method could overcome difficulties that SI and synthetic acceleration methods have for particular problems in XY-geometry.

### **C. Goal of the Research**

The goal of this research was to develop and demonstrate a new algorithm for rapid solutions of the discrete ordinates equations in two dimensions. It is desirable that the algorithm be:

Robust – able to handle a broad range of cross sections and scattering ratios without significant changes in convergence rates;

Flexible – able to easily implement additional spatial methods without requiring another derivation and change to the algorithm. The method should also be able to change angular quadratures with no changes to the algorithm;

Parallelizable – although the method was implemented and demonstrated on a desktop machine, it is desirable that the method be parallelizable to be able to handle large problems efficiently; and

Readily extendable to 3D – the methodology used in deriving and implementing the method should provide a clear path to implementing the algorithm in three dimensions.

### **D. Objectives:**

1. Extend the method to 2-d Cartesian Geometry.
2. Use other spatial and angular quadratures to inherit correct diffusion limits.

3. Evaluate the utility of a partial current problem (a finite-volume particle conservation formulation) as an alternative to Wager's use of partial range angular integrals of the directional flux for coupling cells in a global problem.
4. Formulate the method to minimize the size of the global problem when applied to higher order linear methods.
5. Demonstrate success where both DSA and TSA fail or become ineffective and extend testing to even more challenging problems.
6. Evaluate the ability of a PARDISO-based direct solver routine (6: 11-1) to solve the partial current problem efficiently.
7. a) Maximize the opportunity for parallelization.  
b) Enhance serial performance.
8. Distribution iteration should have the desirable properties described as goals of the research.

## **E. Scope**

The scope of this research is to derive and implement a new method for solutions to the discrete ordinates equations using linear spatial methods for slab and XY – geometry with discrete ordinates quadratures. Slab geometry testing, for both zeroth and first spatial moment methods, was used to validate method choices for XY-geometry testing. Implementation of the DI method, for both



zeroth and first spatial moment methods, show general performance of the method for a variety of parameters. In addition, tests in XY-geometry show the improvement the new method has over other methods currently used to solve these same equations. The code implementation was written to be able to demonstrate this; it is not intended to be incorporated in a production code.

## **F. Assumptions and Limitations**

This research uses linear spatial methods that provide solutions to the time independent, mono-energetic BTE for isotropic scatter and non-multiplying systems in two dimensions. Energy dependence is not tested explicitly.

Nevertheless, the emission source can include scatter into a group from other groups, so the derivations would apply to a multigroup formulation without loss of generality. Similarly, my testing assumes isotropic scattering, but this influences only the numerical values of the elements of the scattering matrix,  $\Sigma$ . Extension to anisotropic scatter requires only the formulation of  $\Sigma$  consistent with the anisotropic scatter approximations to be employed.

The new method solves the discrete ordinates equations and therefore inherits the strengths and weaknesses of the angular and spatial quadratures and the cross section approximations used.

## G. Approach

The first step was to examine the appropriate choice for cell particle flow for implementation in the distribution iteration method. A change in the representation for the problem by transforming the angular flux representation of the AI method into a current representation for the cell transport coefficients is appropriate. This allows changing the “global” problem for the AI method into a partial current problem. This was done for several reasons. This is a more physical problem which is based on the conservation of particles as opposed to a pseudo scalar flux which was used in the AI method. Using this representation, the extensions to three spatial dimensions are more apparent and the same methodology can be used. Also, test problems in chapter three showed that the method converges in fewer iterations for this representation. The flux weights used in the AI method are replaced by current distributions on the cell edges. This motivates the name of the new method: distribution iteration (DI).

The angular integrals described in the BTE were done using an angular quadrature. The discrete elements quadrature used in the AI method did not meet the diffusion limit, which is needed for the highly scattering problems this research attempted. The discrete ordinates quadratures that are commonly used do meet the diffusion limit. Two different quadratures were implemented for two reasons, to compare with previously published results and to demonstrate the flexibility of the method in implementing different angular quadratures.

Different methods to couple the scattering among cells are presented in chapter two and tested for efficiency in chapter three. Next, the DI method for zeroth spatial moment methods is reviewed and first spatial moment methods in slab geometry are derived in chapter three. Implementation of two spatial methods, step characteristic (SC) and linear discontinuous (LD) are covered. Test problems were used to validate choices for the distribution iteration method implementation in XY - geometry.

The DI method is derived for zeroth and first spatial moment methods in two dimensions in chapter four. The following methods were implemented: step characteristic (SC); weighted diamond difference (WDD); linear characteristic (LC); and linear discontinuous (LD). The zeroth spatial moment methods (SC and WDD) validate the extension from one dimension to two dimensions, while the derivation and implementation of the more complicated first moment methods (LC and LD) further demonstrate the flexibility of the method. The partial current problem description and implementation for both the zeroth and first moment methods are also described in chapter four. The validation of the code is presented in chapter five as well as testing designed to demonstrate that the DI method performs at least as well as other methods for routine problems.

The DI method is tested on a variety of problems in the remaining chapters. The testing is designed to illustrate two points: the DI method performs at least as well as other methods and the DI method works for those

problems where other methods fail or have difficulties. The testing is also designed to determine the limitations of the DI method. The problems where other methods have difficulties are presented in chapter six and problems that stress the DI method are presented in chapter seven.

## II. Theory

### A. The Discrete Ordinates System of Equations

The discrete ordinates system of equations is derived from the linear BTE by discretizing in space and angle. The system of equations may be expressed (9: 166) as:

$$\hat{\Omega}_n \cdot \bar{\nabla} \psi(\vec{r}, \hat{\Omega}_n) + \sigma_t(\vec{r}) \psi(\vec{r}, \hat{\Omega}_n) = S(\vec{r}, \hat{\Omega}_n) + E(\vec{r}, \hat{\Omega}_n), \quad (2.1)$$

with an appropriate spatial discretization. This results in a system of simultaneous equations that is too large to solve directly. Therefore, this system of equations is solved by source iteration. Advances in computing speed and available memory suggest another approach is appropriate, motivating this research.

Rather than try to solve the large problem directly, the intent is to break a single large problem into two smaller problems that can be coupled together. The two problems can be described as a local detailed balance problem in each cell of a spatial grid and a global flow balance problem. Both problems assemble the discrete ordinates system of equations in a form that gives the outgoing particle flow in terms of the inward particle flow and emissions. By determining the proper balance on both scales, using the local balance to improve the coefficients in the global balance equations, and the solution to the improved

global balance to improve the local balances, the problem can be solved iteratively.

In general, a cell system of equations is written:

$$\vec{j}^{out} = \mathbf{K}_{OI} \vec{j}^{in} + \mathbf{K}_{OS} \bar{S} + \mathbf{K}_{OE} \bar{E}, \quad (2.2)$$

$$\bar{\psi} = \mathbf{K}_{\psi I} \vec{j}^{in} + \mathbf{K}_{\psi S} \bar{S} + \mathbf{K}_{\psi E} \bar{E}, \quad (2.3)$$

and

$$\bar{S} = \Sigma \bar{\psi}. \quad (2.4)$$

In equations (2.2) through (2.4),  $\vec{j}^{out}$  is a vector of coefficients of basis functions in an approximation to the distribution of current on the faces of the cell for the outward directions,  $\vec{j}^{in}$  is a vector of coefficients of basis functions in an approximation to the distribution of current on the faces of the cell for the inward directions,  $\bar{\psi}$  is a vector of coefficients of basis functions in an approximation to the distribution of the angular flux within the cell,  $\bar{S}$  is a vector of coefficients of basis functions in an approximation to the distribution of the scattering source within the cell,  $\bar{E}$  is the vector of coefficients of basis functions in an approximation to the distribution of emissions within the cell. The matrices,  $\mathbf{K}_{OI}$ ,  $\mathbf{K}_{OS}$ ,  $\mathbf{K}_{OE}$ ,  $\mathbf{K}_{\psi I}$ ,  $\mathbf{K}_{\psi S}$ , and  $\mathbf{K}_{\psi E}$  are the relations between the vectors for the spatial quadrature. The matrix  $\Sigma$  contains the scattering contribution and angular quadrature weights to relate the scattering source and the angular flux. These equations are developed further in Chapters three and

four. The particle flow variable at the cell faces in equations (2.2) and (2.3) could be expressed either as angular flux or as angular current. The reason for using currents is presented in section B. These equations are used for the local detailed balance problem within a cell.

The global balance problem uses the flow of particles across cell faces for all the cells in the mesh, and removes the angular dependence by integrating a modification to equation (2.2) over a hemisphere to determine the particle flow. A discussion of both problems follows.

### 1. Local Detailed Balance

Local detailed balance is found by eliminating the scattering source from the system of equations in a cell. This allows the direct calculation of the detailed flow of particles in a cell from the flow from adjacent cells and emissions within the cell, again accounting for all of the scatters a particle can undergo within the cell. The local detailed balance relation for a cell is:

$$\vec{j}^{Out} = \mathbf{m}_{OI} \vec{j}^{In} + \mathbf{m}_{OE} \bar{E}. \quad (2.5)$$

Again,  $\vec{j}$  is the current at a cell edge for all the ordinates in the angular quadrature set,  $\bar{E}$  is the emissions in the cell along each ordinate, and  $\mathbf{m}_{OI}$  and  $\mathbf{m}_{OE}$  are matrices which give the contributions of the inward particle flow and emissions respectively.

To convert equations (2.2) through (2.4) into the form of equation (2.5), substitute equation (2.4) into equation (2.3) and solve for the angular flux:

$$\vec{\psi} = \mathbf{L}\mathbf{K}_{\psi I}\vec{j}^{in} + \mathbf{L}\mathbf{K}_{\psi E}\vec{E}, \quad (2.6)$$

where

$$\mathbf{L} = (\mathbf{I} - \mathbf{K}_{\psi S}\Sigma)^{-1} \quad (2.7)$$

This result and equation (2.4) are substituted into equation (2.2) for the current:

$$\vec{j}^{out} = \mathbf{K}_{OI}\vec{j}^{in} + \mathbf{K}_{OS}\Sigma(\mathbf{L}\mathbf{K}_{\psi I}\vec{j}^{in} + \mathbf{L}\mathbf{K}_{\psi E}\vec{E}) + \mathbf{K}_{OE}\vec{E}. \quad (2.8)$$

Collecting terms yields:

$$\vec{j}^{out} = (\mathbf{K}_{OI} + \mathbf{K}_{OS}\Sigma\mathbf{L}\mathbf{K}_{\psi I})\vec{j}^{in} + (\mathbf{K}_{OE} + \mathbf{K}_{OS}\Sigma\mathbf{L}\mathbf{K}_{\psi E})\vec{E}. \quad (2.9)$$

The matrices in the parentheses are in the form of equation (2.5). Further, the first matrix represents the contribution to first flight of particles, while the product term represents the contribution from particles after scattering. The convention of bold symbols represents matrices, while lower case  $\mathbf{m}$  is a reminder that this is a cell formula. This provides the needed formulas for the coefficient matrices:

$$\mathbf{m}_{OI} = \mathbf{K}_{OI} + \mathbf{K}_{OS}\Sigma\mathbf{L}\mathbf{K}_{\psi I}, \quad (2.10)$$

and

$$\mathbf{m}_{OE} = \mathbf{K}_{OE} + \mathbf{K}_{OS}\Sigma\mathbf{L}\mathbf{K}_{\psi E}. \quad (2.11)$$

## 2. Global Flow Balance

The global flow problem solves directly across the problem for the flow of particles across cell edges with no angular dependence. Equation (2.5) is



integrated over the appropriate angles to determine the outward particle flow for a cell and this is used to create a system of equations across the spatial mesh:

$$\underline{\underline{\mathbf{A}}}\bar{x} = \bar{b}, \quad (2.12)$$

where the flow of particles across cell edges,  $\bar{x}$  is only dependent on the forcing term,  $\bar{b}$ .

The global flow problem is much smaller than the discrete ordinates system of equations. The matrix  $\underline{\underline{\mathbf{A}}}$  is so sparse that the system can be solved directly. The detailed angular information for the flow of particles is implicit (in the elements of  $\underline{\underline{\mathbf{A}}}$ ); the partial currents of particles passing through all cell edges are the only (explicit) unknowns. This uses the spatial quadrature to model the contribution of particles entering the cell from any direction, scattering any number of times, and exiting the cell edge.

The cell flow of particles in the local balance problem contains the detailed angular information that is implicit in the global balance solution. However, the detailed cell flow does not necessarily include the contribution from particles that flow from nonadjacent cells after any number of scatters. To overcome this shortcoming and retain angular information for the global flow problem the two problems must be linked. Coupling the global and detailed balance problems solves this.

### 3. Coupling the Local Balances

The cell local balances are coupled across the spatial mesh and with the global balance problem through cell coupling. The level of particles scattering among cells is contained in the global balance solution, but the distributions of particles in angle is not. Coupling the local balances addresses the role of these distributions. This allows, through an angular integration, the relative importance of an angular direction to be used in the global balance solution and the distribution of the appropriate level for a particular direction back to the local detailed balance problem from the global balance solution.

If the correct coupling were known, both problems could be solved exactly and the detailed and global flow of particles could be calculated directly. As it is not known, an estimate is used and iteration is used to improve the estimate of the coupling. This is not source iteration; instead, this iteration seeks to improve the estimate of the coupling of the local balances rather than improving the scattering source estimate. The general method is shown in figure 2.1.

The figure shows the general phases of the distribution iteration method. An assumption is made for cell edge distributions. This assumption is used to set up and solve the global flow problem, taking into account emissions within the problem and boundary conditions to set approximate cell edge flow values. The cell edge values are used as inflows for neighboring cells to find cell outflows and improve the estimate of the edge distributions.

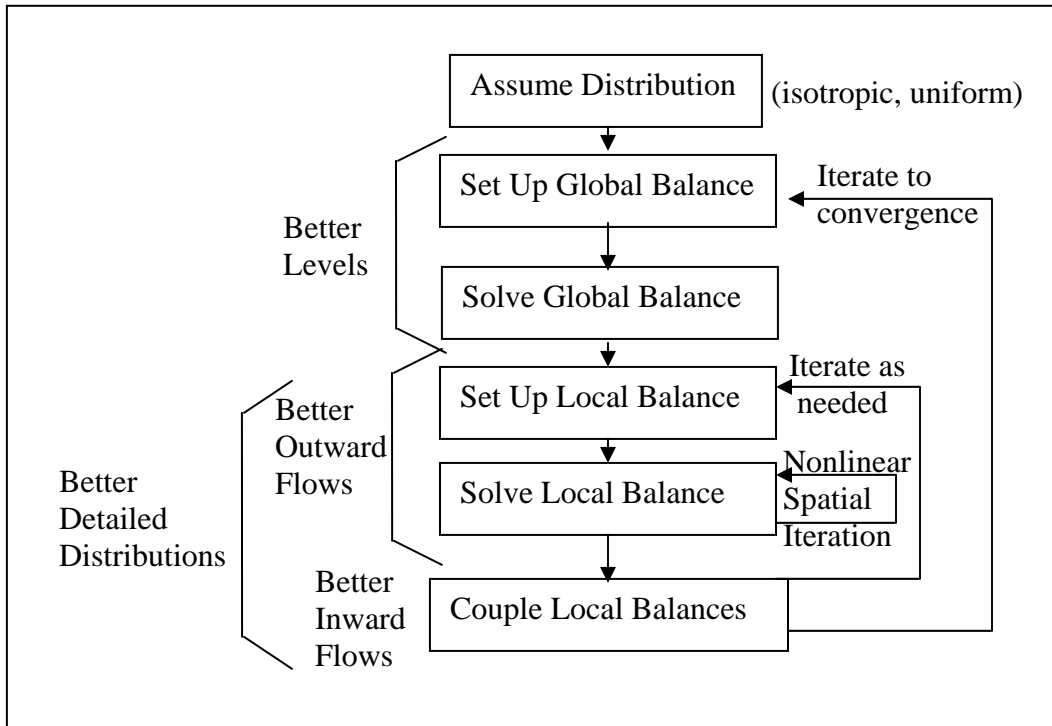


Figure 2.1 Flowchart describing the general distribution iteration method.

This inflow to outflow can be repeated until the estimate of the edge distribution is sufficiently improved. The innermost loop shows where additional iteration is done for nonlinear spatial methods, which are not included in this research. Better inward and outward detailed particle flow solutions, through iteration if needed, provide better coupling with detailed distributions. The updated edge distribution is used to set up another global flow problem and improve the estimate for the global flow problem solution, and the process repeats until a convergence criterion is met.

## B. Choices that Define a Method

The discrete ordinates system of equations is defined by the angular and spatial discretizations that are used. These choices, along with the possible implementation choices shown in figure 2.1 define a distribution iteration method. A review of the choices and considerations for implementation follow.

### 1. Angular Quadrature Sets

In general, the angular quadrature sets are used to evaluate the angular integrals needed for solutions to the discrete ordinate equations.

#### a. Slab Geometry Angular Quadrature Sets

In slab geometry, two different quadrature sets were considered. A brief description of these quadratures follows.

#### Discrete Elements Quadrature Set

Discrete elements (DE) quadratures were used by Wager to demonstrate the Angle Iteration method in one dimension (16: 2-3-5). The discrete elements quadratures do not exactly compute the factor of 1/3 in the diffusion coefficient. The angular quadrature should exactly integrate the following integral:

$$\int_{-1}^1 \frac{d\mu}{2} \mu^2 = \frac{1}{3}, \quad (2.13)$$

where  $\mu$  represents the direction cosine. In slab geometry for a discrete elements quadrature set with an even number,  $N$ , of equal weight elements, the general expression for the mean  $\mu_n$  in an element is:

$$\mu_n = 1 - \frac{(2n-1)}{N}, \quad (2.14)$$

where the element size is:

$$\Delta\mu_n = \frac{2}{N}. \quad (2.15)$$

This particular case for discrete elements is akin to a composite mid-point method. Using the DE angular quadrature, the integral in equation (2.13) is approximated as:

$$\int_{-1}^1 \frac{d\mu}{2} \mu^2 \approx \frac{1}{2} \sum_{n=1}^N \mu_n^2 \Delta\mu_n = \frac{1}{3} \left( 1 - \frac{1}{N^2} \right) \neq \frac{1}{3}. \quad (2.16)$$

As shown in equation (2.16), higher resolution DE quadratures (larger  $N$ ) are closer to meeting the diffusion limit, but are still not exact.

While this quadrature set made the visualization of collapsing and allocating the angular flux easier, the discrete elements quadratures do not meet the diffusion limit. Problems which are highly scattering, which are the type of problems where synthetic acceleration and source iteration have difficulty, and that this research will examine, need an angular quadrature that meets the diffusion limit.

### **Discrete Ordinate Quadrature Sets**

In the case of discrete ordinates angular quadratures, an exact relation for the integral in equation (2.13) is often considered to be a requirement for useful quadratures. Lewis and Miller provide a description of common discrete

ordinates angular quadrature sets for slab geometry (9: 119-126) and XY-geometry. In general, these are even quadratures which are symmetric about  $\mu = 0$  since positive and negative particle flows are generally of equal importance. A discussion of two popular quadrature sets for slab geometry follows.

### Single Range Gauss-Legendre

This quadrature set is also known as  $P_N$  quadratures. The ordinates,  $\mu_n$ , are the  $N$  roots of the Legendre polynomial:

$$P_N(\mu_n) = 0, \quad n = 1, 2, \dots, N. \quad (2.17)$$

The weights are found such that the quadrature set correctly integrates all polynomials through order  $2N - 1$ . The symmetry of the  $P_N$  quadrature set and the properties of the Legendre polynomials make this quadrature set popular for certain problems (9: 119-121).

### Double Range Gauss-Legendre

Double range or  $DP_N$  quadrature sets (9: 121-126) are similar to  $P_N$  except that quadratures are developed for the integrals over  $-1 \leq \mu < 0$  and  $0 < \mu \leq 1$ . These quadrature sets are used for their improved treatment of vacuum boundaries. In our case, these are desirable because partial currents are defined as integrals over these two domains. For example, consider the function defined as:

$$\begin{aligned} f(\mu) &= 0 & -1 \leq \mu \leq 0, \\ f(\mu) &= \mu & 0 < \mu \leq 1. \end{aligned} \quad (2.18)$$

The integral over the whole domain is

$$\int_{-1}^1 f(\mu) d\mu = \frac{1}{2}. \quad (2.19)$$

Double range quadrature sets can integrate this function exactly (even for the lowest order), while single range quadratures do not. Table 2.1 shows the integration results for several single range quadrature sets for equation (2.19) and demonstrates this. The single range quadratures of order 2 -12 and the integration results of equation (2.19) are shown. The error listed in the last column is the absolute difference from the exact solution.

Table 2.1 Single range Gauss quadrature results for equation (2.19)

$P_N$	Integration Results	Error (Difference)
$P_2$	0.57735	0.07735
$P_4$	0.52126	0.02126
$P_6$	0.50994	0.00994
$P_8$	0.50576	0.00576
$P_{10}$	0.50376	0.00376
$P_{12}$	0.50264	0.00264

### b. XY - Geometry Angular Quadrature Sets

The discrete ordinates quadratures were implemented to evaluate the angular integrations needed for solutions to the discrete ordinates equations in XY - geometry because they meet the diffusion limit. Two different quadratures

were implemented in order to compare with previously published results and to show the facility of the method in implementing different angular quadratures.

### **Level Symmetric**

Level symmetric quadratures are widely used (9: 158-162), and this quadrature set was used to compare with published results. These quadrature sets are referred to as  $S_N$  quadratures and contain the same set of  $N/2$  direction cosines with respect to each axis. There are  $\frac{N(N+2)}{8}$  ordinates per octant. The quadrature weights meet the condition that all weights must be equal for points obtained by permuting the direction cosines. A useful property of the  $S_N$  quadratures is that the ordinate directions are invariant to  $90^\circ$  rotations about any axis. The quadratures sets  $S_4$ ,  $S_6$ , and  $S_8$  were implemented for XY - geometry.

### **Product Quadratures**

A product quadrature was also implemented to show the facility with which different angular quadratures could be used. Abu-Shumays (1: 299-301) showed that a quadruple range quadrature set was competitive for improving accuracy. In this quadrature method, the polar angle,  $\phi$ , is integrated using a Gauss-Cristoffel quadrature and the azimuthal angle,  $\omega$ , is integrated using a Gauss-Chebychev quadrature. The direction cosines are calculated using these two quadratures:



$$\begin{aligned}\mu_n &= \cos(\omega_{m(n)})\sin(\phi_{l(n)}), \\ \eta_n &= \sin(\omega_{m(n)})\sin(\phi_{l(n)}),\end{aligned}\tag{2.20}$$

and the final quadrature weights are the product of the quadrature weights,

$$w_n = w_{m(n)}^\omega w_{l(n)}^\phi,\tag{2.21}$$

for both the Chebychev and Cristoffel quadratures. Cristoffel quadratures with 1-3 levels per octant and Chebychev quadratures with 2-5 levels per octant were implemented for XY - geometry.

## 2. Spatial Quadratures

Spatial quadratures methods can be characterized by the highest-order spatial moment balance that is satisfied exactly. Zeroth-moment and first-moment methods are used here. An advantage of linear methods is that for the distribution iteration methods, the matrix relationships providing the flow of particles and defined by the angular and spatial quadratures are fixed and do not need to be calculated for each iteration. For this reason, only linear methods are used here.

Several attributes of spatial quadrature methods are of especial interest: positivity, linearity, and (2<sup>nd</sup> order or better) accuracy. Positivity means that the outgoing face flow value (and the flux within the cell) returned by the spatial method is nonnegative, given nonnegative inflow flux and source. Negative flow values are non-physical and are strictly an artifact of the spatial method.

Linearity refers to the superposition of solutions, a solution for a source that is

the sum of other sources is also the sum of the solutions for the other sources (11: 33). Accuracy refers to the truncation error on fine meshes (9: 371). A spatial method has at most two of the three attributes (9: 135). The description of how these attributes align with the choice of spatial quadrature follows.

Step characteristic (SC) is a zeroth spatial moment method. It is a linear and positive method, but it is 1<sup>st</sup> order accurate. The SC method was implemented for slab and XY-geometry to demonstrate the method and to compare with Wager's results.

Weighted diamond difference (WDD) is a zeroth spatial moment method that is also a linear and positive method, but has less than 2<sup>nd</sup> order accuracy. The method is used in production codes and was used by Azmy to demonstrate the loss of effectiveness for DSA. The WDD method was implemented in XY-geometry to compare with published results.

Linear discontinuous (LD) is a first spatial moment method that is linear and 3<sup>rd</sup> order accurate, but is not a positive method. The LD method is also used in production codes and is one of the spatial quadratures that meets the diffusion limit on thick cells. The LD method was implemented for slab and XY-geometry to demonstrate the DI method for first spatial moment methods.

Linear characteristic (LC) is another non-positive first spatial moment method that is linear and 4<sup>th</sup> order accurate. It is used for better accuracy, but does not (like all characteristic methods) meet the thick-cell diffusion limit. The

LC method was implemented for XY-geometry to demonstrate the flexibility of the DI method for first spatial moment methods.

### **b. Nonlinear Methods**

Wager demonstrated the feasibility of using the exponential characteristic (EC) method for his work in slab geometry, a nonlinear method (16: 6-1).

Nonlinear methods add additional complexity, but have the attributes of accuracy (EC has 4<sup>th</sup> order accuracy), ability to use a coarser spatial mesh for accurate solutions, and positivity. However, additional calculations are needed for the innermost loop, as noted in Figure 2.1. Due to the additional complexity required for nonlinear methods, implementation of DI with EC is left for future efforts.

## **3. Cell Face Flow Variables**

Two choices for cell face flow variable are readily apparent: angular flux,  $\psi$ , and angular current,  $j$ .

### **a. Angular Flux as Cell Face Variable**

Angular flux is commonly used for the cell face flow variable. Spatial quadratures are presented in the literature in terms of angular fluxes. However, with this choice, the global flow balance variable lacks physical meaning; it is the angular integral of the angular flux over a hemisphere, which is neither a partial current nor a scalar flux.

## b. Angular Current as Cell Face Variable

Angular current has not been used for the cell face flow variable (to my knowledge), but can be determined easily from the angular flux and the direction cosines from the angular quadrature. The angular current is

$$j_{face}^{in/out} = \hat{\Omega} \cdot \hat{n}_{face} \psi(\hat{\Omega}),$$
 where in or out is chosen for a given  $\hat{\Omega}$  such that the dot product is positive.

Also, the global flow variable,  $J^\pm$ , is now a physical quantity: the partial current through the cell face. This changes the global flow problem to a partial current problem that is an explicit statement of conservation of particles within each cell. This motivated my choice of face flow variable for the distribution iteration method. The difference is more than one of bookkeeping; distribution iteration using the partial current problem converges in fewer iterations, as demonstrated by the testing presented in chapter 3.

## 4. Coupling the Local Balances

Coupling the local balances requires carrying information about particle flow from each cell in the spatial mesh to other cells, including cells that are not adjacent and may be distant. In order to obtain a rapidly converging method, an efficient coupling method is needed. Three different options are presented: local balance sweeping; red/black; and discrete ordinates sweeping.

### a. Local Balance Sweeping

In the local balance sweeping method, the current cell uses the outflows from the adjacent cell as inflows. This method is easy to implement, but requires

multiple sweeps to communicate between nonadjacent cells. Additionally, the outflow in the direction of the sweep, which is the inflow for the next cell has more improvement than the inflow at far side of the next cell. There is a possibility that the inflow estimate on the cell edges may not have equal improvement across the cell, which may introduce a bias across the cell. This is the method Wager used in his efforts (16: 2-68). The sweep is sequential in 1d, and has some parallelism in higher dimensions.

### **b. Red/Black**

The red/black method divides the spatial mesh into alternating cells and assigns a color, similar to a checkerboard. All the red cells can be done in parallel. The red cell outflows are the black cell inflows so that the black cells can then be done in parallel. Each cell communicates only locally – to its immediate neighbors in the spatial grid. This is the ideal situation for fully parallel computations with efficient scaling to many-processor systems.

However, the region influenced by a localized source in a problem with little scattering is extended by only one cell (in all directions) for each red or black calculation, hence two cells per red/black iteration. Thus convergence may be slow for such cases. These are the conditions in which SI works best, because the sweeps along the ordinate carry the first-flight influence of a localized source throughout the problem in one iteration. This motivated the next approach.

### **c. Discrete Ordinate Sweeping**

Rather than calculate the outflow values directly, the inflow values and emissions in a cell can be used to improve the current estimate of the cell scattering source including all numbers of scatters within the cell. This way of calculating the scattering source overcomes the difficulties of traditional discrete ordinates methods of estimating the scattering source, particularly for high scattering ratios. The cell scattering source calculations can be done in any order, and are also parallelizable. The cell scattering sources are then used for a single discrete ordinates sweep for each ordinate to determine the cell outflow values. For code implementation, two different discrete ordinates sweeping methods were used. The first was a single source calculation followed by one discrete ordinates sweep. This proved sufficient for most problems. The other method was an adaptive technique which varied between one and ten sweeps depending on the properties of the problem. For each sweep, the scattering source was updated using the cell edge values and the scattering source was used to calculate new cell edge values. This was used for slab geometry problems and some of the XY-geometry problems. A further analysis and description is presented in chapter seven.

A strength of the discrete ordinates sweep is that it rapidly communicates cell information across the spatial mesh as the angular flux calculations in an

ordinate are done over the spatial mesh. The sweep is limited in parallelism, but the method may have merit for serial machine implementation.

#### d. Parallel Efficiency of Red/Black vs. Sweeping

Any algorithm that sweeps through a regular, orthogonal grid, such as a checkerboard or its extension to 3d, in a compound direction, for example upward and to the right, is constrained by data dependencies. For example, after the bottom-left cell is done, the data for both the cell to its right and the cell above it are available. These two cells can be done in parallel, after which the three cells above and/or right of them can be done in parallel and so on. Thus, one sweeps a diagonal line of cells (crosswise to the flow) in XY-geometry, or a diagonal plane of cells in XYZ-geometry. This is partially parallel, but much less efficient than red/black (per iteration). Let  $d$  be the number of spatial dimensions and  $n$  be the size of the mesh (in each dimension).

Table 2.2. Parallel Efficiency considerations.

$d$	Sweeps	Stages per Sweep	Stages	Asymptotic Stage Ratio, Sweeps : Red/Black
1	2	$n$	$2n$	$n$
2	4	$2n-1$	$8n-4$	$4n$
3	6	$3n-2$	$18n-12$	$9n$

For large  $n$ , the asymptotic ratio (large  $n$ ) of the number of parallel stages per iteration for sweeping to the number of parallel stages for red/black (two stages) per iteration is  $d^2n$ . This analysis applies to both discrete ordinates

sweeping and to local balance sweeping because all the ordinates that have the same data dependency (such as upward and to the right) can be done in parallel in the diagonal sweep.

Consequently, it is reasonable to expect that red/black will be more efficient for large problems on MMP systems because the number of red/black iterations should be much less than the grid size  $n$ .



### III. Slab Geometry Implementation and Testing

#### A. Local Detailed Balance Problem

##### 1. Zeroth Spatial Moment Methods

Wager presented the foundation for the zeroth spatial moment methods (16: 2-22-27) using the angular flux formulation. The analogous angular current formulation is presented here. For the zeroth spatial moment methods, the system of equations for a cell are:

$$\vec{j}^{out} = \mathbf{K}_{OI} \vec{j}^{in} + \mathbf{K}_{OSA} \vec{S}^A + \mathbf{K}_{OEA} \vec{E}^A, \quad (3.1)$$

$$\vec{\psi}^A = \mathbf{K}_{AI} \vec{j}^{in} + \mathbf{K}_{ASA} \vec{S}^A + \mathbf{K}_{AEA} \vec{E}^A, \quad (3.2)$$

and 
$$\vec{S}^A = \sum_S \vec{\psi}^A. \quad (3.3)$$

In these equations,  $\mathbf{K}_{OI}$ ,  $\mathbf{K}_{OSA}$ ,  $\mathbf{K}_{OEA}$ ,  $\mathbf{K}_{AI}$ ,  $\mathbf{K}_{ASA}$  and  $\mathbf{K}_{AEA}$ , are diagonal matrices of transport coefficients that define the relations of the inputs of a cell to the calculated quantity. For example,  $\mathbf{K}_{OI}$  represents the contribution to the outgoing flux from the incoming flux and  $\mathbf{K}_{ASA}$  represents the contribution to the average flux from the average scatter. The values of the transport coefficients are determined from the spatial quadrature used. Letting  $\mathbf{D}(\vec{x})$  be the diagonalization operator that creates a diagonal matrix from vector  $\vec{x}$ , the general matrices become:

$$\mathbf{K} = \mathbf{D}(\vec{k}). \quad (3.4)$$

The quantities  $\vec{j}^{out}$ ,  $\vec{j}^{in}$  and  $\vec{\psi}^A$  are the variables to represent the cell outward angular current, inward angular current and average angular flux respectively.

The zeroth spatial moment over a cell is normalized to be the average value.

Thus, the quantities  $\vec{S}^A$  and  $\vec{E}^A$  are the variables to represent the average scatter and average emissions in a cell. The vector notation represents an array for the variable with all the ordinates in the angular quadrature. Also, for isotropic scatter:

$$\underline{\Sigma}_S = \sigma_s \underline{\mathbf{1}} \underline{\mathbf{D}}(\vec{w}), \quad (3.5)$$

where  $\underline{\mathbf{D}}(\vec{w})$  is the diagonal operator on quadrature weight vector,  $\sigma_s$  is the isotropic scattering source and  $\underline{\mathbf{1}}$  is a matrix with one for every element. In general, this matrix,  $\underline{\Sigma}_S$  contains the scattering cross sections with the appropriate quadrature weights to calculate the scattering source from the average flux.

Equations (3.3) can be substituted into equation (3.2) to solve for the average flux in a cell in terms of the incoming cell angular current and the emission in a cell:

$$\vec{\psi}^A = (\mathbf{I} - \mathbf{K}_{ASA} \underline{\Sigma}_S)^{-1} \mathbf{K}_{AI} \vec{j}^{in} + (\mathbf{I} - \mathbf{K}_{ASA} \underline{\Sigma}_S)^{-1} \mathbf{K}_{AEA} \vec{E}^A. \quad (3.6)$$

Equations (3.6) and (3.3) can be substituted into equation (3.1) to solve for the outgoing angular current in a cell in terms of the incoming cell angular current and the emission in a cell:

$$\begin{aligned} \vec{j}^{out} = & (\mathbf{K}_{OI} + \mathbf{K}_{OSA} \Sigma_S (\mathbf{I} - \mathbf{K}_{ASA} \Sigma_S)^{-1} \mathbf{K}_{AI}) \vec{j}^{in} + \\ & (\mathbf{K}_{OEA} + \mathbf{K}_{OSA} \Sigma_S (\mathbf{I} - \mathbf{K}_{ASA} \Sigma_S)^{-1} \mathbf{K}_{AEA}) \vec{E}^A. \end{aligned} \quad (3.7)$$

Again, the factor  $(\mathbf{I} - \mathbf{K}_{ASA} \Sigma_S)^{-1}$  can be thought of as modeling infinite within cell scattering (16: 2-55). The terms in the outer parentheses can be expressed as a single matrix:

$$\vec{j}^{out} = \mathbf{m}_{OI} \vec{j}^{in} + \mathbf{m}_{OE} \vec{E}^A. \quad (3.8)$$

An exactly analogous derivation is done for the angular flux formulation. For the zeroth spatial moment methods, these matrices need only be calculated one time for each material (with a uniform spatial mesh). Equation (3.8) can be used to solve the cell detailed balance problem for both the local balance sweeping and the red/black methods. Equations (3.6) and (3.3) are used to determine the cell scattering sources for the discrete ordinates sweep method.

### **Zeroth Moment Transport Coefficients**

For the testing in slab geometry, the transport coefficients for the step characteristic will be discussed for zeroth spatial moment methods. The transport coefficients are used to build the diagonal matrices used in the local detailed balance problem. Other zeroth spatial moment methods would be implemented using the same procedure.

## 1. Angular Flux Formulation

Lathrop introduced the step characteristic method in 1969 (11: 24) and the quadrature equations can also be found in the literature (10: v-8). Wager presented SC relations (16: 2-18,2-22) in a more compact notation using the exponential moment functions of order  $m$  developed by Mathews et al. (11: 27) where:

$$M_m(x) = \int_0^1 dt (1-t)^m e^{-xt} . \quad (3.9)$$

The cell optical thickness measured along ordinate  $n$  is used in these relations and is defined as:

$$\varepsilon_n = \frac{\sigma \Delta x}{|\mu_n|} , \quad (3.10)$$

where  $\sigma$  is the total cross section,  $\Delta x$  is the cell width and  $\mu_n$  is the direction cosine from the angular quadrature. As an example, consider a quadrature set with four ordinates, (1 and 2 to the right, 3 and 4 to the left). The cell SC equations for the outgoing angular fluxes are:

$$\psi_1^R = e^{-\varepsilon_1} \psi_1^L + \frac{\Delta x}{|\mu_1|} M_0(\varepsilon_1) S_1^A + \frac{\Delta x}{|\mu_1|} M_0(\varepsilon_1) E_1^A , \quad (3.11)$$

$$\psi_2^R = e^{-\varepsilon_2} \psi_2^L + \frac{\Delta x}{|\mu_2|} M_0(\varepsilon_2) S_2^A + \frac{\Delta x}{|\mu_2|} M_0(\varepsilon_2) E_2^A , \quad (3.12)$$

$$\psi_3^L = e^{-\varepsilon_3} \psi_3^R + \frac{\Delta x}{|\mu_3|} M_0(\varepsilon_3) S_3^A + \frac{\Delta x}{|\mu_3|} M_0(\varepsilon_3) E_3^A , \quad (3.13)$$

and 
$$\psi_4^L = e^{-\varepsilon_4} \psi_4^R + \frac{\Delta x}{|\mu_4|} M_0(\varepsilon_4) S_4^A + \frac{\Delta x}{|\mu_4|} M_0(\varepsilon_4) E_4^A, \quad (3.14)$$

where R and L designate the right and left faces of the cell. Equations (3.11)

through (3.14) take the form of equation (3.1), with  $\mathbf{K}_{OI} = D(\vec{k}_{OI})$ ,

$\mathbf{K}_{OSA} = D(\vec{k}_{OSA})$  and  $\mathbf{K}_{OEA} = D(\vec{k}_{OEA})$ , where the  $k$  vectors are:

$$(k_{OI})_n = e^{-\varepsilon_n}, \quad (3.15)$$

$$(k_{OSA})_n = \frac{\Delta x}{|\mu_n|} M_0(\varepsilon_n), \quad (3.16)$$

and 
$$(k_{OEA})_n = \frac{\Delta x}{|\mu_n|} M_0(\varepsilon_n). \quad (3.17)$$

For the same quadrature set, the SC equations for the average angular flux are:

$$\psi_1^A = M_0(\varepsilon_1) \psi_1^L + \frac{\Delta x}{|\mu_1|} M_1(\varepsilon_1) S_1^A + \frac{\Delta x}{|\mu_1|} M_1(\varepsilon_1) E_1^A, \quad (3.18)$$

$$\psi_2^A = M_0(\varepsilon_2) \psi_2^L + \frac{\Delta x}{|\mu_2|} M_1(\varepsilon_2) S_2^A + \frac{\Delta x}{|\mu_2|} M_1(\varepsilon_2) E_2^A, \quad (3.19)$$

$$\psi_3^A = M_0(\varepsilon_3) \psi_3^R + \frac{\Delta x}{|\mu_3|} M_1(\varepsilon_3) S_3^A + \frac{\Delta x}{|\mu_3|} M_1(\varepsilon_3) E_3^A, \quad (3.20)$$

and 
$$\psi_4^A = M_0(\varepsilon_4) \psi_4^R + \frac{\Delta x}{|\mu_4|} M_1(\varepsilon_4) S_4^A + \frac{\Delta x}{|\mu_4|} M_1(\varepsilon_4) E_4^A. \quad (3.21)$$

Equations (3.18) through (3.21) take the form of equation (3.2), with

$\mathbf{K}_{AI} = D(\vec{k}_{AI})$ ,  $\mathbf{K}_{ASA} = D(\vec{k}_{ASA})$  and  $\mathbf{K}_{AEA} = D(\vec{k}_{AEA})$ , where the  $k$  vectors are:

$$(k_{AI})_n = M_0(\varepsilon_n), \quad (3.22)$$

$$(k_{ASA})_n = \frac{\Delta x}{|\mu_n|} M_1(\varepsilon_n), \quad (3.23)$$

and

$$(k_{AEA})_n = \frac{\Delta x}{|\mu_n|} M_1(\varepsilon_n). \quad (3.24)$$

## 2. Angular Current Formulation

The x component of current along an ordinate in slab geometry is  $j_n = |\mu_n| \psi_n$ .

The general form for the angular flux equations is exactly analogous to the angular current equations (3.1) through (3.3), but the formulas for some of the  $k$  vectors are different. To change the transport coefficients to the current representation requires multiplying or dividing the transport coefficient by  $|\mu_n|$  where appropriate. The system of equations for the outgoing flow and cell average flux shown in equations (3.11) through (3.14) and equations (3.18) through (3.21) must also be changed. Multiply equation (3.11) by  $|\mu_1|$  to get the corresponding angular current formulation equation:

$$j_1^R = e^{-\varepsilon_1} j_1^L + \Delta x M_0(\varepsilon_1) S_1^A + \Delta x M_0(\varepsilon_1) E_1^A. \quad (3.25)$$

Thus the  $k$  vectors for the outward currents are:

$$(k_{OI})_n = e^{-\varepsilon_n}, \quad (3.26)$$

$$(k_{OSA})_n = \Delta x M_0(\varepsilon_n), \quad (3.27)$$

and 
$$(k_{OEA})_n = \Delta x M_0(\varepsilon_n). \quad (3.28)$$

Replacing  $\psi_1^L$  with the equivalent  $\frac{j_1^L}{|\mu_1|}$  in equation (3.18) yields the

corresponding angular current formulation equation:

$$\psi_1^A = \frac{1}{|\mu_1|} M_0(\varepsilon_1) j_1^L + \frac{\Delta x}{|\mu_1|} M_1(\varepsilon_1) S_1^A + \frac{\Delta x}{|\mu_1|} M_1(\varepsilon_1) E_1^A; \quad (3.29)$$

hence, the  $k$  vectors for the average flux are:

$$(k_{AI})_n = \frac{1}{|\mu_n|} M_0(\varepsilon_n), \quad (3.30)$$

$$(k_{ASA})_n = \frac{\Delta x}{|\mu_n|} M_1(\varepsilon_n), \quad (3.31)$$

and 
$$(k_{AEA})_n = \frac{\Delta x}{|\mu_n|} M_1(\varepsilon_n). \quad (3.32)$$

## 2. First Spatial Moment Methods

The slab geometry zeroth-moment methods are in the general form of equations (2.3) through (2.5); the only difference is the addition of “A” to some of the subscripts and superscripts. The first-moment methods are also of that form, as is shown in this section. First, however, the first-moment methods are presented in a form that follows naturally from the way such spatial quadratures are normally written. This requires several additional terms and equations to

account for the contribution to the flux from the first moment of the scattering source:

$$\vec{j}^{out} = \mathbf{K}_{OI} \vec{j}^{in} + \mathbf{K}_{OSA} \bar{S}^A + \mathbf{K}_{OSX} \bar{S}^X + \mathbf{K}_{OEA} \bar{E}^A + \mathbf{K}_{OEX} \bar{E}^X, \quad (3.33)$$

$$\bar{\psi}^A = \mathbf{K}_{AI} \vec{j}^{in} + \mathbf{K}_{ASA} \bar{S}^A + \mathbf{K}_{ASX} \bar{S}^X + \mathbf{K}_{AEA} \bar{E}^A + \mathbf{K}_{AEX} \bar{E}^X, \quad (3.34)$$

$$\bar{\psi}^X = \mathbf{K}_{XI} \vec{j}^{in} + \mathbf{K}_{XSA} \bar{S}^A + \mathbf{K}_{XSX} \bar{S}^X + \mathbf{K}_{XEA} \bar{E}^A + \mathbf{K}_{XEX} \bar{E}^X, \quad (3.35)$$

$$\bar{S}^A = \sum_S \bar{\psi}^A, \quad (3.36)$$

and 
$$\bar{S}^X = \sum_S \bar{\psi}^X. \quad (3.37)$$

The new matrices,  $\mathbf{K}_{OEX}$ ,  $\mathbf{K}_{AEX}$ ,  $\mathbf{K}_{XI}$ ,  $\mathbf{K}_{XSA}$ ,  $\mathbf{K}_{XEA}$ ,  $\mathbf{K}_{XSX}$  and  $\mathbf{K}_{XEX}$ , are also diagonal matrices of transport coefficients that define the relations of the inputs of particles to the calculated quantity. For example  $\mathbf{K}_{XI}$  represents the contribution to the first spatial moment of the flux in the cell from the incoming flux. The diagonal values, or transport coefficients, are also determined from the spatial quadrature used. The new quantities  $\bar{\psi}^X$ ,  $\bar{S}^X$  and  $\bar{E}^X$  are the variables to represent the x-moments of the angular flux, scatter and emissions respectively.

This system takes the general form by collecting the zeroth and first moments together into single, larger vectors. The easiest way to do this is blockwise:



$$\bar{\psi} = \begin{bmatrix} \bar{\psi}^A \\ \bar{\psi}^X \end{bmatrix}, \quad (3.38)$$

$$\bar{S} = \begin{bmatrix} \bar{S}^A \\ \bar{S}^X \end{bmatrix}, \quad (3.39)$$

and

$$\bar{E} = \begin{bmatrix} \bar{E}^A \\ \bar{E}^X \end{bmatrix}. \quad (3.40)$$

Equation (3.33) can be written in the general form

$$\bar{j}^{out} = \mathbf{K}_{OI} \bar{j}^{in} + \mathbf{K}_{OS} \bar{S} + \mathbf{K}_{OE} \bar{E}, \quad (3.41)$$

by joining  $\mathbf{K}$  matrices blockwise:

$$\mathbf{K}_{OS} = [\mathbf{K}_{OSA} \quad \mathbf{K}_{OSX}], \quad (3.42)$$

and

$$\mathbf{K}_{OE} = [\mathbf{K}_{OEA} \quad \mathbf{K}_{OEX}]. \quad (3.43)$$

Similarly, equations (3.34) and (3.35) are

$$\bar{\psi} = \mathbf{K}_{\psi I} \bar{j}^{in} + \mathbf{K}_{\psi S} \bar{S} + \mathbf{K}_{\psi E} \bar{E}, \quad (3.44)$$

where

$$\mathbf{K}_{\psi I} = \begin{bmatrix} \mathbf{K}_{AI} \\ \mathbf{K}_{XI} \end{bmatrix}, \quad (3.45)$$

$$\mathbf{K}_{\psi S} = \begin{bmatrix} \mathbf{K}_{ASA} & \mathbf{K}_{ASX} \\ \mathbf{K}_{XSA} & \mathbf{K}_{XSX} \end{bmatrix}, \quad (3.46)$$

and

$$\mathbf{K}_{\psi E} = \begin{bmatrix} \mathbf{K}_{AEA} & \mathbf{K}_{AEX} \\ \mathbf{K}_{XEA} & \mathbf{K}_{XEX} \end{bmatrix}. \quad (3.47)$$

Finally, equations (3.36) and (3.37) can be also represented as:

$$\vec{S} = \Sigma \vec{\psi}, \quad (3.48)$$

where

$$\Sigma = \begin{bmatrix} \Sigma_S & 0 \\ 0 & \Sigma_S \end{bmatrix}. \quad (3.49)$$

With these matrices that include first moments, the first-moment system of equations,

$$\vec{j}^{out} = \mathbf{K}_{OI} \vec{j}^{in} + \mathbf{K}_{OS} \vec{S} + \mathbf{K}_{OE} \vec{E}, \quad (3.50)$$

$$\vec{\psi} = \mathbf{K}_{\psi I} \vec{j}^{in} + \mathbf{K}_{\psi S} \vec{S} + \mathbf{K}_{\psi E} \vec{E}, \quad (3.51)$$

and

$$\vec{S} = \Sigma \vec{\psi}, \quad (3.52)$$

is of the same form as equations (2.2) through (2.4). Equation (3.52) can be substituted into equation (3.51) to eliminate the scatter:

$$\vec{\psi} = (\mathbf{I} - \mathbf{K}_{\psi S} \Sigma)^{-1} \mathbf{K}_{\psi I} \vec{j}^{in} + (\mathbf{I} - \mathbf{K}_{\psi S} \Sigma)^{-1} \mathbf{K}_{\psi E} \vec{E}. \quad (3.53)$$

This result with equation (3.52) can be substituted into equation (3.50) to again eliminate scatter:

$$\begin{aligned} \vec{j}^{out} = & (\mathbf{K}_{OI} + \mathbf{K}_{OS} \Sigma (\mathbf{I} - \mathbf{K}_{\psi S} \Sigma)^{-1} \mathbf{K}_{\psi I}) \vec{j}^{in} + \\ & (\mathbf{K}_{OE} + \mathbf{K}_{OS} \Sigma (\mathbf{I} - \mathbf{K}_{\psi S} \Sigma)^{-1} \mathbf{K}_{\psi E}) \vec{E}. \end{aligned} \quad (3.54)$$

The quantities in the parenthesis can be combined to form a single matrix yielding the general form,

$$\vec{j}^{out} = \mathbf{m}_{OI} \vec{j}^{in} + \mathbf{m}_{OE} \vec{E}, \quad (3.55)$$

of equation (2.5). As with the zeroth spatial moment methods, these matrices are only calculated once for each material for first spatial moment methods. Again, equation (3.55) can be used to solve the cell detailed balance problem for both the local balance sweeping and the Red/Black methods. Equation (3.53) is used to determine the cell scattering sources for the discrete ordinates sweep method. The scope of this research is limited to single energy group problems, therefore the x-moments of emissions are zero and the related transport coefficients,  $\mathbf{K}_{OEX}$ ,  $\mathbf{K}_{AEX}$  and  $\mathbf{K}_{XEX}$ , were not used. The code implementation used an equivalent elimination of the scattering sources, in which a block forward elimination and back substitution produces the inverse matrix in equation (3.53). Details are presented in Appendix E.

### **First Moment Transport Coefficients**

For the testing in slab geometry, the transport coefficients for linear discontinuous methods are used as an example of a first-moment, linear spatial quadrature. The transport coefficients are used to build the diagonal matrices used in the local detailed balance problem. Other first spatial moment methods would be implemented using the same procedure.

## Angular Flux Formulation

The LD method has also been used for many years, and the equations are presented by Larson (8: 222) and also by Lewis and Miller (9: 134). Similarly to the zeroth moment methods, a system of equations for a cell is set up for all the ordinates in the angular quadrature set for the outgoing flux in a cell, the average angular flux in a cell, and the x-moment of angular flux in a cell. As was done for SC, the LD angular flux transport coefficients are found from the angular flux equations in a cell, which are shown in appendix A. The current equations are also derived in appendix A. The LD  $k$  vectors for the outgoing fluxes are:

$$(k_{OI})_n = \frac{6 - 2\varepsilon_n}{6 + 4\varepsilon_n + \varepsilon_n^2}, \quad (3.56)$$

$$(k_{OSA})_n = \frac{\Delta x(6 + \varepsilon_n)}{(6 + 4\varepsilon_n + \varepsilon_n^2)|\mu_n|}, \quad (3.57)$$

$$(k_{OSX})_n = \frac{\Delta x \varepsilon_n}{(6 + 4\varepsilon_n + \varepsilon_n^2)|\mu_n|}, \quad (3.58)$$

and

$$(k_{OEA})_n = \frac{\Delta x(6 + \varepsilon_n)}{(6 + 4\varepsilon_n + \varepsilon_n^2)|\mu_n|}. \quad (3.59)$$

The LD  $k$  vectors for the average flux are:

$$(k_{AI})_n = \frac{6 + \varepsilon_n}{6 + 4\varepsilon_n + \varepsilon_n^2}, \quad (3.60)$$

$$(k_{ASA})_n = \frac{\Delta x(3 + \varepsilon_n)}{(6 + 4\varepsilon_n + \varepsilon_n^2)|\mu_n|}, \quad (3.61)$$

$$(k_{ASX})_n = \frac{-\Delta x}{(6+4\epsilon_n + \epsilon_n^2)|\mu_n|}, \quad (3.62)$$

and

$$(k_{AEA})_n = \frac{\Delta x(3 + \epsilon_n)}{(6+4\epsilon_n + \epsilon_n^2)|\mu_n|}. \quad (3.63)$$

The LD x-moment angular flux  $k$  vectors are:

$$(k_{XI})_n = \frac{-3\epsilon_n}{6+4\epsilon_n + \epsilon_n^2}, \quad (3.64)$$

$$(k_{XSA})_n = \frac{3\Delta x}{(6+4\epsilon_n + \epsilon_n^2)|\mu_n|}, \quad (3.65)$$

$$(k_{XSX})_n = \frac{\Delta x(\epsilon_n + 1)}{(6+4\epsilon_n + \epsilon_n^2)|\mu_n|}, \quad (3.66)$$

and

$$(k_{XEA})_n = \frac{3\Delta x}{(6+4\epsilon_n + \epsilon_n^2)|\mu_n|}. \quad (3.67)$$

### Angular Current Formulation

The translation to the current representation is done in the same way as for the zeroth spatial moment method shown in equation (3.25) using the relation  $j_n = |\mu_n|\psi_n$ . The LD  $k$  vectors for the outgoing currents are:

$$(k_{OI})_n = \frac{6 - 2\epsilon_n}{6+4\epsilon_n + \epsilon_n^2}, \quad (3.68)$$

$$(k_{OSA})_n = \frac{\Delta x(6 + \epsilon_n)}{6+4\epsilon_n + \epsilon_n^2}, \quad (3.69)$$

$$(k_{OSX})_n = \frac{\Delta x \varepsilon_n}{6 + 4\varepsilon_n + \varepsilon_n^2}, \quad (3.70)$$

and

$$(k_{OEA})_n = \frac{\Delta x(6 + \varepsilon_n)}{6 + 4\varepsilon_n + \varepsilon_n^2}. \quad (3.71)$$

The LD  $k$  vectors for the average flux are:

$$(k_{AI})_n = \frac{6 + \varepsilon_n}{(6 + 4\varepsilon_n + \varepsilon_n^2)|\mu_n|}, \quad (3.72)$$

$$(k_{ASA})_n = \frac{\Delta x(3 + \varepsilon_n)}{(6 + 4\varepsilon_n + \varepsilon_n^2)|\mu_n|}, \quad (3.73)$$

$$(k_{ASX})_n = \frac{-\Delta x}{(6 + 4\varepsilon_n + \varepsilon_n^2)|\mu_n|}, \quad (3.74)$$

and

$$(k_{AEA})_n = \frac{\Delta x(3 + \varepsilon_n)}{(6 + 4\varepsilon_n + \varepsilon_n^2)|\mu_n|}. \quad (3.75)$$

The LD x-moment angular flux  $k$  vectors are:

$$(k_{XI})_n = \frac{-3\varepsilon_n}{(6 + 4\varepsilon_n + \varepsilon_n^2)|\mu_n|}, \quad (3.76)$$

$$(k_{XSA})_n = \frac{3\Delta x}{(6 + 4\varepsilon_n + \varepsilon_n^2)|\mu_n|}, \quad (3.77)$$

$$(k_{XSX})_n = \frac{\Delta x(\varepsilon_n + 1)}{(6 + 4\varepsilon_n + \varepsilon_n^2)|\mu_n|}, \quad (3.78)$$

and

$$(k_{XEA})_n = \frac{3\Delta x}{(6 + 4\varepsilon_n + \varepsilon_n^2)|\mu_n|}. \quad (3.79)$$

## B. Global Flow Balance Problem

The global flow balance problem determines the proper level of flow values across the problem. Setting up the global flow balance problem with the updated cell valued information uses an array similar to the flux weights used by Wager (16: 2-73). However, a brief discussion of angular quadrature weights is needed first. In the transport equations, the angular quadrature weights are used to calculate the scalar flux and partial currents. In slab geometry the scalar flux,  $\phi$ , is:

$$\phi = \frac{1}{2} \int_{-1}^1 \psi(\mu) d\mu \approx \frac{1}{2} \sum_{\forall n} w_n \psi(\mu_n). \quad (3.80)$$

The partial currents,  $J^\pm$ , in slab geometry are:

$$J^+ = \int_0^1 \mu \psi(\mu) d\mu \approx \sum_{n \ni \mu_n > 0} \tilde{w}_n^+ \mu_n \psi(\mu_n), \quad (3.81)$$

and

$$J^- = \int_{-1}^0 |\mu| \psi(\mu) d\mu \approx \sum_{n \ni \mu_n < 0} \tilde{w}_n^- |\mu_n| \psi(\mu_n), \quad (3.82)$$

where the quadrature weights are renormalized for each direction:

$$\tilde{w}_n^\pm = \frac{w_n}{\sum_{n' \ni \text{sign} n' = \pm} w_{n'}}. \quad (3.83)$$

If there are no ordinates where  $\mu_n = 0$ , (which is standard practice) and:

$$\sum_{n \ni \mu_n > 0} w_n = 1, \quad (3.84)$$

and 
$$\sum_{n \ni \mu_n < 0} w_n = 1, \quad (3.85)$$

then 
$$\sum_{\forall n} w_n = 2, \quad (3.86)$$

and the quadrature rules in equations (3.80) through (3.82) are exact for

$\psi(\mu) = \text{constant}$  ( $-1 \leq \mu \leq 1$ ). It is sufficient for  $\sum_{\forall n} w_n = 2$ , no  $\mu_n = 0$  and a

symmetric angular quadrature set (which is the case for the angular quadratures tested in this research). For these quadrature sets, the renormalized weights in equation (3.83) are equal,  $\tilde{w}_n = w_n$  and the  $\tilde{w}_n$  notation is dropped for convenience.

The edge distribution,  $\zeta$ , is a weight indicating the relative importance of the current along an ordinate to the partial current. The edge distribution,  $\zeta$ , is defined for the angular flux and current as follows:

$$\zeta_n^\psi = \frac{\psi_n}{\sum_{n' \ni \text{Sign}(\mu_{n'}) = \text{Sign}(\mu_n)} w_{n'} \psi_{n'}}, \quad (3.87)$$

and 
$$\zeta_n^j = \frac{j_n}{\sum_{n' \ni \text{Sign}(\mu_{n'}) = \text{Sign}(\mu_n)} w_{n'} j_{n'}}, \quad (3.88)$$

where  $w_{n'}$  is the angular quadrature weight. The use of the edge distributions to set up the global problem begins by referring to the general form for the cell system of equations in the current formulation in equation (3.8):

$$\vec{j}^{\text{out}} = \mathbf{m}_{OI} \vec{j}^{\text{in}} + \mathbf{m}_{OE} \vec{E}. \quad (3.89)$$



The denominator of equation (3.88) is a partial current as defined in equations (3.81) and (3.82). Arranging the edge distributions and angular currents as vectors for the edge of the cell in equation (3.88), the inward angular current for a given direction is:

$$\vec{j}^{in} = \vec{\zeta}^{in} J_{in}, \quad (3.90)$$

where  $J_{in}$  is the inward partial current. Substituting this back into equation (3.89) yields:

$$\vec{j}^{out} = \mathbf{m}_{OI} \vec{\zeta}^{in} J_{in} + \mathbf{m}_{OE} \vec{E}. \quad (3.91)$$

The outward partial current for a given outward direction is:

$$J_{out} = \sum_{n \in out} w_n j_n^{out}. \quad (3.92)$$

Equation (3.91) is used to calculate the outward partial current:

$$J_{out} = \sum_{n \in out} w_n (\mathbf{m}_{OI} \vec{\zeta}^{in})_n J_{in} + \sum_{n \in out} w_n (\mathbf{m}_{OE} \vec{E})_n. \quad (3.93)$$

The quantities:

$$M_{OI} = \sum_{n \in out} w_n \left( \mathbf{m}_{OI} \vec{\zeta}^{in} \right)_n, \quad (3.94)$$

and

$$J_E = \sum_{n \in out} w_n \left( \mathbf{m}_{OE} \vec{E} \right)_n, \quad (3.95)$$

are collapsed coefficients representing the contribution to the outward partial current in a given direction from the inward partial current and emissions

respectively. This process of using the appropriate quadrature weights to integrate over a hemisphere and reduce the cell matrices to a single coefficient is what I call *collapsing*. For equation (3.95) the quantity  $J^E$  represents the outward partial current of particles emitted in the cell that have scattered any number of times (0 through infinity) before leaving the cell for the first time. It is a known value for the problem. For a cell in slab geometry, the partial current equations with the collapsed coefficients are:

$$\begin{bmatrix} J_{Out}^L \\ J_{Out}^R \end{bmatrix} = \begin{bmatrix} M_{OI}^{LL} & M_{OI}^{LR} \\ M_{OI}^{RL} & M_{OI}^{RR} \end{bmatrix} \begin{bmatrix} J_{In}^L \\ J_{In}^R \end{bmatrix} + \begin{bmatrix} J_E^L \\ J_E^R \end{bmatrix}, \quad (3.96)$$

where the superscripts  $R$  and  $L$  indicate the right or left sides of the cell. The double superscripts indicate the contribution to the outward partial current from the respective inward partial current,  $RL$  is the contribution to the right outward partial current from the left inward partial current. A similar relation can be defined across the spatial mesh. Recognizing that the inflow variables are outflows of adjacent cells, a system of equations,  $\underline{\underline{A}}\bar{x} = \bar{b}$  can be set up with the emissions shown in equation (3.95) as the forcing term and the global flow variables as the unknowns. Wager showed how the global flow variables permutation resulted in a penta-diagonal matrix that could be solved directly (14: 2-47) using the angular flux formulation. The current formulation is exactly analogous. To explore the efficacy of sparse matrix methods, a Compaq

Extended Math Library (CXML) direct sparse matrix solver (cxml\_dss.f90) (6:11-1) was used to solve this system of equations in slab geometry.

To distribute the partial current (or global flow variable) solution back to the detailed cell edge angular currents, the distributions are used as follows:

$$\vec{j}_{new}^L = J_{Sol'n}^L \vec{\zeta}^L, \quad (3.97)$$

and 
$$\vec{j}_{new}^R = J_{Sol'n}^R \vec{\zeta}^R. \quad (3.98)$$

A similar technique is used in the angular flux formulation. This completes the equations needed to complete an iteration as described in chapter two.

### C. Test Results In Slab Geometry

#### 1. Preliminaries: Measuring Convergence Tolerance

The symmetric relative difference (SRD) was developed by Minor and Mathews (13: 182) to determine when the difference in the desired quantities between iterations met the chosen convergence tolerance. The relation for the SRD is:

$$SRD(x, y) = \begin{cases} 0 & x = y = 0, \\ \frac{2|x-y|}{|x|+|y|} & Else. \end{cases} \quad (3.99)$$

This function returns a value between zero, for values that are exactly the same, and two as the limit for values that are very different, are of opposite signs, or

only one of which is 0. Most often this function is applied to two arrays to find the maximum SRD between corresponding array values:

$$SRD_{Max}(\vec{x}, \vec{y}) = \underset{i}{Max}(SRD(x_i, y_i)). \quad (3.100)$$

To check for convergence tolerance, the SRD function is applied to corresponding values in two arrays (for two successive iterations) and the maximum value is compared to the convergence criterion.

## 2. Test Problems

The test problems were a series of single material problems with a reflective boundary on the left and a vacuum boundary on the right. In the series of problems, the material was totally scattering with total cross section  $\sigma = 1.0$  and an emission source  $S = 1.0$  uniformly distributed throughout the material. The cell size was fixed at  $\Delta x = 1.0$  and the number of cells varied from 10 to 300 for the problems. The tests were done using a  $DP_8$  angular quadrature (16 ordinates). The convergence tolerance was  $10^{-5}$  for the maximum symmetric relative difference (SRD) in the cell average scalar flux between two iterations. This tested the performance of the code for various combinations of methods for a series of increasingly larger problems.

## 3. Edge Flow Variable Formulation

The first series of tests examined how DI performed with the angular flux formulation as opposed to the angular current formulation as discussed in chapter

two. The measure of performance is the number of iterations needed to reach convergence. The results of these tests are shown in table 3.1.

Table 3.1. Iterations to convergence for current vs. angular flux.

Spatial Quadrature	SC	SC	LD	LD
Formulation	Current	Flux	Current	Flux
Number of cells				
10	3	6	3	6
50	3	6	3	7
100	3	6	3	7
150	3	6	3	7
200	3	6	3	7
250	3	6	3	7
300	3	6	3	7

For these tests, discrete ordinates sweeping was used. Table 3.1 shows that the performance of the current formulation was substantially better than angular flux formulation. The number of iterations needed to reach the convergence criterion in the current representation is at most half the number needed for the angular flux representation. This validates the choice of using the current formulation for additional implementation in XY – geometry.

#### 4. Coupling the Local Balances

The next tests examined the efficiency of different methods for coupling the local balances presented in chapter two. The test conditions were the same

and the tests were done using the current formulation. The measure of performance is the total time required to converge the test problem. This was measured using the (CPU time) intrinsic FORTRAN function and included only the computations, not file I/O. The results for the step characteristic method are presented in figure 3.1.

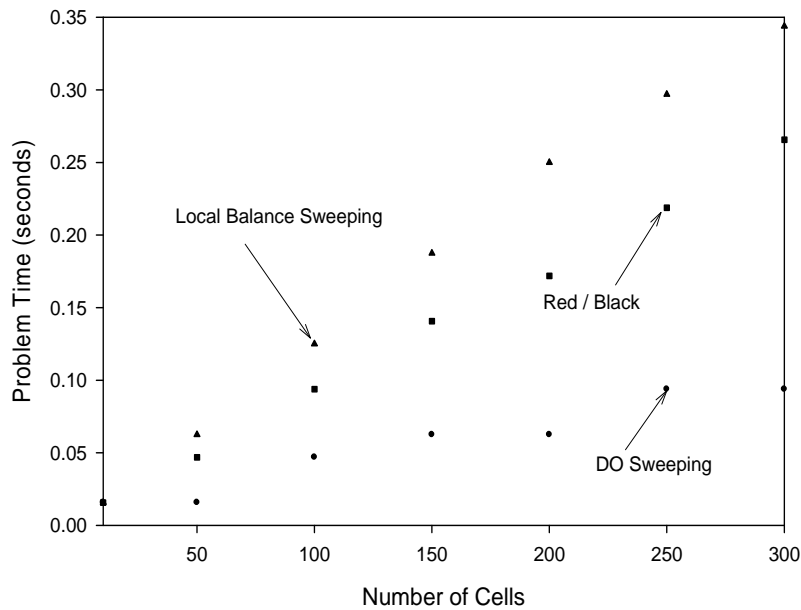


Figure 3.1. The problem solution time versus number of cells for different cell flow coupling methods with step characteristic.

Figure 3.1 shows that the discrete ordinates sweep is the most efficient method for coupling the local balance among cells for this single processor implementation. The Red/Black method performance was less efficient than the discrete ordinates sweep but still an improvement over the local balance sweeping method.

The results of the same test for linear discontinuous with the current representation are shown in figure 3.2.

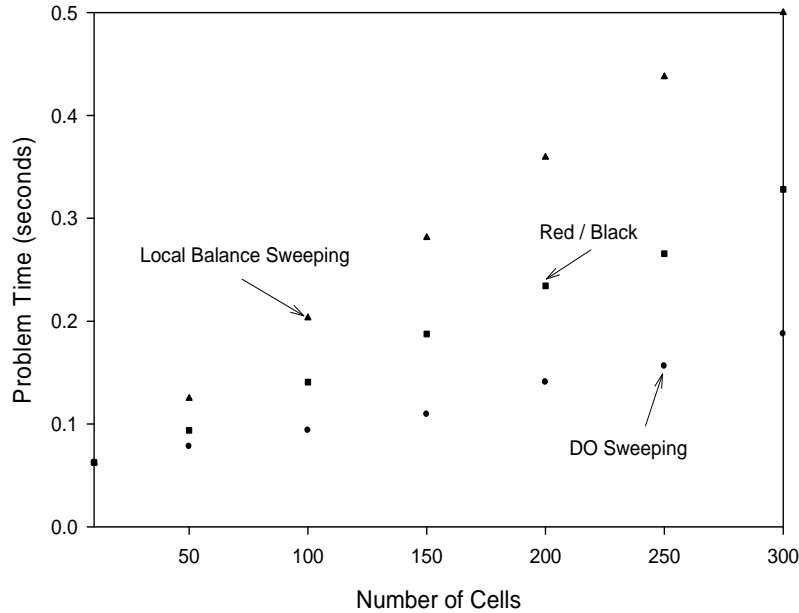


Figure 3.2. The problem solution time versus number of cells for different cell flow coupling methods with linear discontinuous.

The results for linear discontinuous method confirm the results shown by the step characteristic method. A similar timing test was run for a two material problem, with an absorbing ( $c = \frac{\sigma_s}{\sigma_t} = 0.3$ ) region and a scattering ( $c = 0.3$ ) region. The total times were again consistent with the previous series of one material problems: the discrete ordinates sweep method had the fastest time and local balance sweeping the slowest. The overall efficiency of the discrete ordinates sweep method makes it a good choice for implementation in XY – geometry because it will be demonstrated on a serial machine. For problems large enough

to need parallel implementation, the Red/Black method may be the method of choice.



## IV. Implementation in XY – Geometry

This chapter presents the derivations for the local balance problems for both zeroth and first spatial moments problems using the current representation. The global balance problem, subsequently called the partial current problem, is also presented.

### A. Zeroth Spatial Moment Methods Distribution Iteration Derivation

The zeroth spatial moment methods are an extension of the method presented in slab geometry in chapter three. The general representation used in chapter three is changed to explicitly account for the contributions for each cardinal direction, even though in some cases the contribution is zero.

The desired form is to assemble the equations for zeroth spatial moment methods in a relation that gives the cell face outgoing currents in terms of the cell face inward currents and cell emissions. A general method for all zeroth spatial moment methods, such as step characteristic (SC) or weighted diamond difference (WDD), is presented here.

The form of the system of equations is:

$$\vec{j}^{out} = \mathbf{K}_{OI} \vec{j}^{in} + \mathbf{K}_{OS} \vec{S} + \mathbf{K}_{OE} \vec{E}, \quad (4.1)$$

$$\vec{\psi} = \mathbf{K}_{\psi I} \vec{j}^{in} + \mathbf{K}_{\psi S} \vec{S} + \mathbf{K}_{\psi E} \vec{E}, \quad (4.2)$$

and 
$$\vec{S} = \sum_S \vec{\psi}. \quad (4.3)$$

In equation (4.3), the scattering matrix  $\Sigma_S$  has the same representation as in equation (3.3). The vectors are defined:

$$\vec{j}^{out} = \begin{bmatrix} \vec{j}_L^{out} & \vec{j}_R^{out} & \vec{j}_T^{out} & \vec{j}_B^{out} \end{bmatrix}^T, \quad (4.4)$$

$$\vec{j}^{in} = \begin{bmatrix} \vec{j}_L^{in} & \vec{j}_R^{in} & \vec{j}_T^{in} & \vec{j}_B^{in} \end{bmatrix}^T, \quad (4.5)$$

$$\vec{S} = \vec{S}^A, \quad (4.6)$$

and 
$$\vec{E} = \vec{E}^A. \quad (4.7)$$

In equations (4.4) and (4.5) the directions for the sub-vectors are given by the capital subscript, for example  $L$  for left. The matrices are defined:

$$\mathbf{K}_{OI} = \begin{bmatrix} \mathbf{K}_{OI}^{LL} & \mathbf{K}_{OI}^{LR} & \mathbf{K}_{OI}^{LT} & \mathbf{K}_{OI}^{LB} \\ \mathbf{K}_{OI}^{RL} & \mathbf{K}_{OI}^{RR} & \mathbf{K}_{OI}^{RT} & \mathbf{K}_{OI}^{RB} \\ \mathbf{K}_{OI}^{TL} & \mathbf{K}_{OI}^{TR} & \mathbf{K}_{OI}^{TT} & \mathbf{K}_{OI}^{TB} \\ \mathbf{K}_{OI}^{BL} & \mathbf{K}_{OI}^{BR} & \mathbf{K}_{OI}^{BT} & \mathbf{K}_{OI}^{BB} \end{bmatrix}, \quad (4.8)$$

$$\mathbf{K}_{OS} = \begin{bmatrix} \mathbf{K}_{OSA}^L \\ \mathbf{K}_{OSA}^R \\ \mathbf{K}_{OSA}^T \\ \mathbf{K}_{OSA}^B \end{bmatrix}, \quad (4.9)$$

$$\mathbf{K}_{OE} = \begin{bmatrix} \mathbf{K}_{OEA}^L \\ \mathbf{K}_{OEA}^R \\ \mathbf{K}_{OEA}^T \\ \mathbf{K}_{OEA}^B \end{bmatrix}, \quad (4.10)$$

$$\mathbf{K}_{AI} = \begin{bmatrix} \mathbf{K}_{AI}^L & \mathbf{K}_{AI}^R & \mathbf{K}_{AI}^T & \mathbf{K}_{AI}^B \end{bmatrix}, \quad (4.11)$$

$$\mathbf{K}_{\psi S} = \mathbf{K}_{ASA}, \quad (4.12)$$

and 
$$\mathbf{K}_{\psi E} = \mathbf{K}_{AEA}. \quad (4.13)$$

In equations (4.8) through (4.11) the sub-matrices are diagonal matrices similar to those used in slab geometry. In equation (4.8) the sub-matrices are matrices that give outgoing currents from inward currents, hence the subscript  $OI$ , and the two directions in the superscript correspond to the outward direction from the inward direction. For example,  $\mathbf{K}_{OI}^{RL}$  is the sub-matrix that gives the right outward currents from the left inward currents. In equations (4.9) through (4.10), the superscript directions correspond to the outgoing direction and the subscripts have the same meaning as in slab geometry. For example,  $\mathbf{K}_{OSA}^T$  is the matrix giving the current out the top from the average scatter,  $\mathbf{K}_{OEA}^L$  is the matrix giving the current out the left from the average emissions, and  $\mathbf{K}_{AI}^R$  is the matrix giving the average flux from the right inward current.

Similar to the slab geometry case, scatter is eliminated from equations (4.1) and (4.2):

$$\vec{\psi} = (\mathbf{I} - \mathbf{K}_{\psi S} \Sigma_S)^{-1} [\mathbf{K}_{\psi I} \vec{j}^{in} + \mathbf{K}_{\psi E} \vec{E}]. \quad (4.14)$$

Equation (4.14) can now be used to eliminate scatter from equation (3.50). The resulting equation is:

$$\begin{aligned} \vec{j}^{out} = & (\mathbf{K}_{OI} + \mathbf{K}_{OS} \Sigma_S (\mathbf{I} - \mathbf{K}_{\psi S} \Sigma_S)^{-1} \mathbf{K}_{\psi I}) \vec{j}^{in} + \\ & (\mathbf{K}_{OE} + \mathbf{K}_{OS} \Sigma_S (\mathbf{I} - \mathbf{K}_{\psi S} \Sigma_S)^{-1} \mathbf{K}_{\psi E}) \vec{E}. \end{aligned} \quad (4.15)$$

This equation can be used to calculate the cell outgoing currents from the cell inward currents and cell emissions. Looking at the terms in each parentheses,

the first matrix is the uncollided contribution to the respective outgoing current from the respective incoming current as modeled by the spatial quadrature method. The product or second term represents the respective incoming current that contributes to the respective outgoing current after all scattering takes place, again as modeled by the spatial quadrature method.

In addition, the final matrix represented by the sum in each parentheses, only needs to be calculated once for each combination of cell size and material.

The final matrices for equation (4.15) can be expressed as a matrix equation:

$$\vec{j}^{out} = \mathbf{m}_{OI} \vec{j}^{in} + \mathbf{m}_{OE} \vec{E}^A, \quad (4.16)$$

where  $m_{OI}$  is a matrix that gives outward currents from inward currents and  $m_{OE}$  is a matrix that gives outward currents from emissions. The current vectors and emission vector with the respective sub-matrices for each direction is:

$$\begin{bmatrix} \vec{j}_{Out}^R \\ \vec{j}_{Out}^L \\ \vec{j}_{Out}^T \\ \vec{j}_{Out}^B \end{bmatrix} = \begin{bmatrix} \mathbf{m}_{OI}^{RL} & \mathbf{m}_{OI}^{RR} & \mathbf{m}_{OI}^{RT} & \mathbf{m}_{OI}^{RB} \\ \mathbf{m}_{OI}^{LL} & \mathbf{m}_{OI}^{LR} & \mathbf{m}_{OI}^{LT} & \mathbf{m}_{OI}^{LB} \\ \mathbf{m}_{OI}^{TL} & \mathbf{m}_{OI}^{TR} & \mathbf{m}_{OI}^{TT} & \mathbf{m}_{OI}^{TB} \\ \mathbf{m}_{OI}^{BL} & \mathbf{m}_{OI}^{BR} & \mathbf{m}_{OI}^{BT} & \mathbf{m}_{OI}^{BB} \end{bmatrix} \begin{bmatrix} \vec{j}_{In}^L \\ \vec{j}_{In}^R \\ \vec{j}_{In}^T \\ \vec{j}_{In}^B \end{bmatrix} + \begin{bmatrix} \mathbf{m}_{OEA}^R \vec{E}^A \\ \mathbf{m}_{OEA}^L \vec{E}^A \\ \mathbf{m}_{OEA}^T \vec{E}^A \\ \mathbf{m}_{OEA}^B \vec{E}^A \end{bmatrix}. \quad (4.17)$$

Here, the sub-matrices represent the outward contribution from the inward current after any number of scatters. The emissions vector represents the forcing term for this system of equations. Later, the relation between the inward and outward currents will be used to set up the partial current problem across the spatial mesh. The next section will show how to calculate the values for the diagonal sub-matrices in equations (4.8) through (4.13).

## 1. Step Characteristic Transport Coefficients

The first spatial method implemented in XY - geometry was step characteristic (SC). This method was chosen for its relative simplicity, and as a way to validate the extension to XY - geometry before attempting other more complicated spatial methods. Miller (10: 21) presents the cell equations in the angular flux representation using the exponential moment functions. The derivation for the current equations is in appendix B.

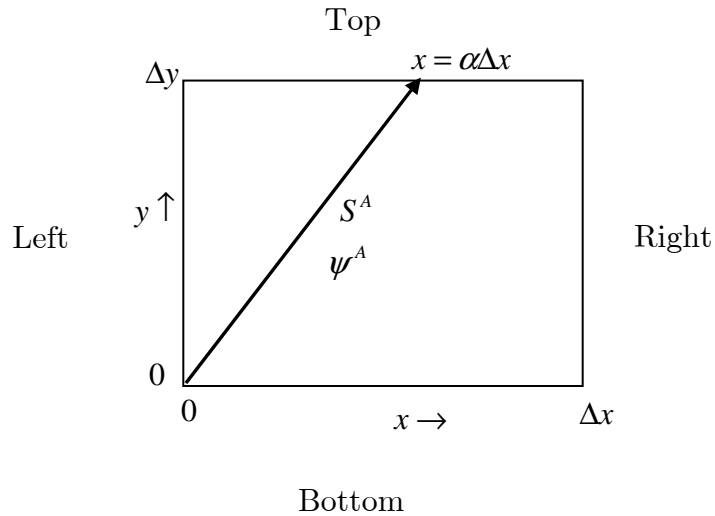


Figure 4.1. Rectangular cell for implementation of the zeroth spatial moment methods.

For the cell in figure 4.1 showing ordinate  $n$  out the top face,  $\mu_n$  and  $\eta_n$  are the direction cosines along the x and y axis respectively from the angular quadrature set, the optical thickness along an ordinate in the y and x direction is:

$$\varepsilon_{y_n} = \frac{\sigma \Delta y}{|\eta_n|}, \quad (4.18)$$

$$\varepsilon_{x_n} = \frac{\sigma \Delta x}{|\mu_n|}, \quad (4.19)$$

and

$$\alpha_n = \frac{\varepsilon_{y_n}}{\varepsilon_{x_n}} = \frac{|\mu_n| \Delta y}{|\eta_n| \Delta x}. \quad (4.20)$$

These equations are used for the spatial quadratures in XY - geometry. For a rectangular cell as shown in figure 4.1, the equations for the outgoing currents in ordinate  $n$ ,  $j_n^{top}$  and  $j_n^{right}$ , in terms of the incoming currents  $j_n^{bottom}$  and  $j_n^{left}$ , scattering within the cell,  $S_{An}$ , and emissions,  $E_{An}$ , for ordinate  $n$  with  $\eta_n > \mu_n > 0$  and  $\alpha_n \leq 1$  are:

$$j_n^{Top} = \frac{|\eta_n|}{|\mu_n|} \alpha_n M_0(\varepsilon_{y_n}) j_n^{Left} + (1 - \alpha_n) e^{-\varepsilon_{y_n}} j_n^{Bottom} + \Delta y [(1 - \alpha_n) M_0(\varepsilon_{y_n}) + \alpha_n M_1(\varepsilon_{y_n})] S_n^A + \Delta y [(1 - \alpha_n) M_0(\varepsilon_{y_n}) + \alpha_n M_1(\varepsilon_{y_n})] E_n^A, \quad (4.21)$$

$$j_n^{Right} = \frac{|\mu_n|}{|\eta_n|} M_0(\varepsilon_{y_n}) j_n^{Bottom} + \frac{|\mu_n| \Delta y}{|\eta_n|} M_1(\varepsilon_{y_n}) S_n^A + \frac{|\mu_n| \Delta y}{|\eta_n|} M_1(\varepsilon_{y_n}) E_n^A, \quad (4.22)$$

and

$$\psi_n^A = \frac{1}{|\mu_n|} \alpha_n M_0(\varepsilon_{y_n}) j_n^{Left} + \frac{1}{|\eta_n|} [(1 - \alpha_n) M_0(\varepsilon_{y_n}) + \alpha_n M_1(\varepsilon_{y_n})] j_n^{Bottom} + \frac{\Delta y}{|\eta_n|} [(1 - \alpha_n) M_1(\varepsilon_{y_n}) + \alpha_n M_2(\varepsilon_{y_n})] S_n^A + \frac{\Delta y}{|\eta_n|} [(1 - \alpha_n) M_1(\varepsilon_{y_n}) + \alpha_n M_2(\varepsilon_{y_n})] E_n^A, \quad (4.23)$$

where  $M_0(\varepsilon_{y_n})$ ,  $M_1(\varepsilon_{y_n})$  and  $M_2(\varepsilon_{y_n})$  are the exponential moment functions defined in equation (3.9). Because the ratio of the direction cosines is frequently used, let:

$$\tau_n = \frac{|\eta_n|}{|\mu_n|}. \quad (4.24)$$

The transport coefficients are the values used to build the diagonal coefficient matrices described previously. Equations (4.21), (4.22) and (4.23) can be written as:

$$j_{out_n}^{Top} = (k_{OI}^{TB})_n j_{in_n}^{bottom} + (k_{OI}^{TL})_n j_{in_n}^{left} + (k_{OI}^{TR})_n j_{in_n}^{right} + (k_{OI}^{TT})_n j_{in_n}^{top} + (k_{OSA}^T)_n S_n^A + (k_{OEA}^T)_n E_n^A, \quad (4.25)$$

$$j_{out_n}^{right} = (k_{OI}^{RB})_n j_{in_n}^{bottom} + (k_{OI}^{RL})_n j_{in_n}^{left} + (k_{OI}^{RR})_n j_{in_n}^{right} + (k_{OI}^{RT})_n j_{in_n}^{top} + (k_{OSA}^R)_n S_n^A + (k_{OEA}^R)_n E_n^A, \quad (4.26)$$

and

$$\psi_n^A = (k_{AI}^B)_n j_{in_n}^{bottom} + (k_{AI}^L)_n j_{in_n}^{left} + (k_{AI}^R)_n j_{in_n}^{right} + (k_{AI}^T)_n j_{in_n}^{top} + (k_{ASA})_n S_n^A + (k_{AEA})_n E_n^A. \quad (4.27)$$

This form is a variation of equation (3.50) giving the outgoing currents from the inward currents, scattering and emissions for an ordinate. As was done in slab geometry, the  $k$  vectors, which are used to form the diagonal matrices  $\mathbf{K} = \mathbf{D}(\vec{k})$ , can also be found by inspection of equations (4.21), (4.22) and (4.23).

Thus the  $k$  vectors for the top outward angular currents are:

$$(k_{OI}^{TB})_n = (1 - \alpha_n) e^{-\varepsilon_{y_n}}, \quad (4.28)$$

$$(k_{OI}^{TL})_n = \tau_n \alpha_n M_0(\varepsilon_{y_n}), \quad (4.29)$$

$$(k_{OI}^{TR})_n = (k_{OI}^{TT})_n = 0, \quad (4.30)$$

and 
$$(k_{OSA}^T)_n = (k_{OEA}^T)_n = \Delta y [(1 - \alpha_n) M_0(\varepsilon_{y_n}) + \alpha_n M_1(\varepsilon_{y_n})]. \quad (4.31)$$

The  $k$  vectors for the right outward angular currents are:

$$(k_{OI}^{RB})_n = \frac{M_0(\varepsilon_{y_n})}{\tau_n}, \quad (4.32)$$

$$(k_{OI}^{RL})_n = (k_{OI}^{RR})_n = (k_{OI}^{RT})_n = 0, \quad (4.33)$$

and

$$(k_{OSA}^R)_n = (k_{OEA}^R)_n = \frac{\Delta y}{\tau_n} M_1(\varepsilon_{y_n}). \quad (4.34)$$

The  $k$  vectors for the average angular flux are:

$$(k_{AI}^B)_n = \frac{1}{|\eta_n|} [(1 - \alpha_n) M_0(\varepsilon_{y_n}) + \alpha_n M_1(\varepsilon_{y_n})], \quad (4.35)$$

$$(k_{AI}^L)_n = \frac{1}{|\mu_n|} \alpha_n M_0(\varepsilon_{y_n}), \quad (4.36)$$

$$(k_{AI}^R)_n = (k_{AI}^T)_n = 0, \quad (4.37)$$

and

$$(k_{ASA})_n = (k_{AEA})_n = \frac{\Delta y}{|\eta_n|} [(1 - \alpha_n) M_1(\varepsilon_{y_n}) + \alpha_n M_2(\varepsilon_{y_n})]. \quad (4.38)$$

Each ordinate is evaluated to determine the outgoing face and the respective transport coefficient. Not shown in figure 4.1 are ordinates exiting the right, bottom, or left cell edges instead of the top edge; however, the same basic relations are used. For these cases, an x-y reversal, a right-left exchange or a top-bottom exchange are used where appropriate. In all, there are 30 transport coefficients to find for each ordinate of which only 11 are nonzero.

These transport coefficients are used to build the diagonal matrices listed in equations (4.8) through (4.13). Once the diagonal matrices are calculated, the final matrices described in equations (4.15) and (4.17) can be constructed. For



the DI method, these matrices will be calculated one time for each material (assuming the spatial mesh is uniform).

## 2. Weighted Diamond Difference Transport Coefficients

Another zeroth spatial moment method that was implemented was weighted diamond difference (WDD). This positive method was chosen to demonstrate the ease of adding other zeroth spatial moment methods and to compare with published results. Azmy (3: 215-216) presents the angular flux formulation of the WDD method, which is changed to the current formulation in appendix B. For the same rectangular cell shown in figure 4.1, the equations for the outgoing currents  $j_n^{top}$  and  $j_n^{right}$ , in terms of the incoming currents  $j_n^{bottom}$  and  $j_n^{left}$  scattering within the cell  $S_n^A$  and emissions  $E_n^A$ , for ordinate  $n$  with  $\eta_n > \mu_n > 0$  and  $\alpha_n \leq 1$  are presented in Appendix B. To avoid bad numerical conditioning, the WDD equations are cast in terms of

$$\delta_{In}^{y_n} = 1 - \rho(\varepsilon_{y_n}) \quad (4.39)$$

and

$$\delta_{Out}^{y_n} = \rho(\varepsilon_{y_n}), \quad (4.40)$$

where

$$\rho(\varepsilon_{y_n}) = \frac{M_1(\varepsilon_{y_n})}{M_0(\varepsilon_{y_n})}. \quad (4.41)$$

Here,  $\delta_{In}^{y_n}$  and  $\delta_{Out}^{y_n}$  are the adaptive weights for the spatial method and  $M_0(\varepsilon_y)$

and  $M_1(\varepsilon_y)$  are the exponential moment functions defined in equation (3.9).

Also  $\delta_{In}^{x_n}$  and  $\delta_{Out}^{x_n}$  are defined exactly analogously. In addition, a ratio of weights and optical thicknesses is defined:

$$h_n = \frac{\delta_{out}^{x_n} \boldsymbol{\varepsilon}_{x_n} \delta_{out}^{y_n} \boldsymbol{\varepsilon}_{y_n}}{\delta_{out}^{x_n} \boldsymbol{\varepsilon}_{x_n} + \delta_{out}^{y_n} \boldsymbol{\varepsilon}_{y_n} + \delta_{out}^{x_n} \boldsymbol{\varepsilon}_{x_n} \delta_{out}^{y_n} \boldsymbol{\varepsilon}_{y_n}}. \quad (4.42)$$

Determining the values of the  $k$  vectors used to form the diagonal matrices

$\mathbf{K} = \mathbf{D}(\vec{k})$  is done the same way that was used for the SC quadrature. The  $k$

vectors for the top outward angular currents are:

$$(k_{OI}^{TB})_n = \frac{h_n}{(\delta_{Out}^{y_n})^2 \boldsymbol{\varepsilon}_{y_n}} - \frac{\delta_{In}^{y_n}}{\delta_{Out}^{y_n}}, \quad (4.43)$$

$$(k_{OI}^{TL})_n = \frac{h_n |\eta_n|}{\delta_{Out}^{x_n} \delta_{Out}^{y_n} \boldsymbol{\varepsilon}_{x_n} |\mu_n|}, \quad (4.44)$$

$$(k_{OI}^{TR})_n = (k_{OI}^{TT})_n = 0, \quad (4.45)$$

and

$$(k_{OSA}^T)_n = (k_{OEA}^T)_n = \frac{h_n |\eta_n|}{\delta_{Out}^{y_n} \boldsymbol{\sigma}}. \quad (4.46)$$

The  $k$  vectors for the right outward angular currents are:

$$(k_{OI}^{RB})_n = \frac{h_n |\mu_n|}{\delta_{Out}^{x_n} \delta_{Out}^{y_n} \boldsymbol{\varepsilon}_{y_n} |\eta|}, \quad (4.47)$$

$$(k_{OI}^{RL})_n = \frac{h_n}{(\delta_{Out}^{x_n})^2 \boldsymbol{\varepsilon}_{x_n}} - \frac{\delta_{In}^{x_n}}{\delta_{Out}^{x_n}}, \quad (4.48)$$

$$(k_{OI}^{RR})_n = (k_{OI}^{RT})_n = 0, \quad (4.49)$$

and

$$(k_{OSA}^R)_n = (k_{OEA}^R)_n = \frac{h_n |\mu_n|}{\delta_{Out}^{x_n} \boldsymbol{\sigma}}. \quad (4.50)$$

The  $k$  vectors for the average angular flux are:

$$(k_{AI}^B)_n = \frac{h_n}{\delta_{Out}^{x_n} |\eta_n| \boldsymbol{\varepsilon}_{y_n}}, \quad (4.51)$$

$$(k_{AI}^L)_n = \frac{h_n}{\delta_{Out}^{y_n} |\mu_n| \varepsilon_{x_n}}, \quad (4.52)$$

$$(k_{AI}^R)_n = (k_{AI}^T)_n = 0, \quad (4.53)$$

and

$$(k_{ASA})_n = (k_{AEA})_n = \frac{h_n}{\sigma}. \quad (4.54)$$

Unlike characteristic methods, the WDD equations need not treat  $\Delta x / |\mu| < \Delta y / |\eta|$  differently than  $\Delta x / |\mu| > \Delta y / |\eta|$ . For convenience in sharing code, I use the equations for the case in figure 4.1 to fill the WDD matrices in the same way as I described above for SC. Again, for the DI method, these WDD matrices (or any other linear, zeroth spatial methods) use the same solver algorithm as SC.

## B. Derivation of First Spatial Moment Methods Distribution Iteration

Similar to the zeroth spatial moments derivation, it is desirable to assemble the discrete ordinates system of equations in a form that gives the cell outgoing currents in terms of the cell inward currents and cell emissions. However, unlike the zeroth spatial moment methods, there is the addition of the first spatial moment of the current along edges  $\vec{\theta}$  and first spatial moment of the scattering sources in each dimension to consider. The equations could again be cast into the general form:

$$\vec{j}^{out} = \mathbf{K}_{OI} \vec{j}^{in} + \mathbf{K}_{OS} \vec{S} + \mathbf{K}_{OE} \vec{E}, \quad (4.55)$$

$$\vec{\psi} = \mathbf{K}_{\psi I} \vec{j}^{in} + \mathbf{K}_{\psi S} \vec{S} + \mathbf{K}_{\psi E} \vec{E}, \quad (4.56)$$

and

$$\vec{S} = \sum_S \vec{\psi}, \quad (4.57)$$

where the angular current vectors include the first spatial moment of the current:

$$\vec{j}^{in} = \begin{bmatrix} \vec{j}^{in} & \vec{\theta}^{in} \end{bmatrix}^T, \quad (4.58)$$

and

$$\vec{j}^{out} = \begin{bmatrix} \vec{j}^{out} & \vec{\theta}^{out} \end{bmatrix}^T. \quad (4.59)$$

This approach was not used; instead, the spatial moments of the angular currents are explicit in the system of equations. This simplifies the indexing for the code and allows use of the same routine for the partial current problem as for the zeroth spatial moment quadratures. This routine is presented later in this chapter. The cell system of equations for the first spatial moment spatial quadratures in general can be written:

$$\vec{j}^{out} = \mathbf{K}_{OI} \vec{j}^{in} + \mathbf{K}_{O\theta} \vec{\theta}^{in} + \mathbf{K}_{OS} \bar{S} + \mathbf{K}_{OE} \bar{E}, \quad (4.60)$$

$$\vec{\theta}^{out} = \mathbf{K}_{\theta I} \vec{j}^{in} + \mathbf{K}_{\theta\theta} \vec{\theta}^{in} + \mathbf{K}_{\theta S} \bar{S} + \mathbf{K}_{\theta E} \bar{E}, \quad (4.61)$$

$$\bar{\psi} = \mathbf{K}_{\psi I} \vec{j}^{in} + \mathbf{K}_{\psi\theta} \vec{\theta}^{in} + \mathbf{K}_{\psi S} \bar{S} + \mathbf{K}_{\psi E} \bar{E}, \quad (4.62)$$

and

$$\bar{S} = \Sigma \bar{\psi}. \quad (4.63)$$

The vectors for equations (2.2) through (2.4) are defined as:

$$\vec{j}^{out} = \begin{bmatrix} \vec{j}_L^{out} & \vec{j}_L^{out} & \vec{j}_L^{out} & \vec{j}_L^{out} \end{bmatrix}^T, \quad (4.64)$$

$$\vec{j}^{in} = \begin{bmatrix} \vec{j}_L^{in} & \vec{j}_L^{in} & \vec{j}_L^{in} & \vec{j}_L^{in} \end{bmatrix}^T, \quad (4.65)$$

$$\vec{\theta}^{out} = \begin{bmatrix} \vec{\theta}_L^{out} & \vec{\theta}_L^{out} & \vec{\theta}_L^{out} & \vec{\theta}_L^{out} \end{bmatrix}^T, \quad (4.66)$$

$$\vec{\theta}^{in} = \begin{bmatrix} \vec{\theta}_L^{in} & \vec{\theta}_L^{in} & \vec{\theta}_L^{in} & \vec{\theta}_L^{in} \end{bmatrix}^T, \quad (4.67)$$

$$\vec{\psi} = \begin{bmatrix} \vec{\psi}^A & \vec{\psi}^X & \vec{\psi}^Y \end{bmatrix}^T, \quad (4.68)$$

$$\vec{S} = \begin{bmatrix} \vec{S}^A & \vec{S}^X & \vec{S}^Y \end{bmatrix}^T, \quad (4.69)$$

and

$$\vec{E} = \begin{bmatrix} \vec{E}^A & \vec{E}^X & \vec{E}^Y \end{bmatrix}^T. \quad (4.70)$$

The matrices for equations (2.2) through (2.4) follow the same methodology as slab geometry. The matrices for equation (2.2) are defined:

$$\mathbf{K}_{OI} = \begin{bmatrix} \mathbf{K}_{OI}^{LL} & \mathbf{K}_{OI}^{LR} & \mathbf{K}_{OI}^{LT} & \mathbf{K}_{OI}^{LB} \\ \mathbf{K}_{OI}^{RL} & \mathbf{K}_{OI}^{RR} & \mathbf{K}_{OI}^{RT} & \mathbf{K}_{OI}^{RB} \\ \mathbf{K}_{OI}^{TL} & \mathbf{K}_{OI}^{TR} & \mathbf{K}_{OI}^{TT} & \mathbf{K}_{OI}^{TB} \\ \mathbf{K}_{OI}^{BL} & \mathbf{K}_{OI}^{BR} & \mathbf{K}_{OI}^{BT} & \mathbf{K}_{OI}^{BB} \end{bmatrix}, \quad (4.71)$$

$$\mathbf{K}_{O\theta} = \begin{bmatrix} \mathbf{K}_{O\theta}^{LL} & \mathbf{K}_{O\theta}^{LR} & \mathbf{K}_{O\theta}^{LT} & \mathbf{K}_{O\theta}^{LB} \\ \mathbf{K}_{O\theta}^{RL} & \mathbf{K}_{O\theta}^{RR} & \mathbf{K}_{O\theta}^{RT} & \mathbf{K}_{O\theta}^{RB} \\ \mathbf{K}_{O\theta}^{TL} & \mathbf{K}_{O\theta}^{TR} & \mathbf{K}_{O\theta}^{TT} & \mathbf{K}_{O\theta}^{TB} \\ \mathbf{K}_{O\theta}^{BL} & \mathbf{K}_{O\theta}^{BR} & \mathbf{K}_{O\theta}^{BT} & \mathbf{K}_{O\theta}^{BB} \end{bmatrix}, \quad (4.72)$$

$$\mathbf{K}_{OS} = \begin{bmatrix} \mathbf{K}_{OSA}^L & \mathbf{K}_{OSX}^L & \mathbf{K}_{OSY}^L \\ \mathbf{K}_{OSA}^R & \mathbf{K}_{OSX}^R & \mathbf{K}_{OSY}^R \\ \mathbf{K}_{OSA}^T & \mathbf{K}_{OSX}^T & \mathbf{K}_{OSY}^T \\ \mathbf{K}_{OSA}^B & \mathbf{K}_{OSX}^B & \mathbf{K}_{OSY}^B \end{bmatrix}, \quad (4.73)$$

and

$$\mathbf{K}_{OE} = \begin{bmatrix} \mathbf{K}_{OEA}^L & \mathbf{K}_{OEX}^L & \mathbf{K}_{OEY}^L \\ \mathbf{K}_{OEA}^R & \mathbf{K}_{OEX}^R & \mathbf{K}_{OEY}^R \\ \mathbf{K}_{OEA}^T & \mathbf{K}_{OEX}^T & \mathbf{K}_{OEY}^T \\ \mathbf{K}_{OEA}^B & \mathbf{K}_{OEX}^B & \mathbf{K}_{OEY}^B \end{bmatrix}. \quad (4.74)$$

The notation is similar to the zeroth spatial moment method notation. For example, the diagonal sub-matrix  $\mathbf{K}_{OI}^{BL}$  represents a matrix that gives bottom

outward currents from left inward currents. The diagonal sub-matrix  $\mathbf{K}_{\theta SX}^L$  gives the left outward current from the x-moment of scatter in the cell  $\bar{S}^x$ . The diagonal sub-matrix  $\mathbf{K}_{\theta EA}^R$  gives the right outward current vector from the average emissions in the cell  $\bar{E}^A$ . The higher moments for the emissions vector, as for the first moments of emissions in slab geometry, represent the higher moments of scatter from other energy groups in a general representation. For the mono-energetic problems used in this research, these vectors and matrices are not used. The matrices for equation (4.61) are defined:

$$\mathbf{K}_{\theta I} = \begin{bmatrix} \mathbf{K}_{\theta I}^{LL} & \mathbf{K}_{\theta I}^{LR} & \mathbf{K}_{\theta I}^{LT} & \mathbf{K}_{\theta I}^{LB} \\ \mathbf{K}_{\theta I}^{RL} & \mathbf{K}_{\theta I}^{RR} & \mathbf{K}_{\theta I}^{RT} & \mathbf{K}_{\theta I}^{RB} \\ \mathbf{K}_{\theta I}^{TL} & \mathbf{K}_{\theta I}^{TR} & \mathbf{K}_{\theta I}^{TT} & \mathbf{K}_{\theta I}^{TB} \\ \mathbf{K}_{\theta I}^{BL} & \mathbf{K}_{\theta I}^{BR} & \mathbf{K}_{\theta I}^{BT} & \mathbf{K}_{\theta I}^{BB} \end{bmatrix}, \quad (4.75)$$

$$\mathbf{K}_{\theta \theta} = \begin{bmatrix} \mathbf{K}_{\theta \theta}^{LL} & \mathbf{K}_{\theta \theta}^{LR} & \mathbf{K}_{\theta \theta}^{LT} & \mathbf{K}_{\theta \theta}^{LB} \\ \mathbf{K}_{\theta \theta}^{RL} & \mathbf{K}_{\theta \theta}^{RR} & \mathbf{K}_{\theta \theta}^{RT} & \mathbf{K}_{\theta \theta}^{RB} \\ \mathbf{K}_{\theta \theta}^{TL} & \mathbf{K}_{\theta \theta}^{TR} & \mathbf{K}_{\theta \theta}^{TT} & \mathbf{K}_{\theta \theta}^{TB} \\ \mathbf{K}_{\theta \theta}^{BL} & \mathbf{K}_{\theta \theta}^{BR} & \mathbf{K}_{\theta \theta}^{BT} & \mathbf{K}_{\theta \theta}^{BB} \end{bmatrix}, \quad (4.76)$$

$$\mathbf{K}_{\theta S} = \begin{bmatrix} \mathbf{K}_{\theta SA}^L & \mathbf{K}_{\theta SX}^L & \mathbf{K}_{\theta SY}^L \\ \mathbf{K}_{\theta SA}^R & \mathbf{K}_{\theta SX}^R & \mathbf{K}_{\theta SY}^R \\ \mathbf{K}_{\theta SA}^T & \mathbf{K}_{\theta SX}^T & \mathbf{K}_{\theta SY}^T \\ \mathbf{K}_{\theta SA}^B & \mathbf{K}_{\theta SX}^B & \mathbf{K}_{\theta SY}^B \end{bmatrix}, \quad (4.77)$$

and

$$\mathbf{K}_{\theta E} = \begin{bmatrix} \mathbf{K}_{\theta EA}^L & \mathbf{K}_{\theta EX}^L & \mathbf{K}_{\theta EY}^L \\ \mathbf{K}_{\theta EA}^R & \mathbf{K}_{\theta EX}^R & \mathbf{K}_{\theta EY}^R \\ \mathbf{K}_{\theta EA}^T & \mathbf{K}_{\theta EX}^T & \mathbf{K}_{\theta EY}^T \\ \mathbf{K}_{\theta EA}^B & \mathbf{K}_{\theta EX}^B & \mathbf{K}_{\theta EY}^B \end{bmatrix}. \quad (4.78)$$

Again, the notation is similar to the previous notation used for equation (2.2).

Here, the outgoing current symbol  $O$  is replaced with the outgoing edge current moment,  $\theta$  so the diagonal sub-matrix  $\mathbf{K}_{\theta I}^{BL}$  represents a matrix that gives bottom outward edge current moment from left inward currents. The matrices for equation (2.3) are defined:

$$\mathbf{K}_{\psi I} = \begin{bmatrix} \mathbf{K}_{AI}^L & \mathbf{K}_{AI}^R & \mathbf{K}_{AI}^T & \mathbf{K}_{AI}^B \\ \mathbf{K}_{XI}^L & \mathbf{K}_{XI}^R & \mathbf{K}_{XI}^T & \mathbf{K}_{XI}^B \\ \mathbf{K}_{YI}^L & \mathbf{K}_{YI}^R & \mathbf{K}_{YI}^T & \mathbf{K}_{YI}^B \end{bmatrix}, \quad (4.79)$$

$$\mathbf{K}_{\psi \theta} = \begin{bmatrix} \mathbf{K}_{A\theta}^L & \mathbf{K}_{A\theta}^R & \mathbf{K}_{A\theta}^T & \mathbf{K}_{A\theta}^B \\ \mathbf{K}_{X\theta}^L & \mathbf{K}_{X\theta}^R & \mathbf{K}_{X\theta}^T & \mathbf{K}_{X\theta}^B \\ \mathbf{K}_{Y\theta}^L & \mathbf{K}_{Y\theta}^R & \mathbf{K}_{Y\theta}^T & \mathbf{K}_{Y\theta}^B \end{bmatrix}, \quad (4.80)$$

$$\mathbf{K}_{\psi S} = \begin{bmatrix} \mathbf{K}_{ASA} & \mathbf{K}_{ASX} & \mathbf{K}_{ASY} \\ \mathbf{K}_{XSA} & \mathbf{K}_{XSX} & \mathbf{K}_{XSY} \\ \mathbf{K}_{YSA} & \mathbf{K}_{YSX} & \mathbf{K}_{YSY} \end{bmatrix}, \quad (4.81)$$

$$\mathbf{K}_{\psi E} = \begin{bmatrix} \mathbf{K}_{AEA} & \mathbf{K}_{AEX} & \mathbf{K}_{AEY} \\ \mathbf{K}_{XEA} & \mathbf{K}_{XEX} & \mathbf{K}_{XEY} \\ \mathbf{K}_{YEA} & \mathbf{K}_{YEX} & \mathbf{K}_{YEY} \end{bmatrix}, \quad (4.82)$$

and

$$\mathbf{\Sigma} = \begin{bmatrix} \Sigma_s & 0 & 0 \\ 0 & \Sigma_s & 0 \\ 0 & 0 & \Sigma_s \end{bmatrix}. \quad (4.83)$$

Similarly, the diagonal sub-matrix  $\mathbf{K}_{AI}^T$  gives the contribution the average angular flux within a cell  $\bar{\psi}^A$  from the top inward current vector, the diagonal sub-matrix  $\mathbf{K}_{X\theta}^R$  gives the contribution the x-moment angular flux within a cell  $\bar{\psi}^X$  from the right inward edge current moment vector, the diagonal sub-matrix  $\mathbf{K}_{XSY}$  gives the contribution the x-moment angular flux within a cell  $\bar{\psi}^X$  from the y-moment of scatter vector, and the sub-matrix  $\Sigma_S$  is the scattering matrix defined in equation (3.5).

Equation (4.63) is substituted into equation (4.62) to eliminate scatter.

This gives:

$$\bar{\psi} = (\mathbf{I} - \mathbf{K}_{\psi S} \Sigma)^{-1} \mathbf{K}_{\psi I} \bar{j}^{in} + (\mathbf{I} - \mathbf{K}_{\psi S} \Sigma)^{-1} \mathbf{K}_{\psi \theta} \bar{\theta}^{in} + (\mathbf{I} - \mathbf{K}_{\psi S} \Sigma)^{-1} \mathbf{K}_{\psi E} \bar{E}. \quad (4.84)$$

Equation (4.84) is then substituted into equations (4.60) and (4.61) to again eliminate scatter. The final equations are:

$$\bar{j}^{out} = (\mathbf{K}_{OI} + \mathbf{K}_{OS} \Sigma (\mathbf{I} - \mathbf{K}_{\psi S} \Sigma)^{-1} \mathbf{K}_{\psi I}) \bar{j}^{in} + (\mathbf{K}_{O\theta} + \mathbf{K}_{OS} \Sigma (\mathbf{I} - \mathbf{K}_{\psi S} \Sigma)^{-1} \mathbf{K}_{\psi \theta}) \bar{\theta}^{in} + (\mathbf{K}_{OE} + \mathbf{K}_{OS} \Sigma (\mathbf{I} - \mathbf{K}_{\psi S} \Sigma)^{-1} \mathbf{K}_{\psi E}) \bar{E}, \quad (4.85)$$

and

$$\bar{\theta}^{out} = (\mathbf{K}_{\theta I} + \mathbf{K}_{\theta S} \Sigma (\mathbf{I} - \mathbf{K}_{\psi S} \Sigma)^{-1} \mathbf{K}_{\psi I}) \bar{j}^{in} + (\mathbf{K}_{\theta\theta} + \mathbf{K}_{\theta S} \Sigma (\mathbf{I} - \mathbf{K}_{\psi S} \Sigma)^{-1} \mathbf{K}_{\psi \theta}) \bar{\theta}^{in} + (\mathbf{K}_{\theta E} + \mathbf{K}_{\theta S} \Sigma (\mathbf{I} - \mathbf{K}_{\psi S} \Sigma)^{-1} \mathbf{K}_{\psi E}) \bar{E}. \quad (4.86)$$

As was done for slab geometry, the code implementation used an equivalent elimination of the scattering sources, in which a block forward elimination and back substitution produces the inverse matrix in equations (4.84) through (4.86), which is shown in appendix C.



As with the zeroth spatial moment methods, the final matrix represented by the sum in each parentheses for equations (4.85) and (4.86), only need to be calculated once per material and cell size. The matrices for these equations can be expressed as:

$$\vec{j}^{out} = \mathbf{m}_{OI} \vec{j}^{in} + \mathbf{m}_{O\theta} \vec{\theta}^{in} + \mathbf{m}_{OE} \vec{E}^A, \quad (4.87)$$

and

$$\vec{\theta}^{out} = \mathbf{m}_{\theta I} \vec{j}^{in} + \mathbf{m}_{\theta\theta} \vec{\theta}^{in} + \mathbf{m}_{\theta E} \vec{E}^A. \quad (4.88)$$

Here  $\mathbf{m}_{OI}$  is a matrix that gives cell outward currents from inward currents,  $\mathbf{m}_{OE}$  is a matrix that gives cell outward currents from emissions,  $\mathbf{m}_{\theta I}$  is a matrix that gives cell outward current edge moments from inward currents, and  $\mathbf{m}_{\theta\theta}$  is a matrix that gives cell outward current edge moments from inward current edge moments. The current vectors, edge moment vectors and emission vectors with the respective sub-matrices for each direction is:

$$\begin{aligned} \begin{bmatrix} \vec{j}_{Out}^L \\ \vec{j}_{Out}^R \\ \vec{j}_{Out}^T \\ \vec{j}_{Out}^B \end{bmatrix} &= \begin{bmatrix} \mathbf{m}_{OI}^{LL} & \mathbf{m}_{OI}^{LR} & \mathbf{m}_{OI}^{LT} & \mathbf{m}_{OI}^{LB} \\ \mathbf{m}_{OI}^{RL} & \mathbf{m}_{OI}^{RR} & \mathbf{m}_{OI}^{RT} & \mathbf{m}_{OI}^{RB} \\ \mathbf{m}_{OI}^{TL} & \mathbf{m}_{OI}^{TR} & \mathbf{m}_{OI}^{TT} & \mathbf{m}_{OI}^{TB} \\ \mathbf{m}_{OI}^{BL} & \mathbf{m}_{OI}^{BR} & \mathbf{m}_{OI}^{BT} & \mathbf{m}_{OI}^{BB} \end{bmatrix} \begin{bmatrix} \vec{j}_{In}^L \\ \vec{j}_{In}^R \\ \vec{j}_{In}^T \\ \vec{j}_{In}^B \end{bmatrix} + \\ &\begin{bmatrix} \mathbf{m}_{O\theta}^{LL} & \mathbf{m}_{O\theta}^{LR} & \mathbf{m}_{O\theta}^{LT} & \mathbf{m}_{O\theta}^{LB} \\ \mathbf{m}_{O\theta}^{RL} & \mathbf{m}_{O\theta}^{RR} & \mathbf{m}_{O\theta}^{RT} & \mathbf{m}_{O\theta}^{RB} \\ \mathbf{m}_{O\theta}^{TL} & \mathbf{m}_{O\theta}^{TR} & \mathbf{m}_{O\theta}^{TT} & \mathbf{m}_{O\theta}^{TB} \\ \mathbf{m}_{O\theta}^{BL} & \mathbf{m}_{O\theta}^{BR} & \mathbf{m}_{O\theta}^{BT} & \mathbf{m}_{O\theta}^{BB} \end{bmatrix} \begin{bmatrix} \vec{\theta}_{In}^L \\ \vec{\theta}_{In}^R \\ \vec{\theta}_{In}^T \\ \vec{\theta}_{In}^B \end{bmatrix} + \begin{bmatrix} \mathbf{m}_{OEA}^L \vec{E}^A \\ \mathbf{m}_{OEA}^R \vec{E}^A \\ \mathbf{m}_{OEA}^T \vec{E}^A \\ \mathbf{m}_{OEA}^B \vec{E}^A \end{bmatrix}. \end{aligned} \quad (4.89)$$

A similar system can be constructed for the outward current edge moments for a cell:

$$\begin{aligned}
\begin{bmatrix} \vec{\theta}_{Out}^L \\ \vec{\theta}_{Out}^R \\ \vec{\theta}_{Out}^T \\ \vec{\theta}_{Out}^B \end{bmatrix} &= \begin{bmatrix} \mathbf{m}_{\theta I}^{LL} & \mathbf{m}_{\theta I}^{LR} & \mathbf{m}_{\theta I}^{LT} & \mathbf{m}_{\theta I}^{LB} \\ \mathbf{m}_{\theta I}^{RL} & \mathbf{m}_{\theta I}^{RR} & \mathbf{m}_{\theta I}^{RT} & \mathbf{m}_{\theta I}^{RB} \\ \mathbf{m}_{\theta I}^{TL} & \mathbf{m}_{\theta I}^{TR} & \mathbf{m}_{\theta I}^{TT} & \mathbf{m}_{\theta I}^{TB} \\ \mathbf{m}_{\theta I}^{BL} & \mathbf{m}_{\theta I}^{BR} & \mathbf{m}_{\theta I}^{BT} & \mathbf{m}_{\theta I}^{BB} \end{bmatrix} \begin{bmatrix} \vec{j}_{In}^L \\ \vec{j}_{In}^R \\ \vec{j}_{In}^T \\ \vec{j}_{In}^B \end{bmatrix} + \\
&\begin{bmatrix} \mathbf{m}_{\theta\theta}^{LL} & \mathbf{m}_{\theta\theta}^{LR} & \mathbf{m}_{\theta\theta}^{LT} & \mathbf{m}_{\theta\theta}^{LB} \\ \mathbf{m}_{\theta\theta}^{RL} & \mathbf{m}_{\theta\theta}^{RR} & \mathbf{m}_{\theta\theta}^{RT} & \mathbf{m}_{\theta\theta}^{RB} \\ \mathbf{m}_{\theta\theta}^{TL} & \mathbf{m}_{\theta\theta}^{TR} & \mathbf{m}_{\theta\theta}^{TT} & \mathbf{m}_{\theta\theta}^{TB} \\ \mathbf{m}_{\theta\theta}^{BL} & \mathbf{m}_{\theta\theta}^{BR} & \mathbf{m}_{\theta\theta}^{BT} & \mathbf{m}_{\theta\theta}^{BB} \end{bmatrix} \begin{bmatrix} \vec{\theta}_{In}^L \\ \vec{\theta}_{In}^R \\ \vec{\theta}_{In}^T \\ \vec{\theta}_{In}^B \end{bmatrix} + \begin{bmatrix} \mathbf{m}_{\theta EA}^L \vec{E}^A \\ \mathbf{m}_{\theta EA}^R \vec{E}^A \\ \mathbf{m}_{\theta EA}^T \vec{E}^A \\ \mathbf{m}_{\theta EA}^B \vec{E}^A \end{bmatrix}.
\end{aligned} \tag{4.90}$$

Again, the sub-matrices represent the outward contribution for the respective vectors from the inward vector after completing any number of scatters. The emissions vector represents the forcing term for these systems of equations. These equations will be used to set up the partial current problem across the spatial mesh. The next section will show how to calculate the values for the diagonal sub-matrices in equations (4.71) through (4.82).

### 1. Linear Characteristic Transport Coefficients

The first method implemented was linear characteristic (LC) which was initially developed by Alcouffe et al. in 1979 (11: 24). This first spatial moment method was chosen as an extension of SC and to show the implementation of first order spatial methods. Miller (12: 23) also provided the LC cell equations in the angular flux representation using the exponential moment functions. The derivation for the cell current equations are presented in Appendix D. The process of determining the equations for the  $k$  vectors used to form the diagonal

matrices  $\mathbf{K} = \mathbf{D}(\vec{k})$  is analogous to the procedure used for SC. The  $k$  vectors for the top outward angular currents are:

$$(k_{OI}^{TB})_n = (1 - \alpha_n) e^{-\varepsilon_{y_n}}, \quad (4.91)$$

$$(k_{OI}^{TL})_n = \tau_n \alpha_n M_0(\varepsilon_{y_n}), \quad (4.92)$$

$$(k_{O\theta}^{TB})_n = -\alpha_n (1 - \alpha_n) e^{-\varepsilon_{y_n}}, \quad (4.93)$$

$$(k_{O\theta}^{TL})_n = \tau_n \alpha_n [2M_1(\varepsilon_{y_n}) - M_0(\varepsilon_{y_n})], \quad (4.94)$$

$$(k_{OSA}^T)_n = (k_{OEA}^T)_n = \alpha_n \Delta y [-(1 - \alpha_n) M_0(\varepsilon_{y_n}) + (1 - 2\alpha_n) M_1(\varepsilon_{y_n}) + \alpha_n M_2(\varepsilon_{y_n})], \quad (4.95)$$

$$(k_{OSX}^T)_n = \alpha_n \Delta y [-(1 - \alpha_n) M_0(\varepsilon_{y_n}) + (1 - 2\alpha_n) M_1(\varepsilon_{y_n}) + \alpha_n M_2(\varepsilon_{y_n})], \quad (4.96)$$

and  $(k_{OSY}^T)_n = \Delta y [-(1 - \alpha_n) M_0(\varepsilon_{y_n}) + (2 - 3\alpha_n) M_1(\varepsilon_{y_n}) + \alpha_n M_2(\varepsilon_{y_n})]. \quad (4.97)$

The  $k$  vectors for the right outward angular currents are:

$$(k_{OI}^{RB})_n = \frac{1}{\tau_n} M_0(\varepsilon_{y_n}), \quad (4.98)$$

$$(k_{O\theta}^{RB})_n = \frac{1}{\tau_n} [(1 - 2\alpha_n) M_0(\varepsilon_{y_n}) + 2\alpha_n M_1(\varepsilon_{y_n})], \quad (4.99)$$

$$(k_{OI}^{RL})_n = (k_{O\theta}^{RL})_n = 0, \quad (4.100)$$

$$(k_{OSY}^R)_n = \frac{\Delta y}{\tau_n} [M_2(\varepsilon_{y_n}) - M_1(\varepsilon_{y_n})], \quad (4.101)$$

$$(k_{OSX}^R)_n = \frac{\Delta y}{\tau_n} [(1 - 2\alpha_n) M_1(\varepsilon_{y_n}) + 2\alpha_n M_2(\varepsilon_{y_n})], \quad (4.102)$$

and  $(k_{OSA}^R)_n = (k_{OEA}^R)_n = \frac{\Delta y}{\tau_n} M_1(\varepsilon_{y_n}). \quad (4.103)$

The  $k$  vectors for the top outward first moment of the angular currents are:

$$(k_{\theta I}^{TB})_n = 3\alpha_n (1 - \alpha_n) e^{-\varepsilon_{y_n}}, \quad (4.104)$$

$$(k_{\theta I}^{TL})_n = 3\tau_n \alpha_n [(2\alpha_n - 1)M_0(\varepsilon_{y_n}) - 2\alpha_n M_1(\varepsilon_{y_n})], \quad (4.105)$$

$$(k_{\theta\theta}^{TB})_n = (1 - 3\alpha_n + 2\alpha_n^2)e^{-\varepsilon_{y_n}}, \quad (4.106)$$

$$(k_{\theta\theta}^{TL})_n = 3\tau_n \alpha_n [(1 - 2\alpha_n)M_0(\varepsilon_{y_n}) + (6\alpha_n - 2)M_1(\varepsilon_{y_n}) - 4\alpha_n M_2(\varepsilon_{y_n})], \quad (4.107)$$

$$(k_{\theta SA}^T)_n = (k_{\theta EA}^T)_n = 3\alpha_n \Delta y [(1 - \alpha_n)M_0(\varepsilon_{y_n}) + (2\alpha_n - 1)M_1(\varepsilon_{y_n}) - \alpha_n M_2(\varepsilon_{y_n})], \quad (4.108)$$

$$(k_{\theta SX}^T)_n = \Delta y [(1 - 3\alpha_n + 2\alpha_n^3)M_0(\varepsilon_{y_n}) + (3\alpha_n - 6\alpha_n^3)M_1(\varepsilon_{y_n}) + 6\alpha_n^3 M_2(\varepsilon_{y_n}) - 2\alpha_n^3 M_3(\varepsilon_{y_n})], \quad (4.109)$$

$$\text{and} \quad (k_{\theta SY}^T)_n = 3\alpha_n \Delta y [-(1 - \alpha_n)M_0(\varepsilon_{y_n}) + (3 - 4\alpha_n)M_1(\varepsilon_{y_n}) - (2 - 5\alpha_n)M_2(\varepsilon_{y_n}) - 2\alpha_n M_3(\varepsilon_{y_n})]. \quad (4.110)$$

The  $k$  vectors for the right outward first moment of the angular currents are:

$$(k_{\theta I}^{RB})_n = \frac{3}{\tau_n} [M_0(\varepsilon_{y_n}) - 2M_1(\varepsilon_{y_n})], \quad (4.111)$$

$$(k_{\theta\theta}^{RB})_n = \frac{3}{\tau_n} [(1 - 2\alpha_n)M_0(\varepsilon_{y_n}) + (6\alpha_n - 2)M_1(\varepsilon_{y_n}) - 4\alpha_n M_2(\varepsilon_{y_n})], \quad (4.112)$$

$$(k_{\theta I}^{RL})_n = (k_{\theta\theta}^{RL})_n = 0, \quad (4.113)$$

$$(k_{\theta SA}^R)_n = (k_{\theta EA}^R)_n = \frac{3\Delta y}{\tau_n} [M_1(\varepsilon_{y_n}) - M_2(\varepsilon_{y_n})], \quad (4.114)$$

$$(k_{\theta SX}^R)_n = \frac{3\Delta y}{\tau_n} [(1 - 2\alpha_n)M_1(\varepsilon_{y_n}) - (1 - 4\alpha_n)M_2(\varepsilon_{y_n}) - 2\alpha_n M_3(\varepsilon_{y_n})], \quad (4.115)$$

$$\text{and} \quad (k_{\theta SY}^R)_n = \frac{\Delta y}{\tau_n} [-3M_1(\varepsilon_{y_n}) + 6M_2(\varepsilon_{y_n}) - 2M_3(\varepsilon_{y_n})]. \quad (4.116)$$

The  $k$  vectors for the average angular fluxes are:

$$(k_{AI}^B)_n = \frac{1}{|\eta_n|} [(1 - \alpha_n)M_0(\varepsilon_{y_n}) + \alpha_n M_1(\varepsilon_{y_n})], \quad (4.117)$$

$$(k_{AI}^L)_n = \frac{\alpha_n}{|\mu_n|} M_1(\varepsilon_{y_n}), \quad (4.118)$$

$$(k_{A\theta}^B)_n = \frac{\alpha_n}{|\eta_n|} [-(1-\alpha_n)M_0(\varepsilon_{y_n}) + (1-2\alpha_n)M_1(\varepsilon_{y_n}) + \alpha_n M_2(\varepsilon_{y_n})], \quad (4.119)$$

$$(k_{A\theta}^L)_n = \frac{\alpha_n}{|\mu_n|} [M_2(\varepsilon_{y_n}) - M_1(\varepsilon_{y_n})], \quad (4.120)$$

$$(k_{ASA})_n = (k_{AEA})_n = \frac{\Delta y}{|\eta_n|} [(1-\alpha_n)M_1(\varepsilon_{y_n}) + \alpha_n M_2(\varepsilon_{y_n})], \quad (4.121)$$

$$(k_{ASX})_n = \frac{\alpha_n \Delta y}{|\eta_n|} [-(1-\alpha_n)M_1(\varepsilon_{y_n}) + (1-2\alpha_n)M_2(\varepsilon_{y_n}) + \alpha_n M_3(\varepsilon_{y_n})], \quad (4.122)$$

and  $(k_{ASY})_n = \frac{\Delta y}{|\eta_n|} [-(1-\alpha_n)M_1(\varepsilon_{y_n}) + (1-2\alpha_n)M_2(\varepsilon_{y_n}) + \alpha_n M_3(\varepsilon_{y_n})]. \quad (4.123)$

The  $k$  vectors for the x-moment of the angular fluxes are:

$$(k_{XI}^B)_n = \frac{3\alpha_n}{|\eta_n|} [(1-\alpha_n)M_0(\varepsilon_{y_n}) + (2\alpha_n - 1)M_1(\varepsilon_{y_n}) - \alpha_n M_2(\varepsilon_{y_n})], \quad (4.124)$$

$$(k_{XI}^L)_n = \frac{3\alpha_n}{|\mu_n|} [(2\alpha_n - 1)M_1(\varepsilon_{y_n}) - 2\alpha_n M_2(\varepsilon_{y_n})], \quad (4.125)$$

$$(k_{X\theta}^B)_n = \frac{1}{|\eta_n|} [(1-3\alpha_n + 2\alpha_n^3)M_0(\varepsilon_{y_n}) + (3\alpha_n - 6\alpha_n^3)M_1(\varepsilon_{y_n}) + 6\alpha_n^3 M_2(\varepsilon_{y_n}) - 2\alpha_n^3 M_3(\varepsilon_{y_n})], \quad (4.126)$$

$$(k_{X\theta}^L)_n = \frac{3\alpha_n}{|\mu_n|} [(1-2\alpha_n)M_1(\varepsilon_{y_n}) - (4\alpha_n - 1)M_2(\varepsilon_{y_n}) - 2\alpha_n M_3(\varepsilon_{y_n})], \quad (4.127)$$

$$(k_{XI}^B)_n = \frac{3\alpha_n}{|\eta_n|} [(1-\alpha_n)M_0(\varepsilon_{y_n}) + (2\alpha_n - 1)M_1(\varepsilon_{y_n}) - \alpha_n M_2(\varepsilon_{y_n})], \quad (4.128)$$

$$(k_{XSA})_n = (k_{XEA})_n = \frac{3\alpha_n \Delta y}{|\eta_n|} [(1-\alpha_n)M_1(\varepsilon_{y_n}) + (2\alpha_n - 1)M_2(\varepsilon_{y_n}) - \alpha_n M_3(\varepsilon_{y_n})], \quad (4.129)$$

$$(k_{XSS})_n = \frac{\Delta y}{|\eta_n|} [(1 - 3\alpha_n + 2\alpha_n^3)M_1(\varepsilon_{y_n}) + (3\alpha_n - 6\alpha_n^3)M_2(\varepsilon_{y_n}) + 6\alpha_n^3M_3(\varepsilon_{y_n}) - 2\alpha_n^3M_4(\varepsilon_{y_n})], \quad (4.130)$$

and

$$(k_{XSY})_n = \frac{3\alpha_n\Delta y}{|\eta_n|} [-(1 - \alpha_n)M_1(\varepsilon_{y_n}) + (2 - 3\alpha_n)M_2(\varepsilon_{y_n}) - (1 - 3\alpha_n)M_3(\varepsilon_{y_n}) - \alpha_nM_4(\varepsilon_{y_n})]. \quad (4.131)$$

The  $k$  vectors for the y-moment of the angular fluxes are:

$$(k_{YI}^B)_n = \frac{3}{|\eta_n|} [(1 - \alpha_n)M_0(\varepsilon_{y_n}) + (3\alpha_n - 2)M_1(\varepsilon_{y_n}) - 2\alpha_nM_2(\varepsilon_{y_n})], \quad (4.132)$$

$$(k_{YI}^L)_n = \frac{3\alpha_n}{|\mu_n|} [M_1(\varepsilon_{y_n}) - M_2(\varepsilon_{y_n})], \quad (4.133)$$

$$(k_{Y\theta}^B)_n = \frac{3\alpha_n}{|\eta_n|} [-(1 - \alpha_n)M_0(\varepsilon_{y_n}) + (3 - 4\alpha_n)M_1(\varepsilon_{y_n}) + (5\alpha_n - 2)M_2(\varepsilon_{y_n}) - 2\alpha_nM_3(\varepsilon_{y_n})], \quad (4.134)$$

$$(k_{Y\theta}^L)_n = \frac{\alpha_n}{|\mu_n|} [-3M_0(\varepsilon_{y_n}) + 6M_1(\varepsilon_{y_n}) - 2M_2(\varepsilon_{y_n})], \quad (4.135)$$

$$(k_{YSA})_n = (k_{YEA})_n = \frac{3\Delta y}{|\eta_n|} [(1 - \alpha_n)M_1(\varepsilon_{y_n}) + (2\alpha_n - 1)M_2(\varepsilon_{y_n}) - \alpha_nM_3(\varepsilon_{y_n})], \quad (4.136)$$

$$(k_{YSX})_n = \frac{3\alpha_n\Delta y}{|\eta_n|} [-(1 - \alpha_n)M_1(\varepsilon_{y_n}) + (2 - 3\alpha_n)M_2(\varepsilon_{y_n}) - (1 - 3\alpha_n)M_3(\varepsilon_{y_n}) - \alpha_nM_4(\varepsilon_{y_n})], \quad (4.137)$$

and

$$(k_{YSY})_n = \frac{\Delta y}{|\eta_n|} [-3(1 - \alpha_n)M_1(\varepsilon_{y_n}) + (6 - 9\alpha_n)M_2(\varepsilon_{y_n}) - (2 - 8\alpha_n)M_3(\varepsilon_{y_n}) - 2\alpha_nM_4(\varepsilon_{y_n})]. \quad (4.138)$$

As with the zeroth spatial moment methods, each ordinate is evaluated to determine the outgoing face and the respective transport coefficient. Ordinates exiting the right, bottom or left cell edges instead of the top edge use the same

basic equations with an x-y reversal, a right-left exchange or a top-bottom exchange where appropriate.

## 2. Linear Discontinuous Transport Coefficients

The next spatial method implemented was linear discontinuous (LD). This first spatial moment method was chosen to show the implementation of other higher order spatial methods with the same algorithm as LC. Boegers et al (4: 289-290) provided the angular flux representation for the LD equations. A derivation for the LD cell current equations for ordinate  $n$  with  $\eta_n > \mu_n > 0$  and  $\alpha_n \leq 1$ , is presented in Appendix D.

The following definitions are used for the LD quadrature:

$$a_n = 1 + \alpha_n + \varepsilon_{y_n} + \frac{3}{4 + \varepsilon_{y_n}} + \frac{3\alpha_n^2}{1 + 3\alpha_n + \varepsilon_{y_n}}, \quad (4.139)$$

$$b_n = 4 + \varepsilon_{y_n}, \quad (4.140)$$

and 
$$c_n = 1 + 3\alpha_n + \varepsilon_{y_n}. \quad (4.141)$$

Again, the process of determining the equations for the  $k$  vectors used to form the diagonal matrices  $\mathbf{K} = \mathbf{D}(\vec{k})$  is analogous to the procedure used for SC. The  $k$  vectors for the top outward angular currents are:

$$(k_{OI}^{TB})_n = \frac{(9 + 6b_n - 3a_nb_n + b_n^2)}{a_nb_n^2}, \quad (4.142)$$

$$(k_{OI}^{TL})_n = \frac{(3 + b_n)(3 + c_n)\alpha_n|\eta_n|}{a_nb_nc_n|\mu_n|}, \quad (4.143)$$

$$(k_{O\theta}^{TB})_n = -\frac{\alpha_n(b_n+3)}{a_nb_nc_n}, \quad (4.144)$$

$$(k_{O\theta}^{TL})_n = \frac{(-3+(a_n-1)b_n)|\eta_n|}{a_nb_n^2|\mu_n|}, \quad (4.145)$$

$$(k_{OSA}^T)_n = (k_{OEA}^T)_n = \frac{\Delta y(b_n+3)}{a_nb_n}, \quad (4.146)$$

$$(k_{OSX}^T)_n = -\frac{\Delta y\alpha_n(b_n+3)}{a_nb_nc_n}, \quad (4.147)$$

and

$$(k_{OSY}^T)_n = \frac{\Delta y(-3+(a_n-1)b_n)}{a_nb_n^2}. \quad (4.148)$$

The  $k$  vectors for the right outward angular currents are:

$$(k_{OI}^{RB})_n = \frac{(3+b_n)(c_n+3\alpha_n)|\mu_n|}{a_nb_nc_n|\eta_n|}, \quad (4.149)$$

$$(k_{OI}^{RL})_n = \frac{\alpha_n(c_n^2+9\alpha_n+c_n(3-3a_n+3\alpha_n))}{a_nc_n^2}, \quad (4.150)$$

$$(k_{O\theta}^{RB})_n = \frac{(a_nc_n-\alpha_n(c_n+3\alpha_n))|\mu_n|}{a_nc_n^2|\eta_n|}, \quad (4.151)$$

$$(k_{O\theta}^{RL})_n = -\frac{(c_n+3\alpha_n)}{a_nb_nc_n}, \quad (4.152)$$

$$(k_{OSA}^R)_n = (k_{OEA}^R)_n = \frac{\Delta y(c_n+3\alpha_n)|\mu_n|}{a_nc_n|\eta_n|}, \quad (4.153)$$

$$(k_{OSX}^R)_n = \frac{\Delta y(a_nc_n-\alpha_n(c_n+3\alpha_n))|\mu_n|}{a_nc_n^2|\eta_n|}, \quad (4.154)$$

and

$$(k_{OSY}^R)_n = -\frac{\Delta y(c_n+3\alpha_n)|\mu_n|}{a_nb_nc_n|\eta_n|}. \quad (4.155)$$

The  $k$  vectors for the top outward first moment of the angular currents are:



$$(k_{\theta I}^{TB})_n = \frac{3(3+b_n)\alpha_n}{a_n b_n c_n}, \quad (4.156)$$

$$(k_{\theta I}^{TL})_n = \frac{3\alpha_n(-a_n c_n + (3+c_n)\alpha_n)|\eta_n|}{a_n c_n^2 |\mu_n|}, \quad (4.157)$$

$$(k_{\theta\theta}^{TB})_n = \frac{(a_n c_n - 3\alpha_n^2)}{a_n c_n^2}, \quad (4.158)$$

$$(k_{\theta\theta}^{TL})_n = -\frac{3\alpha_n |\eta_n|}{a_n b_n c_n |\mu_n|}, \quad (4.159)$$

$$(k_{\theta SA}^T)_n = (k_{\theta EA}^T)_n = \frac{\Delta y 3\alpha_n}{a_n c_n}, \quad (4.160)$$

$$(k_{\theta SX}^T)_n = \frac{\Delta y (a_n c_n - 3\alpha_n^2)}{a_n c_n^2}, \quad (4.161)$$

and

$$(k_{\theta SY}^T)_n = -\frac{\Delta y 3\alpha_n}{a_n b_n c_n}. \quad (4.162)$$

The  $k$  vectors for the right outward first moment of the angular currents are:

$$(k_{\theta I}^{RB})_n = -\frac{3(-3+(a_n-1)b_n)|\mu_n|}{a_n b_n^2 |\eta_n|}, \quad (4.163)$$

$$(k_{\theta I}^{RL})_n = \frac{3\alpha_n(3+c_n)}{a_n b_n c_n}, \quad (4.164)$$

$$(k_{\theta\theta}^{RB})_n = -\frac{3\alpha_n |\mu_n|}{a_n b_n c_n |\eta_n|}, \quad (4.165)$$

$$(k_{\theta\theta}^{RL})_n = \frac{(-3+a_n b_n)}{a_n b_n^2}, \quad (4.166)$$

$$(k_{\theta SA}^R)_n = (k_{\theta EA}^R)_n = \frac{3\Delta y |\mu_n|}{a_n b_n |\eta_n|}, \quad (4.167)$$

$$(k_{\theta SX}^R)_n = -\frac{3\Delta y \alpha_n |\mu_n|}{a_n b_n c_n |\eta_n|}, \quad (4.168)$$

and 
$$(k_{\theta SY}^R)_n = \frac{\Delta y(a_n b_n - 3)|\mu_n|}{a_n b_n^2 |\eta_n|}. \quad (4.169)$$

The  $k$  vectors for the average angular fluxes are:

$$(k_{AI}^B)_n = \frac{(3 + b_n)}{a_n b_n |\eta_n|}, \quad (4.170)$$

$$(k_{AI}^L)_n = \frac{\alpha_n(3 + c_n)}{a_n c_n |\mu_n|}, \quad (4.171)$$

$$(k_{A\theta}^B)_n = -\frac{\alpha_n}{a_n c_n |\eta_n|}, \quad (4.172)$$

$$(k_{A\theta}^L)_n = -\frac{1}{a_n b_n |\mu_n|}, \quad (4.173)$$

$$(k_{ASA})_n = (k_{AEA})_n = \frac{\Delta y}{a_n |\eta_n|}, \quad (4.174)$$

$$(k_{ASX})_n = -\frac{\Delta y \alpha_n}{a_n c_n |\eta_n|}, \quad (4.175)$$

and 
$$(k_{ASY})_n = -\frac{\Delta y}{a_n b_n |\eta_n|}. \quad (4.176)$$

The  $k$  vectors for the x-moment of the angular fluxes are:

$$(k_{XI}^B)_n = \frac{3(3 + b_n)\alpha_n}{a_n b_n c_n |\eta_n|}, \quad (4.177)$$

$$(k_{XI}^L)_n = \frac{3\alpha_n(-a_n c_n + (3 + c_n)\alpha_n)}{a_n c_n^2 |\mu_n|}, \quad (4.178)$$

$$(k_{X\theta}^B)_n = \frac{(a_n c_n - 3\alpha_n^2)}{a_n c_n^2 |\eta_n|}, \quad (4.179)$$

$$(k_{X\theta}^L)_n = \frac{(a_n c_n - 3\alpha_n^2)}{a_n c_n^2 |\eta_n|}, \quad (4.180)$$

$$(k_{XSA})_n = (k_{XEA})_n = \frac{\Delta y 3\alpha_n}{a_n c_n |\eta_n|}, \quad (4.181)$$

$$(k_{XSX})_n = \frac{\Delta y (a_n c_n - 3\alpha_n^2)}{a_n c_n^2 |\eta_n|}, \quad (4.182)$$

and

$$(k_{XSY})_n = -\frac{\Delta y 3\alpha_n}{a_n b_n c_n |\eta_n|}. \quad (4.183)$$

The  $k$  vectors for the y-moment of the angular fluxes are:

$$k_{YI}^B(n, n) = \frac{(9 + 3b_n - 3a_n b_n)}{a_n b_n^2 |\eta_n|}, \quad (4.184)$$

$$k_{YI}^L(n, n) = \frac{3\alpha_n (3 + c_n)}{a_n b_n c_n |\mu_n|}, \quad (4.185)$$

$$k_{Y\theta}^B(n, n) = -\frac{3\alpha_n}{a_n b_n c_n |\eta_n|}, \quad (4.186)$$

$$k_{Y\theta}^L(n, n) = \frac{(-3 + a_n b_n)}{a_n b_n^2 |\mu_n|}, \quad (4.187)$$

$$(k_{YSA})_n = (k_{YEA})_n = \frac{\Delta y 3}{a_n b_n |\eta_n|}, \quad (4.188)$$

$$(k_{YSX})_n = -\frac{\Delta y 3\alpha_n}{a_n b_n c_n |\eta_n|}, \quad (4.189)$$

and

$$(k_{YSY})_n = \frac{\Delta y (a_n b_n - 3)}{a_n b_n^2 |\eta_n|}. \quad (4.190)$$

As with WDD, LD is treated like LC: each ordinate is evaluated to determine the outgoing face and the respective transport coefficient. For ordinates that are not exiting the top of the cell, the same basic relations are used with an x-y exchange, a right-left reversal or a top-bottom reversal where

appropriate. Again, for the DI method, these LD matrices (or any other linear, first spatial method) use the same solver algorithm as LC.

### C. Partial Current Problem

#### 1. Zeroth Spatial Moment Partial Current Problem

The partial current problem is set up to establish the proper scale of values across the problem. Setting up the partial current problem with the improved cell shape information requires an array similar to equation (3.88). The edge distribution,  $\zeta$ , is defined as the current along an ordinate divided by the partial current found by integrating over the ordinates in that direction or:

$$\zeta_R^n = \frac{j_R^n}{\sum_{n' \in R} w^{n'} j_R^{n'}}, \quad (4.191)$$

where  $w^{n'}$  is the angular quadrature weight. Similarly, an edge distribution can be defined for the top edge as well:

$$\zeta_T^n = \frac{j_T^n}{\sum_{n' \in T} w^{n'} j_T^{n'}}. \quad (4.192)$$

The left and bottom edges are defined in the same way.

The edge distributions allow the cell current shape information to be retained while solving the partial current problem. Using the relations in equation (4.17), the edge current along the right edge in terms of the incoming currents and emissions in a cell is:

$$\vec{j}_{Out}^R = \mathbf{m}_{OI}^{RL} \vec{j}_{In}^L + \mathbf{m}_{OI}^{RR} \vec{j}_{In}^R + \mathbf{m}_{OI}^{RT} \vec{j}_{In}^T + \mathbf{m}_{OI}^{RB} \vec{j}_{In}^B + \mathbf{m}_{OEA}^R \vec{E}_A. \quad (4.193)$$

As was done in slab geometry, the right edge current relation can be transformed into an equivalent relation for the partial currents and emissions in a cell as:

$$\mathbf{J}_{Out}^R = M_{OI}^{RL} \mathbf{J}_{In}^L + M_{OI}^{RR} \mathbf{J}_{In}^R + M_{OI}^{RT} \mathbf{J}_{In}^T + M_{OI}^{RB} \mathbf{J}_{In}^B + M_{OEA}^R \mathbf{E}_A. \quad (4.194)$$

In this case, the coefficients on the partial currents and emissions are collapsed single values determined using the quadrature weights, the coefficient matrices and the edge distributions as follows:

$$M_{OI}^{RR} = \sum_{n \in out} w_n \left( \mathbf{m}_{OI}^{RR} \bar{\zeta}_n^R \right), \quad (4.195)$$

$$M_{OI}^{RL} = \sum_{n \in out} w_n \left( \mathbf{m}_{OI}^{RL} \bar{\zeta}_n^L \right), \quad (4.196)$$

$$M_{OI}^{RT} = \sum_{n \in out} w_n \left( \mathbf{m}_{OI}^{RT} \bar{\zeta}_n^T \right), \quad (4.197)$$

$$M_{OI}^{RB} = \sum_{n \in out} w_n \left( \mathbf{m}_{OI}^{RB} \bar{\zeta}_n^B \right), \quad (4.198)$$

and

$$M_{OEA}^R \mathbf{E}_A = \sum_{n \in out} w_n \left( \mathbf{m}_{OEA}^R \bar{\mathbf{E}}_A \right). \quad (4.199)$$

Equations (4.195) through (4.198) can be applied in a similar manner to determine the remaining partial currents. Applying this to the system of equations described in equation (4.17) yields:

$$\begin{bmatrix} \mathbf{J}_{Out}^L \\ \mathbf{J}_{Out}^R \\ \mathbf{J}_{Out}^T \\ \mathbf{J}_{Out}^B \end{bmatrix} = \begin{bmatrix} M_{OI}^{LL} & M_{OI}^{LR} & M_{OI}^{LT} & M_{OI}^{LB} \\ M_{OI}^{RL} & M_{OI}^{RR} & M_{OI}^{RT} & M_{OI}^{RB} \\ M_{OI}^{TL} & M_{OI}^{TR} & M_{OI}^{TT} & M_{OI}^{TB} \\ M_{OI}^{BL} & M_{OI}^{BR} & M_{OI}^{BT} & M_{OI}^{BB} \end{bmatrix} \begin{bmatrix} \mathbf{J}_{In}^L \\ \mathbf{J}_{In}^R \\ \mathbf{J}_{In}^T \\ \mathbf{J}_{In}^B \end{bmatrix} + \begin{bmatrix} M_{OEA}^L \mathbf{E}_A \\ M_{OEA}^R \mathbf{E}_A \\ M_{OEA}^T \mathbf{E}_A \\ M_{OEA}^B \mathbf{E}_A \end{bmatrix}. \quad (4.200)$$

The partial currents in equation (4.200) are the outgoing partial currents for a cell. The collapsed matrices form coefficients for each cell in the spatial mesh that will be used in the partial current problem.

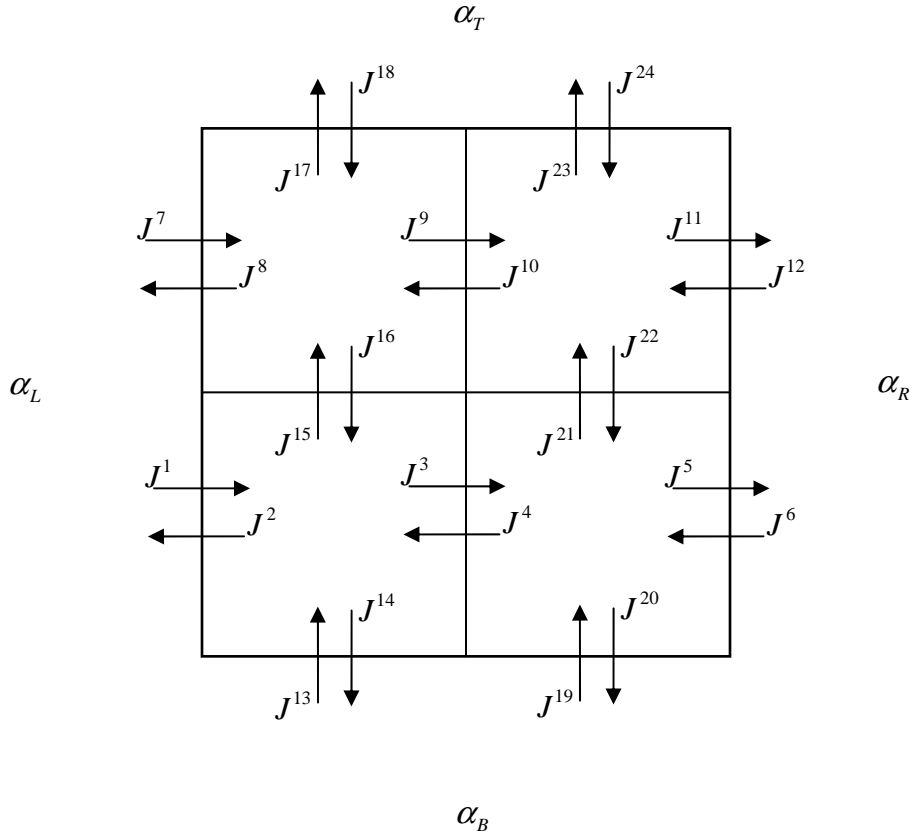


Figure 4.2. Setting up the partial current problem for a two cell by two cell problem showing the ordering of the partial currents.

The ordering of the partial currents in the partial current problem is important in keeping the problem manageable. The scattering contribution from the orthogonal directions increases the bandwidth of the sparse matrix. To keep the matrix bandwidth manageable and provide a consistent pattern to implement into the code, the partial current problem was set up using the ordering shown in



where, for example,  $M_{14}^T$  is the coefficient that corresponds to the cell top incoming partial current that contributes to the outgoing partial current  $J^{14}$ . These values come directly from the cell partial current equation shown in equation (4.200) and are the collapsed matrix coefficients for each cell. The unknowns  $\vec{x}$  in the relation are the partial currents in the ordering shown in figure 4.3:  $\vec{x}^T = (J^1 \ J^2 \ J^3 \ . \ . \ . \ J^{22} \ J^{23} \ J^{24})$  and the forcing vector  $\vec{b}$ , is derived from the cell emissions in the same ordering. The elements of the forcing vector are considered known values for this problem.

As can be seen by the matrix, this is a sparse matrix problem which grows quickly as the number of cells in the problem increase. To solve the sparse matrix problem, a Compaq Extended Math Library (CXML) (6: 11-1) direct sparse matrix solver (cxml\_dss.f90) was used. Fortunately, the library routine did not require actually creating the matrix explicitly; data was entered as vectors which greatly increased to size of the problems that could be solved.

### **Reapportioning Partial Current from the Direct Solver**

The partial current problem solution,  $J_{PCP}$ , from the library routine can then be distributed back to the cell edge currents using the original  $\zeta$ , or edge distribution. This forms the basis of the iterative method. With the correct  $\zeta$  value, the partial current solution does not change from the initial partial current values. Since the correct  $\zeta$  value is not known initially, an iteration with among cell calculations on the cell edge values must be used to improve the current



estimate of  $\zeta$ . To distribute the cell partial current solution back to the cell edge values, the following relations are used for the zeroth spatial moment methods:

$$\vec{j}_{new}^L = J_{PCP}^L \vec{\zeta}^L, \quad (4.201)$$

$$\vec{j}_{new}^R = J_{PCP}^R \vec{\zeta}^R, \quad (4.202)$$

$$\vec{j}_{new}^T = J_{PCP}^T \vec{\zeta}^T, \quad (4.203)$$

and 
$$\vec{j}_{new}^B = J_{PCP}^B \vec{\zeta}^B. \quad (4.204)$$

## 2. First Spatial Moment Partial Current Problem

First spatial moment methods must be handled differently due to the first spatial moment of the edge current  $\theta$  that is used for these methods. The solution can be found through either solving two simultaneous systems of equations or transforming the partial current system of equations to eliminate the  $\theta$  values. The second choice was used in order to allow the use of the same routine for the partial current problem that was used with the zeroth spatial moment methods. To do this, a new parameter is defined:

$$\rho_i = \frac{\theta_i}{j_i}, \quad (4.205)$$

where  $\vec{\rho}$  is a cell edge array containing the number of ordinates in the angular quadrature set. This new parameter permits the first spatial moment methods current to be written in a form similar to equation (4.193). In this case, the equation may be written as:

$$\begin{aligned} \vec{j}_{Out}^R = & (\mathbf{m}_{OI}^{RL} + \mathbf{m}_{O\theta}^{RL} \mathbf{D}(\vec{\rho}_{In}^{-L})) \vec{j}_{In}^L + (\mathbf{m}_{OI}^{RR} + \mathbf{m}_{O\theta}^{RR} \mathbf{D}(\vec{\rho}_{In}^{-R})) \vec{j}_{In}^R + \\ & (\mathbf{m}_{OI}^{RT} + \mathbf{m}_{O\theta}^{RT} \mathbf{D}(\vec{\rho}_{In}^{-T})) \vec{j}_{In}^T + (\mathbf{m}_{OI}^{RB} + \mathbf{m}_{O\theta}^{RB} \mathbf{D}(\vec{\rho}_{In}^{-B})) \vec{j}_{In}^B + \mathbf{m}_{OEA}^R \vec{E}^A, \end{aligned} \quad (4.206)$$

where  $\mathbf{D}$  is an operator that creates a diagonal matrix from a vector. A similar procedure is done for the remaining edge currents. This allows the system of equations in equation (4.89) to be written:

$$\begin{bmatrix} \vec{j}_{Out}^L \\ \vec{j}_{Out}^R \\ \vec{j}_{Out}^T \\ \vec{j}_{Out}^B \end{bmatrix} = \begin{bmatrix} (\mathbf{m}_{OI}^{LL} + \mathbf{m}_{O\theta}^{LL} \mathbf{D}(\vec{\rho}_{In}^{-L})) & \dots & (\mathbf{m}_{OI}^{LB} + \mathbf{m}_{O\theta}^{LB} \mathbf{D}(\vec{\rho}_{In}^{-B})) \\ \vdots & \ddots & \vdots \\ (\mathbf{m}_{OI}^{BL} + \mathbf{m}_{O\theta}^{BL} \mathbf{D}(\vec{\rho}_{In}^{-L})) & \dots & (\mathbf{m}_{OI}^{BB} + \mathbf{m}_{O\theta}^{BB} \mathbf{D}(\vec{\rho}_{In}^{-B})) \end{bmatrix} + \begin{bmatrix} \mathbf{m}_{OEA}^L \vec{E}^A \\ \mathbf{m}_{OEA}^R \vec{E}^A \\ \mathbf{m}_{OEA}^T \vec{E}^A \\ \mathbf{m}_{OEA}^B \vec{E}^A \end{bmatrix}. \quad (4.207)$$

The quantity in the parenthesis can be combined to form a single matrix:

$$\begin{bmatrix} \vec{j}_{Out}^L \\ \vec{j}_{Out}^R \\ \vec{j}_{Out}^T \\ \vec{j}_{Out}^B \end{bmatrix} = \begin{bmatrix} \hat{\mathbf{m}}^{LL} & \hat{\mathbf{m}}^{LR} & \hat{\mathbf{m}}^{LT} & \hat{\mathbf{m}}^{LB} \\ \hat{\mathbf{m}}^{RL} & \hat{\mathbf{m}}^{RR} & \hat{\mathbf{m}}^{RT} & \hat{\mathbf{m}}^{RB} \\ \hat{\mathbf{m}}^{TL} & \hat{\mathbf{m}}^{TR} & \hat{\mathbf{m}}^{TT} & \hat{\mathbf{m}}^{TB} \\ \hat{\mathbf{m}}^{BL} & \hat{\mathbf{m}}^{BR} & \hat{\mathbf{m}}^{BT} & \hat{\mathbf{m}}^{BB} \end{bmatrix} \begin{bmatrix} \vec{j}_{In}^L \\ \vec{j}_{In}^R \\ \vec{j}_{In}^T \\ \vec{j}_{In}^B \end{bmatrix} + \begin{bmatrix} \mathbf{m}_{OEA}^L \vec{E}^A \\ \mathbf{m}_{OEA}^R \vec{E}^A \\ \mathbf{m}_{OEA}^T \vec{E}^A \\ \mathbf{m}_{OEA}^B \vec{E}^A \end{bmatrix}. \quad (4.208)$$

Here the  $\hat{\mathbf{m}}$  indicates the quantities in the parentheses for equation (4.207). Now equation (4.208) is in the same form as equation (4.17) and the collapsing for the partial current problem is done the same as for the zeroth spatial moment method. The first moment partial current problem is identical to the zeroth spatial moment problem. Also, the cell partial current solution is distributed to the cell edge currents as shown in equations (4.201) through (4.204). One difference is the cell edge current first spatial moment values  $\vec{\theta}$ , are distributed as follows:

$$\bar{\theta}_{new}^L = J_{PCP}^L D(\bar{\rho}^L) \bar{\zeta}^L, \quad (4.209)$$

$$\bar{\theta}_{new}^R = J_{PCP}^R D(\bar{\rho}^R) \bar{\zeta}^R, \quad (4.210)$$

$$\bar{\theta}_{new}^T = J_{PCP}^T D(\bar{\rho}^T) \bar{\zeta}^T, \quad (4.211)$$

and

$$\bar{\theta}_{new}^B = J_{PCP}^B D(\bar{\rho}^B) \bar{\zeta}^B. \quad (4.212)$$

Note the partial current problem does not adjust the edge distributions  $\bar{\zeta}$ . This is done during the among cell calculations using the local cell coupling relations.

## V. Validation and Performance

The code must be validated before any comparisons to other methods can be made. The test plan was implemented in three phases: initial checks; consistency checks; and accuracy checks. These checks and their results are described in this chapter.

### A. Validation

#### 1. Initial Checks

Two key areas for initial checks were for both the spatial method and the angular quadrature. For the angular quadrature, the weights and direction cosines were tested using Mathematica to compare the ability of the angular quadrature to exactly integrate the functions  $1$ ,  $\mu$ ,  $\mu^2$ ,  $\mu^3$ ,  $\mu^4$ ,  $\eta$ ,  $\eta^2$ ,  $\eta^3$  and  $\eta^4$  over the interval -1 to 1.

Numerical testing confirmed that cell balance equations were satisfied by each spatial quadrature method as implemented. Most errors would show up as violations of the balance equations (13: 176-177). For the zeroth spatial moment methods, the particle balance equation for a cell is:

$$(j_R - j_L)\Delta y + (j_T - j_B)\Delta x + \sigma\Delta x\Delta y\psi_A = S_A\Delta x\Delta y. \quad (5.1)$$

For the first spatial moment methods, additional balance equations were used.

The x moment balance equation:

$$3(j_R + j_L - 2\mu\psi_A)\Delta y + (\theta_T - \theta_B)\Delta x + \sigma\Delta x\Delta y\psi_X = S_X\Delta x\Delta y, \quad (5.2)$$

and the y moment balance equation:

$$3(j_T + j_B - 2\eta\psi_A)\Delta x + (\theta_R - \theta_L)\Delta y + \sigma\Delta x\Delta y\psi_Y = S_Y\Delta x\Delta y. \quad (5.3)$$

Both the angular quadrature testing and all cell balance relations for all spatial methods were confirmed.

## 2. Consistency Checks

The consistency testing was broken into two portions: symmetry tests and aspect ratio tests.

### Symmetry Tests

In this phase, the testing validated that boundary conditions and indexing were consistently implemented. (This test identifies copy-paste-edit errors.) The quantities,  $\alpha_L$ ,  $\alpha_R$ ,  $\alpha_T$ , and  $\alpha_B$  are used to specify the boundary conditions on the left, right, top and bottom side of the spatial mesh respectively. The same boundary condition was applied to all the cells on a respective edge. Again, two boundary conditions were used: vacuum boundaries (i.e.  $\alpha_R = 0$ ); and reflective boundaries (i.e.  $\alpha_R = 1$ ). The scattering ratio is varied in these tests. It is defined as the ratio of the scattering cross section ( $\sigma_s$ ) to the total cross section ( $\sigma_t$ ):

$$c = \frac{\sigma_s}{\sigma_t}. \quad (5.4)$$

Various symmetries are compared to ensure the same result is calculated when only the orientation of the problem is changed. For the different problems

examined, the cell average scalar flux should be the same value and the rate of convergence should be identical.

The first test problem in this phase is the uniform universe test.

Reflective boundaries are set on all boundaries and the values are set as shown in figure 5.1.

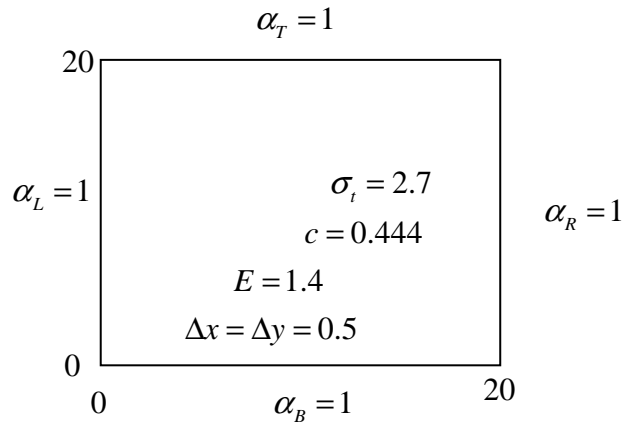


Figure 5.1. Problem values for the uniform universe test problem.

This test problem was chosen because it is one of the few transport problems with a closed form solution. A flux solution is found by integrating the BTE over all angles:

$$\int_{\forall \Omega} [\hat{\Omega} \cdot \vec{\nabla} \psi + \sigma_t \psi = \sigma_s \phi + E] d\Omega, \quad (5.5)$$

but  $\vec{\nabla} \psi = 0$  and  $\psi$  is independent of  $\hat{\Omega}$  for this uniform problem. This also means that:

$$\psi = a\phi, \quad (5.6)$$

where  $a=1$  based on the normalization for the angular quadrature set where:

$$\int_{\forall\Omega} d\Omega = 1. \quad (5.7)$$

Equation (5.5) yields:

$$\sigma_t\phi = \sigma_s\phi + E, \quad (5.8)$$

or,

$$(\sigma_t - \sigma_s)\phi = \sigma_a\phi = E, \quad (5.9)$$

where  $\sigma_a$  is the absorption cross section. The solution for the scalar flux is:

$$\phi = \frac{E}{\sigma_a}. \quad (5.10)$$

Also, for the angular quadrature set normalization, the value of the converged angular and scalar flux in a cell should be the same and equal to  $\frac{E}{\sigma_a}$ .

The next symmetry test problem examined the effect of boundary conditions on the solution by setting three sides of the problem with reflective boundaries and the remaining side with a vacuum boundary. The side with the vacuum boundary is rotated through all possible cases, and the (rotated or reflected) converged solutions should be identical in each case. The problem values for this test are shown in figure 5.2.

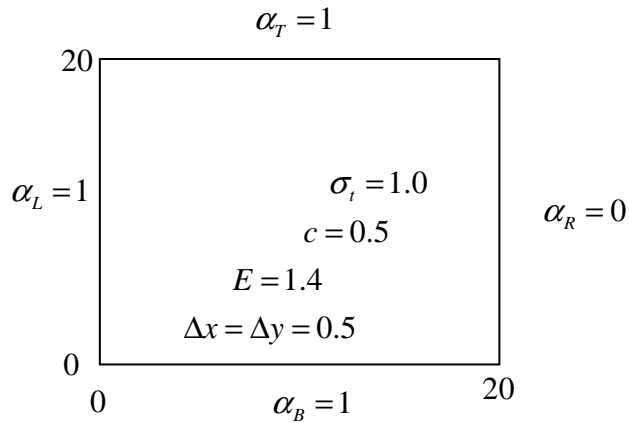


Figure 5.2. Problem values for the single vacuum boundary and three reflective boundary problem.

The last symmetry test problem in this phase examines additional rotational symmetries. In this problem, two adjacent boundaries are reflective and the other two are vacuum, then the boundary conditions are reversed. Again, for both of these cases, the converged results should be identical. The problem values were the same as figure 5.2 with the exception of the vacuum boundaries.

The results of some of the validation tests follow. For brevity, the results of the WDD method are shown for some of the tests, the other spatial quadratures had similar results.

### Symmetry Test Results

The results of the uniform universe test are shown in table 5.1. The test was done using the  $S_6$  angular quadrature and a tolerance of  $10^{-5}$ . Each spatial method converged in one iteration for the DI method. As noted earlier, the value



of the scalar flux in a cell can be calculated and for this test the value should be 0.9325873. An independent source iteration (SI) solution was also done for comparison. Note that while the SI solution meets the requested tolerance, it does not have the precision that the DI methods have for this solution. The number of SI iterations required to meet the same tolerance is listed, which is significant for a relatively simple test problem. In addition, for this test, the average angular flux in a cell had the same value as the scalar flux as expected.

Table 5.1. Results of the uniform universe test.

Spatial method	Distribution Iteration		Source Iteration	
	Scalar Flux	Number of iterations	Scalar Flux	Number of iterations
WDD	0.9325873	1	0.9325859	38
SC	0.9325873	1	0.9325859	35
LD	0.9325873	1	0.9325871	21
LC	0.9325873	1	0.9325871	21

The results of the one vacuum boundary symmetry tests showed that the problems returned identical values for the scalar flux, iterations to convergence and maximum and minimum scalar flux values for each vacuum boundary location. The test was also done using the  $S_6$  angular quadrature and a tolerance of  $10^{-5}$ . As noted earlier, the results of each different vacuum boundary should be identical as the vacuum boundary is rotated around the problem grid if the boundary conditions and indexing are correct for either a

right/left or top/bottom exchange. The other spatial quadratures have similarly identical results.

In addition, the average angular flux in each cell was compared for the results for the right/left and top/bottom tests respectively by exchanging the array indices for the right/top and comparing this to the left/bottom test results. The exchanged right vacuum boundary cell average angular flux values compared to the test left vacuum boundary cell average angular flux with a SRD of  $1.28 \times 10^{-13}$ . Also, the exchanged top vacuum boundary cell average angular flux values compared to the test bottom vacuum boundary cell average angular flux with a SRD of  $1.28 \times 10^{-13}$ . The other spatial quadratures have similar results. These test results all used a convergence tolerance of  $10^{-5}$ , and the SRD is consistent with the rounding errors associated with the machine arithmetic for the different test solutions.

The next symmetry tests, two vacuum boundaries, also returned identical values for the scalar flux, iterations to convergence and maximum and minimum scalar flux values for both vacuum boundary cases. Computations for this test used the  $S_6$  angular quadrature and a tolerance of  $10^{-5}$ . For this test, the results for the different vacuum boundaries should also have been identical as the vacuum boundaries are rotated on the problem grid if boundary conditions and indexing for an x/y exchange are properly implemented. The other spatial quadratures again had similar identical results.

For this case as well, the average angular flux in each cell was compared by doing another exchange of the array indices for the right/top test results. The exchanged right/top vacuum boundary cell average angular flux values compared to the test left/bottom vacuum boundary cell average angular flux with a SRD of  $1.60 \times 10^{-13}$ , which is consistent with rounding errors for the different tests. The other spatial quadratures had similar results.

### **Aspect Ratio Tests**

The symmetry test problems used a 40x40 grid of square cells. The next series of test problems in this phase of testing uses various aspect ratios  $\Delta y : \Delta x$  while keeping the cross section and boundary conditions the same as shown in figure 5.3. Again, the results for the converged solution should be identical when x and y values are interchanged. Aspect ratios of 1:2, 1:4 and 1:8 were compared to aspect ratios of 2:1, 4:1 and 8:1.

The aspect ratio tests returned identical values for the scalar flux, iterations to convergence and maximum and minimum scalar flux values for all spatial quadratures. Again, the test was also done using the  $S_6$  angular quadrature and a tolerance of  $10^{-5}$ . As noted earlier, this test confirms that cells with aspect ratios other than one returned consistent results when x and y values are interchanged.

### 3. Source Iteration Comparison

The last series of tests in this phase compare the converged solution from conventional source iteration with the DI solution. The scattering ratio was kept low so that the SI solution would not suffer from false convergence. An example of the problem and boundary conditions used is shown in figure 5.3 for a 10x10 spatial mesh. The spatial mesh is refined, from 10 cells by 10 cells to 100 cells by 100 cells. The cell scalar flux results for both SI and DI are compared to ensure the converged results are consistent.

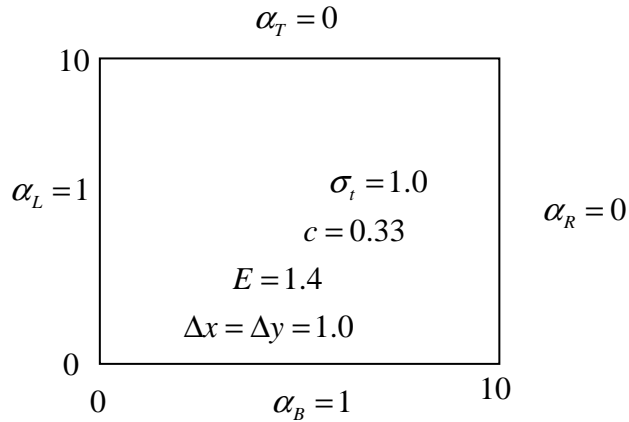


Figure 5.3. Problem variables for the source iteration comparison test problem.

#### Source Iteration Test Results

The results of the source iteration comparison tests are shown in figure 5.4. Again, the test was done using the  $S_6$  angular quadrature and a tolerance of  $10^{-5}$ . The solid line is the requested tolerance of  $10^{-5}$ . As noted earlier, this test confirmed that an independent source iteration calculation returned the same

values for the cell scalar fluxes as the DI method. The  $SRD(\phi_{DI}, \phi_{SI})$  was less than  $3.6 \times 10^{-6}$ , which is less than the  $10^{-5}$  tolerance, in every cell for seven trials with grids ranging from 10x10 to 100x100. This gives confidence that the code is consistent, however it is still possible that both the DI and the SI codes could be off by a common factor. To eliminate this possibility, the results are next compared to an independent solution.

#### 4. Benchmarking

After the initial checks and consistency checks are done, it is evident that the results from the code are consistent. Getting the same results for different problems from two different methods within the code shows consistency, but it does not demonstrate accuracy. To do this, the converged results must be compared to a known solution (benchmarked). Mathews' vacuum duct problem (10: x-8) is used as a benchmark. The benchmark problem is shown in figure 5.5.

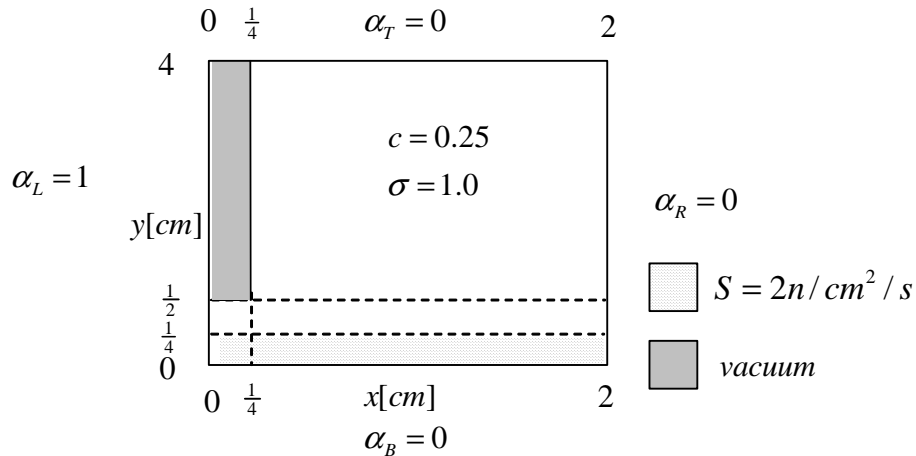


Figure 5.4. Problem variables for the benchmark problem.

## Benchmark Test Results

The results of a benchmark test for the SC spatial quadrature is shown in figure 5.5. Again, the test was also done using the  $S_8$  angular quadrature and a tolerance of  $10^{-5}$ . The solid line shows an independent Monte Carlo solution to the same problem (10: x-8). A ray effect due to the use of the  $S_8$  angular quadrature is seen in the location of the peak of the graph. Physically, the peak should be located over the duct, as shown by the Monte Carlo solution. This ray effect behavior is also consistent with previous results for this problem (10: x-10).

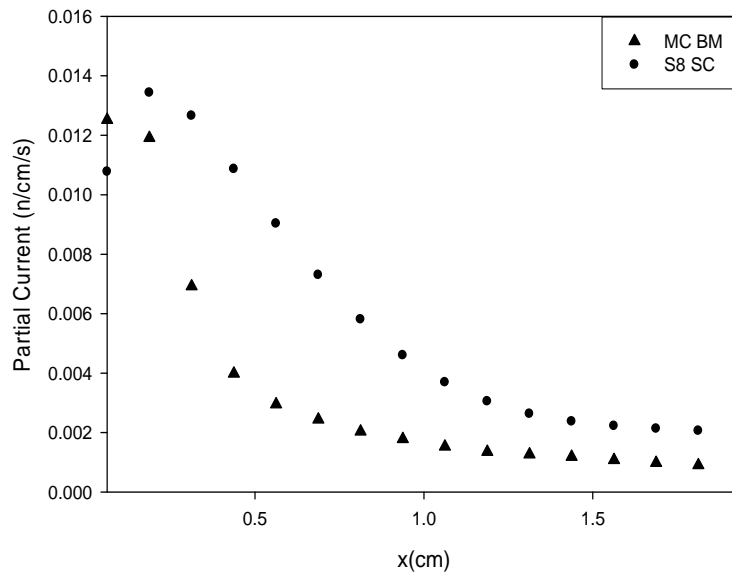


Figure 5.5. Results of the SC comparison with a Monte Carlo solution to the benchmark problem. The plot of the partial current out the top edge is shown for both methods.

The results of a benchmark test for linear discontinuous is shown in figure 5.6. Again, the test was done using the  $S_8$  angular quadrature and a tolerance of  $10^{-5}$ . The solid line shows an independent Monte Carlo solution to the same problem. As with the SC solution, a ray effect due to the use of the  $S_8$  angular quadrature is seen in the location of the peak of the graph. Again, this ray effect behavior is also consistent with previous results for this problem.

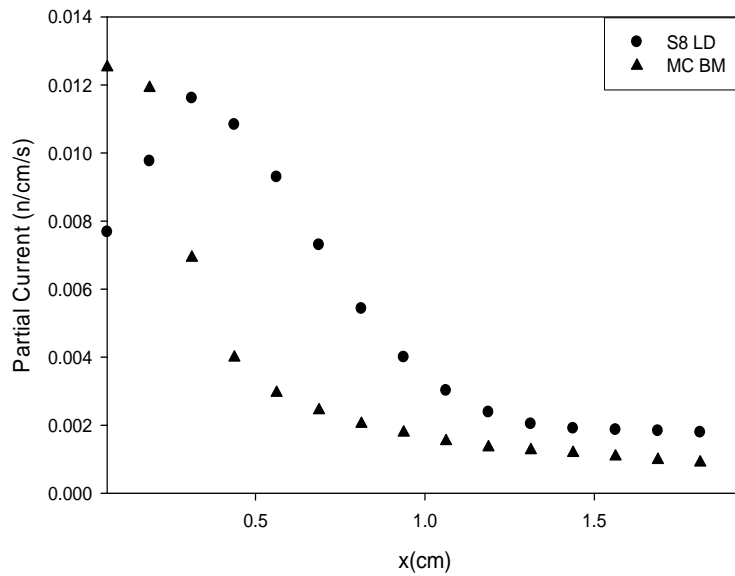


Figure 5.6. Results of the LD comparison with a Monte Carlo solution to the benchmark problem. The plot of the partial current out the top edge is shown for both methods.

For both the SC and LD solutions shown in figures 5.5 and 5.6, the important observation is not the ray effect, but the magnitude of the partial current calculated for both spatial methods. The scale of the DI result is

comparable to the Monte Carlo result in either case and validates the accuracy of the comparison done with SI in figure 5.4.

## **B. Routine Problem Comparison**

This section demonstrates the efficiency of this method by comparing the results for the DI method to published results for DSA methods for three different problems: varying aspect ratios, varying scattering ratios and varying mesh size, for given problems. The three problems were not particularly challenging for either method, but show how DSA methods and SI methods compare to the DI method for relatively straightforward problems. Morel et al. (14: 309-10) published results for DSA using Bi-Linear Nodal (BLN) and Waring et al. (17: 124-25) published results for DSA using Linear Bi-Linear Nodal (LBLN) spatial methods for the same set of three problems. The comparative measure used for each problem is the number of iterations needed to converge the cell scalar flux to a given tolerance. The DSA methods have an inner loop which is used to estimate the residual error at each step. For these problems listed, the DSA inner loop used a minimum of three passes to update the residual error estimate, while the DI method only had one pass through the among cell calculations (14: 306). However, for comparison purposes, an iteration is one complete cycle in each case, which should be a conservative comparison for the DI method.



## 1. Aspect Ratios

The first comparison problem examines results for a set of grids which differ in cell aspect ratio,  $\Delta y:\Delta x$ . The basic parameters for a homogeneous medium problem (14: 309, 17: 124) are shown in figure 5.7. The problem is intended to show for DSA methods the effectiveness in terms of error reduction per iteration. The problem was done using an  $S_4$  angular quadrature and converged to a tolerance of  $10^{-4}$  using the cell average scalar flux. The spatial grid has  $25 \times 25$  rectangular cells in each case; the problem size differs among the cases. The cells are not necessarily square. Aspect ratios of  $\Delta y:\Delta x = 2:1$ ,  $5:1$ ,  $10:1$  and  $20:1$  were tested.

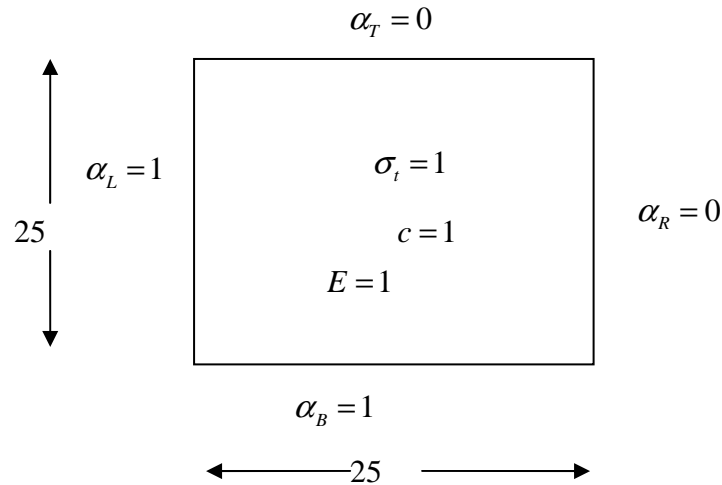


Figure 5.7. Problem variables for the DSA aspect ratio comparison.

The results for the aspect ratio tests for both DI and DSA (14: 309, 17: 124) are shown in table 5.2. As can be seen in the table, the zeroth spatial moment methods using DI (WDD and SC) converged faster than the DSA

methods, while the first moment methods using DI (LD and LC) were comparable to the DSA methods. The stability of the DSA methods shows that the iteration count does not increase as the aspect ratio increases. The zeroth spatial moment methods also show this, while the DI method shows a slight increase for high aspect ratios for first moment methods. For the 20:1 case, DI takes more iterations (10 for LD, 7 for LC) than DSA (6 for BLN, 6 for LBLN) but uses fewer discrete ordinates sweeps (10 for LD, 7 for LC) than DSA ( $\geq 18$  for each DSA calculation). While this problem does not definitely show the DI method as better, it does show that DI requires of the same order of iterations to converge for a totally scattering problem.

Table 5.2. DSA aspect ratio comparison results

		DI Methods				DSA Methods	
$\Delta x$	$\Delta y$	WDD	SC	LD	LC	BLD	LBLN
1.0	1.0	4	5	5	5	8	8
1.0	5.0	3	3	5	5	8	8
1.0	10.0	3	3	8	8	8	8
5.0	5.0	2	2	3	5	6	6
5.0	10.0	2	2	3	4	6	6
5.0	100.0	2	2	10	7	6	6
10.0	10.0	2	2	3	5	5	5
10.0	100.0	2	2	5	5	5	5
100.0	100.0	2	2	4	5	5	5

The same test was done using an adaptive DO sweeping technique in shown chapter two and described later in this chapter. The results are shown in table 5.3 with the original DSA results for comparison. The additional DO sweeps for each iteration only decrease the iteration count for a few of the tests, but this is by design. The adaptive technique is only to use additional DO sweeps for an iteration where the DI method is converging relatively slowly, which is only two of the tests the 1:10 and 1: 20 cases. For these problems, the number of iterations to convergence is a third smaller. For the other cases, the iterations to convergence is about the same or one less.

Table 5.3. DSA aspect ratio comparison adaptive DO sweep results

		DI Methods				DSA Methods	
$\Delta x$	$\Delta y$	WDD	SC	LD	LC	BLD	LBLN
1.0	1.0	4	5	4	3	8	8
1.0	5.0	3	3	4	3	8	8
1.0	10.0	3	3	5	5	8	8
5.0	5.0	2	2	3	3	6	6
5.0	10.0	2	2	3	3	6	6
5.0	100.0	2	2	4	3	6	6
10.0	10.0	2	2	3	3	5	5
10.0	100.0	2	2	4	4	5	5
100.0	100.0	2	2	2	3	5	5

The adaptive DO sweeping technique shows the DI method to be slightly better than DSA for this case in terms of iterations to reach convergence for this problem.

### Scattering Ratios

The next comparison problem examines results for grids which differ in cell scattering ratio. The basic parameters for another homogeneous medium are shown (14: 309, 17: 124) in figure 5.8. The problem is intended to show, for DSA and source iteration methods, the dependence of the efficiency upon the scattering ratio. The problems were solved using an  $S_4$  angular quadrature and cell average scalar fluxes were converged to a tolerance of  $10^{-4}$ . The problem uses a  $25 \times 25$  cell grid with  $\Delta x = \Delta y = 1$  mean free path (mfp).

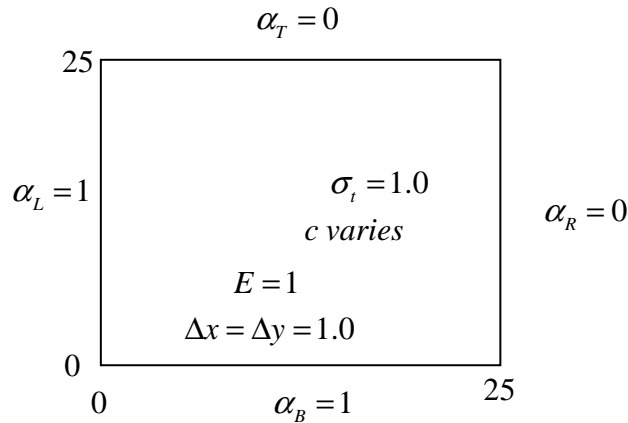


Figure 5.8. Problem variables for the DSA scattering ratio comparison.

The results for the scattering ratio comparison for unaccelerated SI, for DI, and for DSA-SI are shown in table 5.3. First consider SI versus DI. SC and LC have similar relative performance for SI and DI as WDD and LD. Both the

zeroth spatial moment methods using DI converged faster than source iteration using the same spatial method and angular quadrature. The DI zeroth spatial moment methods show that the iteration count went from three to four as the scattering ratio increased for this problem, while the SI methods climbed from twenty to over two thousand with higher scattering ratios. The DI first spatial moment methods again show the iteration count went from three to five as the scattering ratio increased for this problem, while the SI methods increased from ten to over two thousand with higher scattering ratios. It also shows the advantage of first moment methods for source iteration: the iteration count is much lower for the same problem than with a zeroth moment source iteration method. For DI methods, the iteration count was almost identical for both zeroth and first moment methods. This problem demonstrates the DI method as superior to (unaccelerated) source iteration for this case.

Table 5.4. DSA scattering ratio comparison results.

c	SI		DI		DSA	
	WDD	LD	WDD	LD	BLN	LBLN
1.0	2379	2020	4	5	8	8
0.9	171	94	3	4	7	7
0.8	93	50	3	4	7	6
0.7	64	34	3	4	6	6
0.6	49	26	3	4	5	5
0.5	40	20	3	3	5	5
0.4	34	17	3	3	5	4
0.3	29	14	3	3	4	4
0.2	26	12	3	3	4	4
0.1	23	9	3	3	3	3

Next consider DI versus DSA. The DI method converged slightly faster than DSA for almost all scattering ratios. The DI methods show very little increase in iteration (from 3 to 5) with increasing scattering ratio for this problem, while the DSA methods show a larger increase (from 3 to 8). This problem also shows the DI method to be slightly better than DSA for this case in terms of iterations to reach convergence.

### 3. Two Material Problem

The last comparison problem examines results for grids which differ in spatial mesh refinement for a two material problem. The basic parameters for another homogeneous medium are shown (14: 309, 17: 124) in figure 5.9. The problem is intended to show the effectiveness of DSA for inhomogeneous problems. The

problems were solved using an  $S_4$  angular quadrature and cell average scalar fluxes were converged to a tolerance of  $10^{-4}$ . The spatial grid size remained fixed at 50 cm for this problem while  $\Delta x$  and  $\Delta y$  both vary at the same ratio, thereby refining the spatial mesh for the problem. Mesh sizes of 5x5, 10x10, 25x25 and 50x50 were tested. For these mesh sizes, the cell thicknesses were 10 cm, 5 cm, 2 cm and 1 cm respectively.

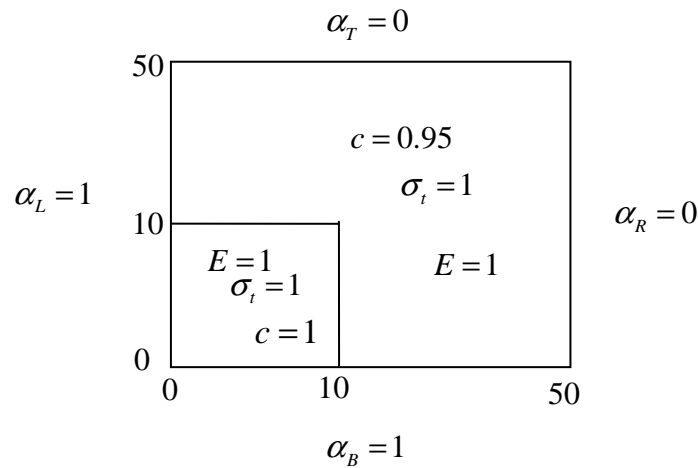


Figure 5.9. Problem variables for the two material DSA comparison problem.

The DI results for the mesh refinement problem, along with the published DSA results (14: 309, 17: 124), are shown in table 5.5. As can be seen in the table, the DI method converged slightly faster than the DSA methods for these cell sizes. Again, while this problem does not definitely show the DI method as better than DSA, it does again show that DI converges in the same number of iteration or slightly fewer iterations for a highly scattering problem.

Table 5.5. DSA two material comparison results.

Mesh	DI Methods				DSA Methods	
	WDD	SC	LD	LC	BLD	LBLN
5x5	2	2	4	5	6	6
10x10	2	3	4	5	8	7
25x25	3	4	4	4	9	8
50x50	4	6	6	5	8	7

In chapter two, figure 2.1 shows an inner loop doing the local balance coupling labeled “iterate as needed”. The discussion following the figure discussed the fact that some problems needed additional loops with discrete ordinates sweeping. For the problems presented so far, only one discrete ordinates sweep was sufficient for the DI method to converge in a few iterations. However, there were problems in which additional loops through the discrete ordinates sweeping were needed but this also depended on the spatial method used. This led to an adaptive technique which varied between one and ten sweeps depending on the properties of the problem. Timing analysis showed that ten sweeps would at most double the time for an iteration. For each sweep, the scattering source was updated using the cell edge currents and the scattering source was used to calculate new cell edge currents. A detailed analysis of the adaptive technique is presented in chapter seven, but the technique was used for some of the problems in chapter six, as well as in the first DSA comparison problem for this chapter.



This chapter showed the validity of the DI results through a variety of test problems. In addition, this chapter showed that the DI method performed much better than SI for higher of scattering ratios. Finally, these problems show the performance of DI is comparable to the effectiveness of DSA with a similar computational effort based on a conservative iteration count. In the next chapter, problems where synthetic acceleration has difficulties are examined.

## VI. Challenging Problems – Comparison with DSA and TSA

### A. Where DSA Loses Effectiveness

The previous chapter shows how DI performance was comparable to DSA on several routine problems. Recently, it has been shown that DSA can lose its effectiveness or converges slowly for a particular problem. (3: 213, 18: 1) This was shown using a test that has alternating layers of two different materials that are highly scattering. The particular problem's parameters given by Azmy (3: 228-229) are shown in figure 6.1. For this problem, different total cross sections will be compared with different mesh sizes which varied from a 10x10 spatial mesh to a 160x160 spatial mesh.

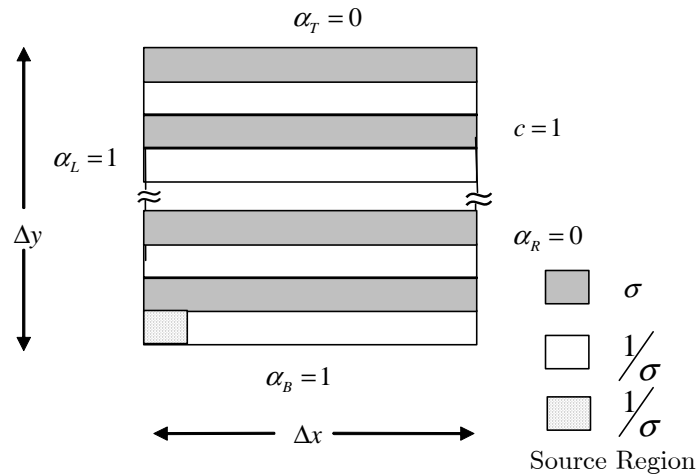


Figure 6.1. Problem variables for the Azmy Periodic Horizontal Interface (PHI).

An  $S_6$  angular quadrature was used for this problem to compare with the published results in the article. The convergence tolerance of  $10^{-6}$  was used for the relative difference in the cell average scalar flux.

The measure of effectiveness used for this problem is the spectral radius. For a converging system of equations, the spectral radius is between zero and one. A spectral radius which is close to zero indicates that the system of equations converges rapidly. Conversely, a spectral radius close to one indicates the system of equations converges slowly. Additionally, a spectral radius of one or greater indicates system of equations that diverges (6: 229). Often calculating the eigenvalues or spectral radius for a large system of equations is impractical. Azmy estimates the spectral radius using the ratio of the  $L_2$  norm of the residual in the cell average scalar flux to the previous iterate as follows:

$$\rho_l \approx \frac{\|\phi_l - \phi_{l-1}\|_2}{\|\phi_{l-1} - \phi_{l-2}\|_2}. \quad (6.1)$$

The spectral radius is computed for the iteration in which the problem met the convergence tolerance (3: 213-216).

For the DI method, testing showed that the spectral radius calculated this way could vary with the chosen tolerance or iteration even though the method was converging in a few iterations. Another method of estimating the spectral radius or convergence rate was developed. The maximum SRD of the scalar flux

between iterations is shown for two different cross sections in figures 6.2 and 6.3.

The solid line represents the convergence tolerance in Azmy's problem.

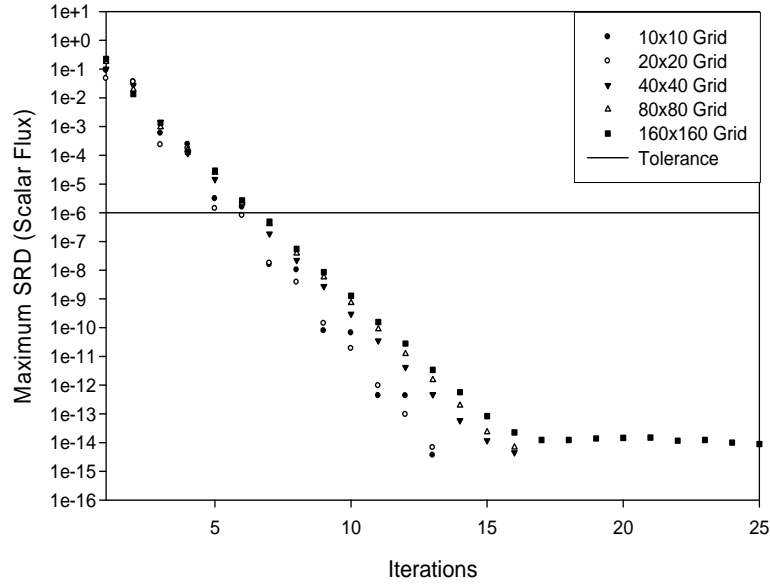


Figure 6.2. Convergence rates for the Azmy Periodic Horizontal Interface (PHI) problem with DI using WDD and  $S_6$  at  $\sigma=10$  cross section for various mesh sizes.

These problems are done to a much tighter tolerance,  $10^{-14}$  and for all the different spatial meshes that the DSA test problem were done. The figures demonstrate two points, the maximum SRD of the scalar flux decreases by a fairly constant amount per iteration and the problem can be run to very tight tolerances which show the problem does not suffer from bad numerical conditioning. The rate of decrease in the maximum SRD is the DI method estimate of the spectral radius or convergence rate. The convergence rate is found by doing a linear regression of the linearized data which is shown in the figures. One note is that this maximum SRD estimate is an asymptotic value.

For problems with reasonable tolerances, for example  $10^{-4}$  is commonly used, the problem would converge faster than the DI estimate of the spectral radius would predict.

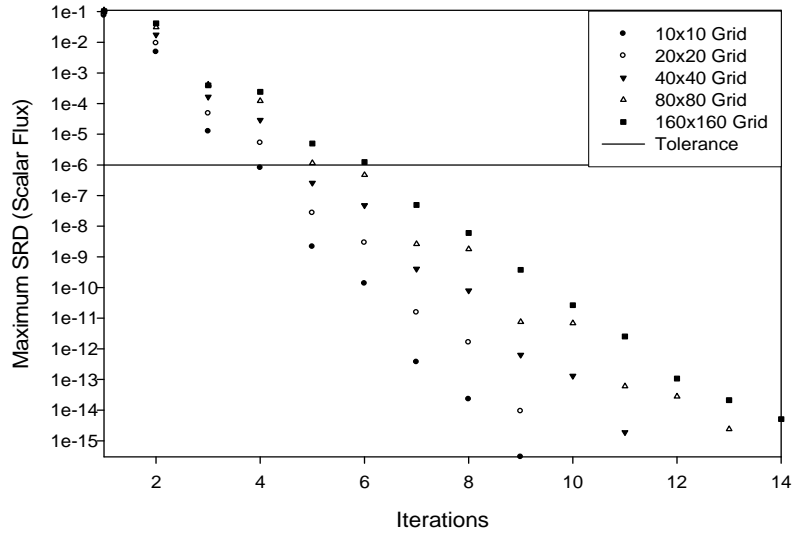


Figure 6.3. Convergence rates for the Azmy Periodic Horizontal Interface (PHI) problem with DI using WDD and  $S_6$  cross section  $\sigma = 160$  for various mesh sizes.

Another observation from the two plots shown in figure 6.2 and 6.3 is that the rate of convergence does change with cross sections and mesh size. For the cross section shown in figure 6.2 the spectral radius is fairly constant as the mesh is refined. This can be seen by the fact the iteration count does not change significantly as the spatial mesh is changed. On the other hand, for the cross section used in figure 6.3, the number of iterations needed to reach the final tolerance almost doubles as the mesh gets larger. The convergence rates for these

plots will be discussed shortly. For the DI results shown in table 6.2 and 6.4, the adaptive DO sweeping technique was used.

### 1. Weighted Diamond Difference Comparison

The published results for the Azmy PHI problem using DSA with WDD and an  $S_6$  angular quadrature are shown in table 6.1 (3: 231). As seen in the table, the spectral radius increases strongly with the number of cells, indicating slower convergence. For this DSA method, going to larger problems of this type will lead to slowly converging solutions. Hence, DSA is no longer accelerating the solution for a large enough problem of this type or loses effectiveness.

Table 6.1. Published DSA with WDD Results.

	Cross Sections				
Mesh	10	20	40	80	160
10x10	0.100	0.039	0.010	0.002	4E-4
20x20	0.241	0.132	0.044	0.010	0.002
40x40	0.422	0.316	0.151	0.046	0.010
80x80	0.581	0.539	0.360	0.160	0.048
160x160	0.683	0.713	0.609	0.386	0.165

The DI results for the Azmy PHI problem using WDD with DI and  $S_6$  angular quadrature are shown in table 6.2. The spectral radii, or convergence rates, listed in the table were determined using the slope of the linearized plots, as described previously. Contrary to the DSA solutions, the DI method does not increase strongly for larger problems. In addition, the total number of iterations needed to solve a difficult problem remains small. For this problem, DI with

WDD showed good performance and was considerably better than DSA with the same spatial and angular quadratures.

Table 6.2. DI with WDD results.

Mesh	Cross Section				
	10	20	40	80	160
10x10	0.079671	0.061348	0.046345	0.001066	0.000303
20x20	0.077822	0.083753	0.057003	0.016199	0.002528
40x40	0.09177	0.07236	0.085153	0.049317	0.012909
80x80	0.08531	0.104472	0.067329	0.081133	0.036083
160x160	0.122462	0.098787	0.110332	0.064091	0.081433

## 2. Linear Discontinuous Comparison

Azmy's results for the Azmy PHI problem using a Bi-Linear Nodal method with DSA and  $S_6$  angular quadrature are shown in table 6.3 (3: 232). Again, the spectral radius increases for larger meshes for certain cross sections. For this DSA method, going to larger problems will lead to slowly converging solutions. For example, the spectral radius listed for the cross section  $\sigma = 20$  and mesh of 160, took 388 iterations to meet the tolerance of  $10^{-6}$  (3: 231). In addition, for several cross sections, this method diverged.

Table 6.3. Published DSA with BLN Results.

	Cross Sections				
Mesh	10	20	40	80	160
10x10	0.355	0.254	0.192	D	D
20x20	0.543	0.417	0.317	D	D
40x40	0.717	0.607	0.452	D	D
80x80	0.836	0.688	0.624	D	D
160x160	0.901	0.392	0.671	D	D

The DI results for the Azmy PHI problem with LD and an  $S_6$  angular quadrature are shown in table 6.4. The spectral radii listed in the table were again determined using the linear regression of the slope of the linearized plots.

Table 6.4. DI with LD results.

	Cross Section				
Mesh	10	20	40	80	160
10x10	0.101	0.115	0.089	0.059	0.044
20x20	0.101	0.117	0.118	0.075	0.053
40x40	0.194	0.099	0.124	0.094	0.055
80x80	0.269	0.216	0.153	0.140	0.099
160x160	0.245	0.302	0.160	0.179	0.133

Unlike the zeroth spatial moment method, the convergence rates for DI method with first spatial moment methods do increase slightly with larger problems. However, the spectral radius is still much better than the DSA methods and the DI method works for all the cross sections tested (did not diverge). Also, and for the WDD results as well, the calculated spectral radii are



an asymptotic value from the plots of convergence rates. Just using the problem set tolerance of  $10^{-6}$  would have given lower spectral radii.

The DI method has demonstrated an improved performance over DSA for this particular problem. The rate of convergence for zeroth spatial moments methods is clearly superior for DI. The convergence rate stays almost constant while the DSA method increased strongly with an increase in the number of cells. The first moment methods also had good improvement in the rate of convergence, and the DI methods were able to solve the problem for cross sections the DSA method diverged on.

### **3. Azmy PHI Timing Analysis**

The DI method showed good improvement over the DSA method performance for the Azmy PHI problem, particularly for the zeroth spatial moment method of WDD. Two questions to be answered are: where does the DI method spend its computational effort; and how does the effort change as the number of cells increase? An intrinsic FORTRAN timing function was used to determine the amount of time spent in each portion of the DI iteration.

The DI iteration is separated into two parts for timing purposes; discrete ordinates sweep cell calculations; and the partial current problem. The discrete ordinates sweep cell calculations will be further broken down into the within cell calculation and the discrete ordinates sweep. For timing purposes, only a single within cell calculation and discrete ordinates sweep will be timed. The actual

times can be scaled from these time values. The partial current problem is further separated into the collapsing / setting up the partial problem and the time needed for the CXML library routine to solve the partial current problem. The timing analysis was done for the DI method with WDD and LD using  $S_6$  and a cross section  $\sigma = 10$ .

### Zeroth Spatial Moment Methods

The WDD results of the time analysis for the main parts of a DI iteration: the iterations time; among cell calculation time; and partial current problem time are shown in table 6.5. As can be seen in the table, the time for the partial current problem is most of the iteration time, more than three times the discrete ordinates sweep cell calculation time. Additionally, separate log-log plot shows that the iteration portions of the code scale linearly with the number of cells, with a slope of 1.00. SC gave nearly identical timing results for the zeroth spatial moment tests.

Table 6.5. WDD Iteration Timing.

Number of Cells	Time (s)		
	Iteration	Partial Current Problem	Among Cell Calculations
100	0.063	0.047	0.019
400	0.234	0.188	0.047
1600	0.938	0.766	0.172
6400	4.000	3.281	0.656

The WDD results of the time analysis for the partial current problem are shown in table 6.6. As can be seen in the figure, the predominance of the time for the partial current problem is used for collapsing and setting up the partial current problem due to the number of matrix multiplications that are done.

Table 6.6. WDD Partial current problem timing.

Number of Cells	Time (s)		
	Partial Current Problem	Collapsing	Direct Solver
100	0.047	0.031	0.016
400	0.188	0.141	0.031
1600	0.766	0.547	0.172
6400	3.281	2.234	0.906

The WDD results of the time analysis for the discrete ordinates sweep cell calculations is shown in table 6.7. As can be seen in the table, most of the time is for within cell calculation, again doing the matrix multiplications, and is about twice the time for the discrete ordinates sweep.

Table 6.7. WDD Discrete ordinates sweep timing.

Number of Cells	Time (s)		
	Among Cell Calculations	Update Scattering Source	DO Sweep
100	0.019	0.016	0.004
400	0.047	0.031	0.016
1600	0.172	0.109	0.063
6400	0.656	0.391	0.266

### First Spatial Moment Methods

A similar analysis was done for the LD spatial method. The LD results of the time analysis for the main parts of a DI iteration: the iterations time; discrete ordinates sweep cell calculation time; and partial current problem time are shown in table 6.8. As can be seen in the table, the time for the partial current problem is most of the iteration time, more than ten times the among cell calculations time. This is significantly more than the zeroth spatial moment methods, and due to the additional matrix multiplications used in collapsing to set up the partial current problem. Additionally, separate log-log plots show that the iteration portions of the code scale linearly with the number of cells with a slope of 0.9969. LC gave nearly identical timing results for the first spatial moment tests.

Table 6.8. LD Iteration timing.

Number of Cells	Time (s)		
	Iteration	Partial Current Problem	Among Cell Calculations
100	0.469	0.422	0.047
400	1.828	1.656	0.172
1600	7.328	6.688	0.609
6400	29.547	26.969	2.484

The LD results of the time analysis for the partial current problem time are shown in table 6.9. As can be seen in the table, the predominance of the time for the partial current problem is collapsing and setting up the partial current problem. The CXML direct solver actually takes the same amount of time as the zeroth spatial moment methods. This is to be expected, the actual problem size is the same for both methods.

Table 6.9. LD Partial current problem timing.

Number of Cells	Time (s)		
	Partial Current Problem	Collapsing	Direct Solver
100	0.422	0.422	0.016
400	1.656	1.625	0.031
1600	6.688	6.469	0.172
6400	26.969	25.875	0.906

The LD results of the time analysis for the discrete ordinates sweep cell calculation time is shown in table 6.10. As can be seen in the table, most of the time is for the within cell calculation again, updating the scattering sources, significantly more than the discrete ordinates sweep.

Table 6.10. LD Discrete ordinates sweep timing.

Number of Cells	Time (s)		
	Among Cell Calculations	Update Scattering Source	DO Sweep
100	0.047	0.031	0.016
400	0.172	0.141	0.031
1600	0.609	0.531	0.078
6400	2.484	2.156	0.328

The timing analysis of the DI method showed three important points. First, the problem iteration time scales linearly with the number of cells. This will be important when using the DI method to solve very large problems in higher dimensions. Second, the among cell calculations using a within cell calculation followed by a discrete ordinates sweep is an efficient way to update the cell edge values. The computation cost of the discrete ordinates sweep cell algorithm is less than doing two within cell calculations to update cell edge values. Lastly, most of the computational effort for an iteration is in setting up and solving the partial current problem. The discrete ordinates sweep cell calculations are a smaller part of the computational effort, particularly with first

moment methods. The timing analysis showed that additional effort could be applied to improving  $\zeta$  without a significant computational cost as is done in the discrete ordinates sweep method.

## **B. Where TSA Fails**

The Azmy PHI problem showed how the DSA method lost effectiveness, or converged slowly across a variety of cross sections and meshes. Another periodic horizontal interface (PHI) problem reported by Chang and Adams (5: 1) demonstrated how TSA methods diverged for certain cross section combinations. This next problem also uses pairs of cross sections, but the layout and source are slightly different from the Azmy PHI used in the last section. This next problem, hereafter referred to as the Chang problem(5: 11), uses a fixed mesh of 100 cm by 200 cm and varies the two different cross sections during these tests. Each cell is set at 1 cm by 1 cm and there are incident boundary currents on the bottom and left sides with no sources within the problem. The layout of this problem is shown in figure 6.4.

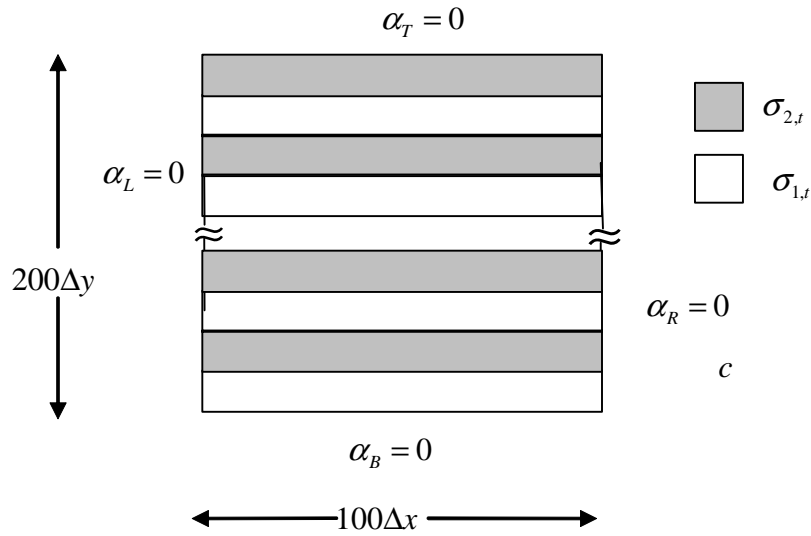


Figure 6.4. Problem variables for the Chang Periodic Horizontal Interface (PHI).

The problem was done for different scattering ratios and to a tolerance of  $10^{-7}$  using the cell average scalar flux. As with the DSA PHI problem, the measure of effectiveness used in this article was the spectral radius, which is determined using the relation described in equation (6.1) for the published results. The numerical results of the TSA method using diamond difference (DD) showed that certain cross sections caused the method to diverge, as can be seen by spectral radii greater than one. This data will be presented later in this chapter. The DI method was done with a single discrete ordinates sweeping method initially for comparison. The DI method used the same linear regression procedure that was used with the Azmy PHI to determine the convergence rates.



## 1. Weighted Diamond Difference Comparison

An example of how the SRD of the scalar flux changed per iteration for the DI method with WDD is shown in figure 6.5 for a scattering ratio of  $c = 0.9$ .

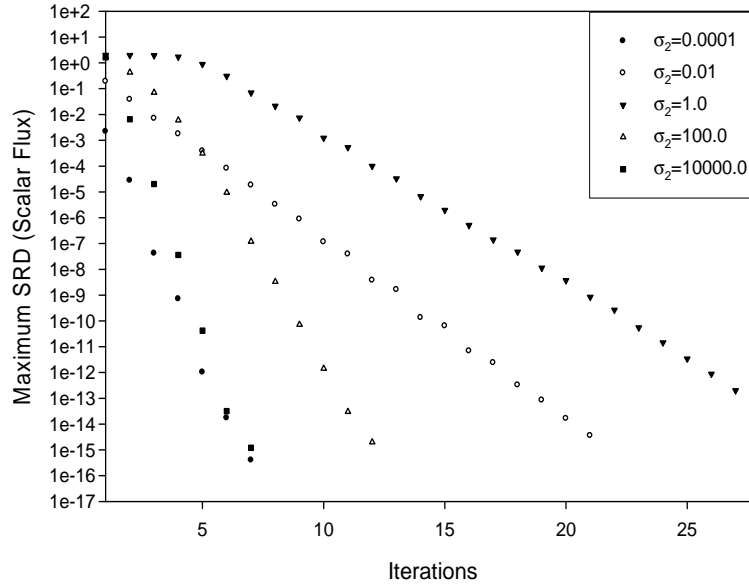


Figure 6.5. Convergence rates for the Chang Periodic Horizontal Interface (PHI) problem with DI using WDD and  $S_6$  for  $\sigma_1 = 10^{-4}$  and  $\sigma_2$  at various cross section combinations with a scattering ratio of 0.9.

As can be seen in figure 6.5, there are particular cross section combinations for which the problem converges slower. The fastest convergence occurs when the two cross sections are the same, making it a homogeneous problem. The rates of convergence are listed in table 6.11 along with TSA results (5: 11) for comparison.

Table 6.11. Chang PHI Test for  $c = 0.9$ , with DI WDD using  $S_4$ , and TSA DD using  $S_4 / S_2$ .

	$\sigma_{1,t} = 0.0001$		$\sigma_{1,t} = 1.00$		$\sigma_{1,t} = 10000.0$	
	Spectral Radius		Spectral Radius		Spectral Radius	
$\sigma_{2,t}$	DI	TSA	DI	TSA	DI	TSA
0.0001	0.004677	0.0014	0.277204	4.5255	0.002214	0.0397
0.01	0.212961	0.0793	0.273905	4.1231	0.019761	0.1745
1.00	0.273779	4.5254	0.119207	0.4639	0.12368	0.4521
100.0	0.023046	1.1009	0.120754	0.4741	0.000194	0.0783
10000.0	0.002211	0.0398	0.12314	0.4562	8.87E-08	0.0089

Note that for four different cross section combinations, the TSA method diverged. This is indicated by a spectral radius greater than one. However, for this case, the DI method performed well having a spectral radius less than 0.3 for all cross sections and only using a single discrete ordinates sweep per iteration. For only one combination of cross sections, where TSA worked well, the TSA spectral radius was smaller than the DI method spectral radius. Note these problems were done with similar spatial methods and similar angular quadratures.

For higher scattering ratios,  $c = 0.99$  and a higher order angular quadrature, the following comparisons (5: 14) can be made in table 6.12.

Table 6.12. Chang PHI Test for  $c = 0.99$  with DI Results WDD using  $S_6$ , and TSA DD Results using  $S_6/S_2$ .

	$\sigma_{1,t}=1.00$	
	Spectral Radius	
$\sigma_{2,t}$	DI	TSA
0.0001	0.4858	32.5264
0.01	0.4802	20.1193
1.00	0.1017	0.5865
100.0	0.0928	1.2958
10000.0	0.1196	0.5458

Note that for the same cross section combinations that diverged in the previous problem, the TSA method also diverges for this case, as well as another combination of cross sections. The DI method converges for this problem using one discrete ordinates sweep per iteration. The performance is somewhat slower for the particular cross section pairs where TSA diverged for this case. However, the rates of convergence for the other cross sections remains about the same or slightly faster than the  $c = 0.9$  scattering ratio case while the TSA method is much slower.

Although TSA method did not give results for scattering ratios of  $c = 1.0$ , since it had already diverged for lower scattering ratios, the DI method was also done for totally scattering problems to see if the DI method would solve these problems with a single discrete ordinates sweep. This would make this particular problem as difficult as it could be.

As can be seen in table 6.13, the rate of convergence for this scattering ratio is again much slower for certain cross sections combinations.

Table 6.13. Chang PHI Test for  $c = 1.0$ , DI with WDD using  $S_6$

$\sigma_{2,t}$	$\sigma_{1,t} = 0.0001$	$\sigma_{1,t} = 1.00$	$\sigma_{1,t} = 10000.0$
	Spectral Radius	Spectral Radius	Spectral Radius
1.00E-04	0.006858	0.653732	0.420436
1.00E-02	0.234153	0.641062	0.406724
1.00E+00	0.651778	0.111584	0.04627
1.00E+02	0.397283	0.038089	3.7E-05
1.00E+04	0.395913	0.038089	2.12E-06

For the combinations where TSA diverged previously, the DI method performance was again slower but still converged. The other cross sections continued to converge at the same or a faster rate.

Again, the DI results with WDD are presented here using only a single discrete ordinates sweep per iteration. The Chang PHI problem was challenging for the DI method for certain cross section combinations, but these are the same cross section combinations which caused the TSA method to diverge for this particular problem.

## 2. Other Spatial Method Comparison for Chang PHI Problem

The next section demonstrates the effect the adaptive discrete ordinates sweep has on convergence rates for this problem. The adaptive technique is applied to the Chang PHI problem for the particular cross sections that challenged the DI method. These cross sections,  $\sigma_{1,t} = 1.0$  and  $\sigma_{2,t} = 0.0001$ , are

the same cross sections where the TSA method diverged for all scattering ratios. The results for these cross sections using the four spatial DI methods are listed in table 6.14 with scattering ratio of  $c = 0.9$ . As a comparison of note, the TSA method using DD had a spectral radius of 4.5255 or diverged (5: 11).

Table 6.14. Chang PHI Problem for  $c=0.9$  using  $S_6$ .

TSA DD	Spectral Radius	
4.5255		
Method	1x DO sweep	Adaptive DO sweep
WDD	0.259	0.198107
SC	0.431519	0.25439
LD	0.466337	0.249747
LC	0.473478	0.243725

All the spatial methods show improvement in the rate of convergence for the adaptive discrete ordinates sweep over a single DO sweep per iteration.

The same case was done again for a scattering ratio of  $c = 0.99$ . The results are listed in table 6.15. Again, note the TSA method diverged (5: 14) for this case. The adaptive discrete ordinates sweep technique shows improvement over a single DO sweep per iteration in the rates of convergence for all the spatial methods tested with the DI method.

Table 6.15. Chang PHI Problem for  $c=0.99$  using  $S_6$ .

TSA DD	Spectral Radius	
32.5264		
Method	1x DO sweep	Adaptive DO sweep
WDD	0.4858	0.3907
SC	0.7217	0.5471
LD	0.8285	0.4851
LC	0.7783	0.5058

Although the TSA method was not done for a scattering ratio of  $c = 1.0$ , this combination of cross sections caused the DI method with SC to diverge as well. The TSA PHI problem was done again using the adaptive discrete ordinates sweep and the results are shown in table 6.16.

Table 6.16. Chang PHI Problem for  $c=1.0$  using  $S_6$

TSA	Spectral Radius	
N/A		
Method	1x DO sweep	Adaptive DO sweep
WDD	0.6537	0.5786
SC	N/A	0.9001
LD	0.9468	0.7140
LC	0.8707	0.6438

The results also show that the adaptive discrete ordinates sweep technique improve the rates of convergence for the DI method. The adaptive DO sweep technique also stabilizes the SC spatial method, which had previously diverged for this problem.

This section showed that the improved performance for the DI method over TSA for this particular problem. The DI WDD method converged reliably where TSA DD did not. The DI method rate of convergence was considerably faster than TSA when TSA did work.

## VII. Additional Tests

This section shows the development and analysis of the adaptive DO sweep technique that was used in chapter six. Earlier testing on the Chang PHI problem showed areas where the DI method performance was challenged for certain spatial methods and scattering ratios. In an attempt to fully challenge the method, another degree of interfaces or a checkerboard of alternating cells was added. Also, to further stress the DI method with this problem, the cross sections that caused the TSA method to diverge and showed slower convergence rates for DI were chosen. The cross section values used were  $\sigma_{1,t} = 1.0$  and  $\sigma_{2,t} = 0.0001$ , and the scattering ratio is set to one.

### A. The Checkerboard Problem

The problem used incident currents on the left and bottom side, like the Chang PHI problem. A diagram of the problem is shown in figure 7.1. For this problem, the  $S_6$  angular quadrature was used. The number of  $x$  and  $y$  cells were the same for each case and varied from 25 to 125 each.



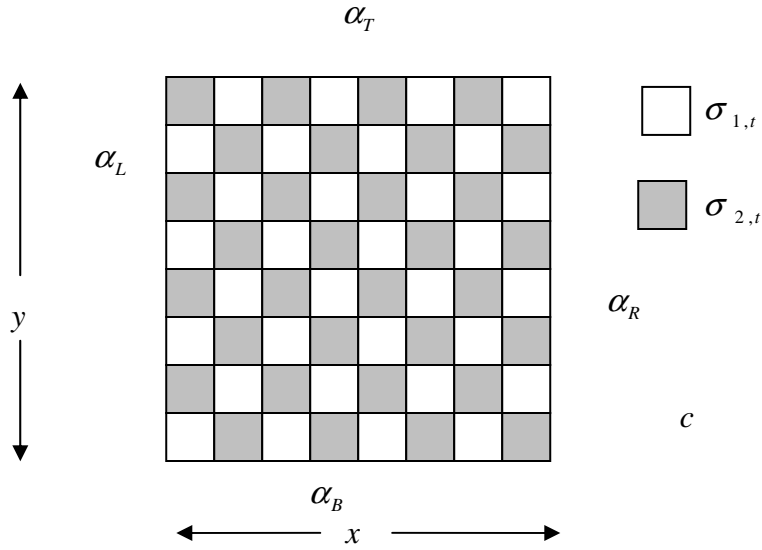


Figure 7.1. Problem variables for the checkerboard problem.

### 1. Spatial Method Performance

As was shown in the chapter six, other spatial methods did not perform as well as WDD for the Chang PHI problem with these particular cross sections and scattering ratio. The rate of convergence for the checkerboard problem can be seen in figure 7.2 for all the spatial methods currently implemented in DI using a single discrete ordinates sweep.

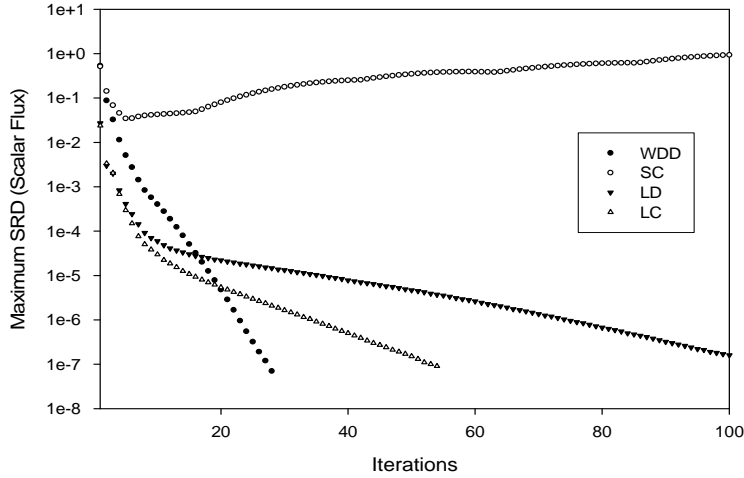


Figure 7.2. DI Convergence rates for different spatial methods on the checkerboard problem for a single DO sweep.

As can be seen in figure 7.2, SC does not converge for this problem (like the Chang PHI problem) with one DO sweep. The first spatial moment methods are slow to converge for tolerance  $>10^{-4}$  while WDD converges in the fewest number of iterations. The performance of the spatial methods for the Chang PHI problem gave similar results. This performance in figure 7.2 for the DI method indicated that the checkerboard problems were taxing the DI method using only one DO sweep per iteration for several spatial methods.

## 2. Edge Distribution Improvement

The initial attempt at how the number of DO sweeps per iteration influences the overall performance is shown in figure 7.3. In this case, the number of discrete ordinate sweeps was increased from one time per iteration to three times per iteration for each of the four spatial methods.

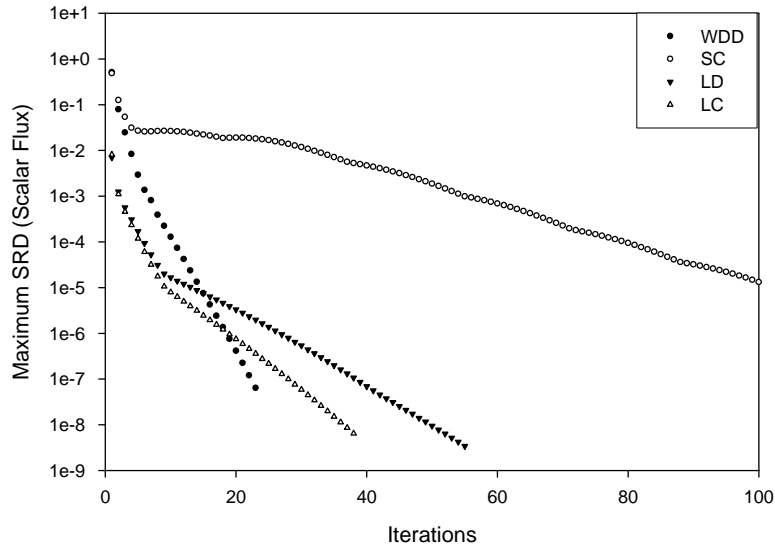


Figure 7.3. DI Convergence rates for different spatial methods on the checkerboard problem for a three DO sweeps.

Figure 7.3 shows several important points. With the additional discrete ordinate sweeps, SC is now converging slowly as opposed to diverging, and the first spatial moment methods are converging faster, especially LD. However, the effect on WDD is small, there is little change in the convergence rate.

This spatial method dependence led to the concept of letting the code decide how much effort to put into discrete ordinate sweeps, or an adaptive technique to estimate how many discrete ordinates sweeping cell calculations to do. For spatial methods that are working well, like WDD, there is little advantage to doing additional discrete ordinate sweeps. For spatial methods that are not performing well, like SC, more effort in the discrete ordinates sweeping cell calculations should help the problem converge quicker. There should be a

limit to the maximum number of discrete ordinates sweeping cell calculations. A first estimate of what the maximum should be is based on the results of the timing analysis. The partial current problem time during an iteration, for the first spatial moment methods, was about ten times longer than the discrete ordinates sweeping cell calculations. Thus ten was chosen as the maximum, as it would at most double the iteration time for the first spatial moment methods. The adaptive technique used the ratio of the maximum value in the SRD of the edge distribution  $\zeta$  for the current and previous iteration.

$$\text{Number of DO sweeps} = \text{Maxvalue} \times \frac{\text{Max}(\text{SRD}(\zeta^l, \zeta^{l-1}))}{\text{Max}(\text{SRD}(\zeta^{l-1}, \zeta^{l-2}))} \quad (7.1)$$

The ratio of the maximum values of the SRD of  $\zeta$  should be less than one for a method that is converging and much less for one that is converging quickly. For methods that are working well, only one discrete ordinates sweeping calculation is enough to improve the estimate of  $\zeta$  and the ratio should reflect that. Methods that need additional effort would have more discrete ordinate sweeps up to ten. The results of the adaptive algorithm are shown in figure 7.4.

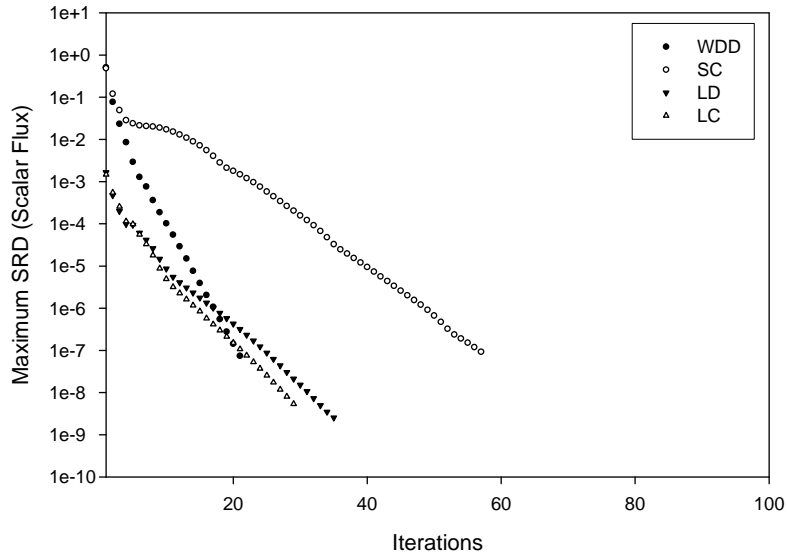


Figure 7.4. DI Convergence rates for different spatial methods on the checkerboard problem for the adaptive DO sweep technique.

As in the multiple calculations shown in figure 7.3, the adaptive technique used in figure 7.4 shows similar results with a few key differences. The performance of the first spatial moment methods, LD and LC, is better, converging in fewer iterations. Also performance of SC which was slow or even diverged in the previous two cases, is much improved. The SC method now converges readily. Again, the improvement of WDD is not significant, it has been working well previously. The number of iterations need to reach a tolerance of  $10^{-7}$  is shown in table 7.1.

Table 7.1. Number of DI iterations for the checkerboard problem.

Spatial Method	DO Sweep Cell Calculation Technique		
	1x	3x	Adaptive
WDD	28	23	21
SC	Div	>100	57
LD	>100	55	35
LC	54	38	29

The improvement in performance for some spatial methods is considerable for this simple adaptive technique. Another optimization of the technique, or different choice for the maximum number, may give even better performance. However, this simple adaptive method is sufficient to show the robustness of the DI method and the importance of efficiently improving the estimate of  $\zeta$  values for difficult problems.

Table 7.2. Total number of DO sweeps for the checkerboard problem

Spatial Method	Number of DO Sweep Calculations		
	1x	3x	Adaptive
WDD	28	69	83
SC	Div	>300	393
LD	>100	165	220
LC	54	114	156

Table 7.2 shows the total number of discrete ordinate sweeps done for each of the different spatial methods. For each case, the total number of discrete ordinate sweeps is two to three times more. However, these calculations are the

comparatively inexpensive part of the overall iteration calculation. Timing analysis shows that setting up and solving the partial current problem is most of the computational time of an iteration. Improving the estimate of  $\zeta$  values during the among cell calculations is more important than setting up and solving more partial current problems.

### **3. Timing Analysis**

The maximum number of discrete ordinate sweeps was chosen so as to at most double the iteration time for the first spatial moment methods. This leads to the question of what does the additional calculations do to the total time to solving the problem? The plot of the total time for the DI WDD method comparing the difference in time as the number of cells increase is shown in figure 7.5.

As can be seen in figure 7.5, the total time is slightly more, even though the number of discrete ordinate sweeps cell calculations tripled as shown in table 7.2. This is due to the fewer number of total number of iterations shown in table 7.1 which offset the time for the additional discrete ordinate sweeps cell calculations.

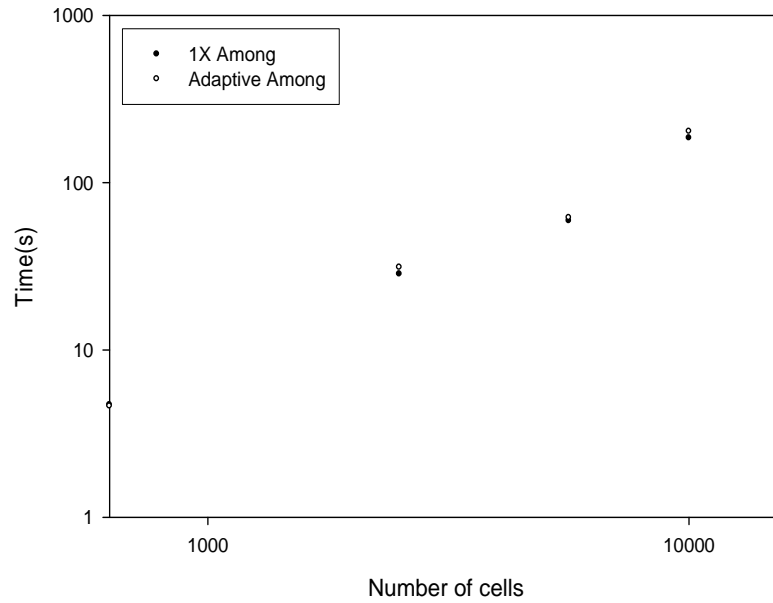


Figure 7.5. Comparison of total convergence time for the checkerboard problem with DI using WDD for a single DO sweep and the adaptive DO sweep technique.

The first spatial moment time is more interesting, as the maximum number of sweeps was chosen for these methods in particular. The plot of the total time for the DI LD method comparing the difference in time as the number of cells increase is shown in figure 7.6.



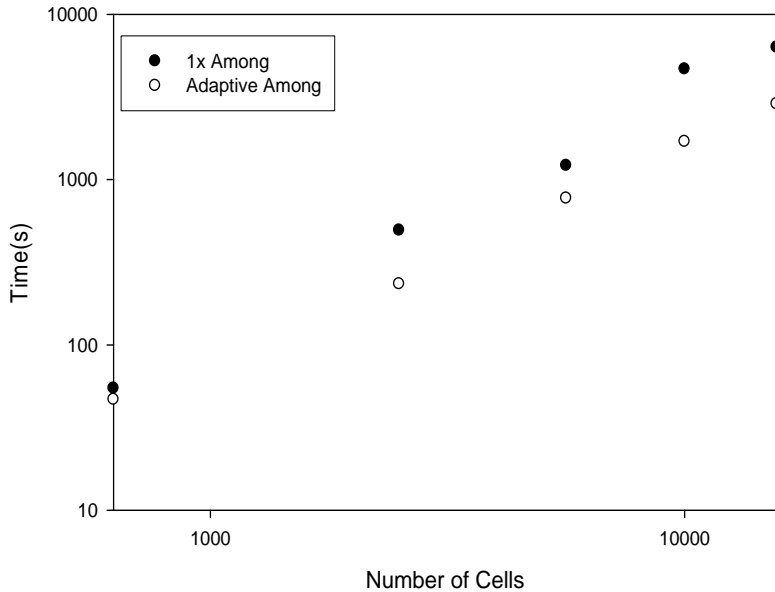


Figure 7.6. Comparison of total convergence time for the checkerboard problem with DI using LD for a single DO sweep and the adaptive DO sweep technique.

As can be seen in the figure, the total time is consistently less for the adaptive technique by as much as a factor of two, even though the number of discrete ordinate sweeps cell calculations doubled as shown in table 7.2. Again, the decrease in time is due to the fewer number of total iterations, as shown in table 7.1, which offset the time for the additional discrete ordinate sweeps cell calculations.

The checkerboard problem demonstrated the robustness of the DI method. The problem challenged the method initially, as some of the PHI problems did for synthetic acceleration methods. The checkerboard problem however, showed a way to both stabilize diverging spatial methods and improve the convergence

rates methods that were converging slowly. Furthermore, the new technique does not come at a computational cost penalty, it actually improves the overall speed of the method for first spatial moment methods.

### B. Scattering Ratio Horizontal Interface Problem

Another problem that was tested is also a periodic horizontal interface, but where the scattering ratio is varied between layers as opposed to the total cross sections. The spatial mesh is 40 cells by 40 cells with  $\Delta x = \Delta y = 1.0$ . A description of the problem is shown in figure 7.13 for a total cross section  $\sigma = 1$ .

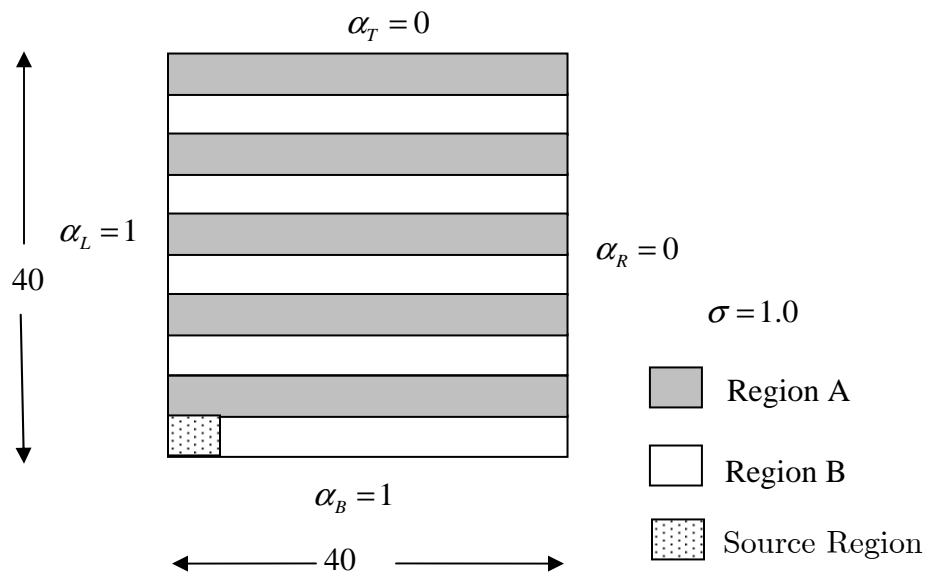


Figure 7.7. Problem variables for the scattering ratio PHI problem.

Each region's scattering ratio are systematically changed and the rates of convergence are checked for total cross sections of 0.1 , 1.0, and 10.0. The problem is intended to stress the DI method for the first moment methods by

creating regions where the current along an ordinate is not continuous and may produce negative current artifacts.

### Spatial Methods

The DI results of the scattering ratio PHI for the total cross section of 0.1 is shown in figure 7.8. All spatial methods converged readily for the scattering ratio of 1.0 and 0.0 for regions A and B respectively. The various combinations of scattering ratios are shown later for WDD at this total cross section in table 7.3.

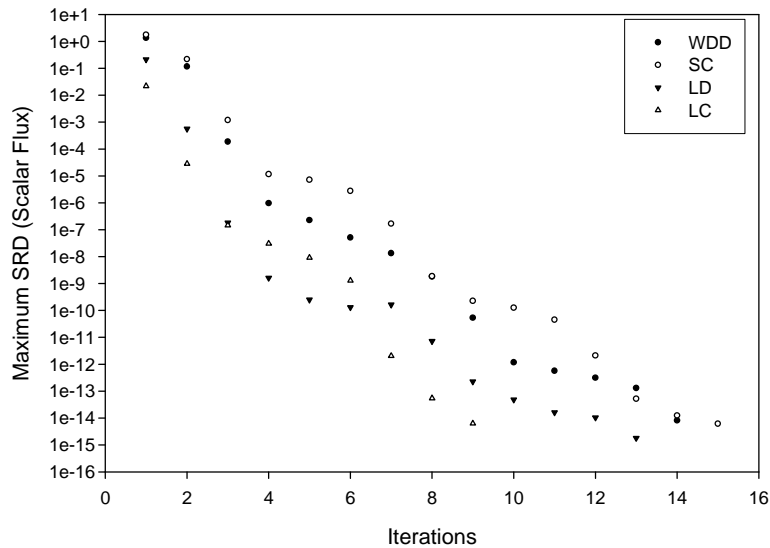


Figure 7.8. Convergence rates for different spatial methods versus iterations using  $S_6$  to the scattering ratio PHI problem. Total cross section is 0.1 and scattering ratios of 1.0 and 0.0 for regions A and B respectively.

The results of the scattering ratio PHI for the total cross section of 1.0 is shown in figure 7.9. Again, all spatial methods converged readily for the scattering ratio of 1.0 and 0.0 for regions A and B respectively. The various combinations of scattering ratios are shown later for WDD at this total cross section in table 7.4.

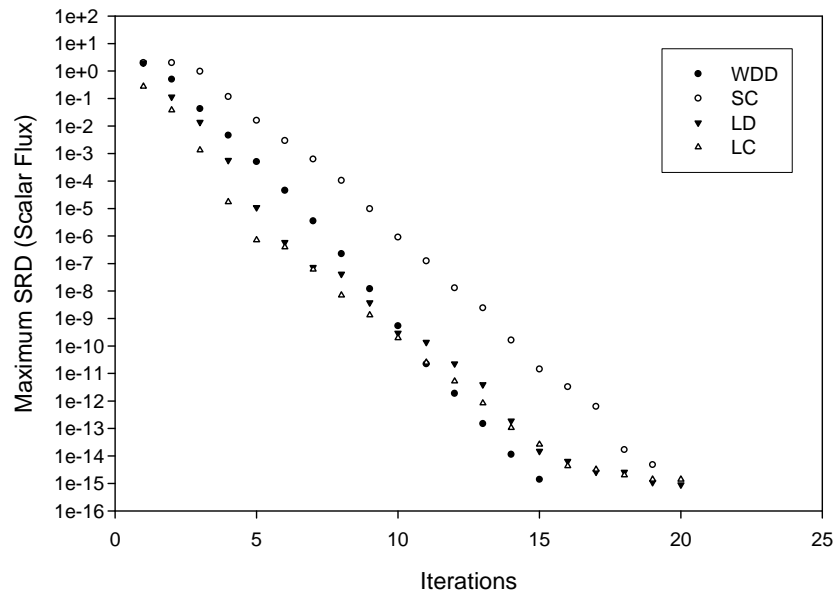


Figure 7.9. Convergence rates for different spatial methods versus iterations using  $S_6$  to the scattering ratio PHI problem. Total cross section is 1.0 and scattering ratios of 1.0 and 0.0 for regions A and B respectively.

The results of the scattering ratio PHI for the total cross section of 10.0 is shown in figure 7.10. As with the previous cases, all spatial methods converged readily for the scattering ratio of 1.0 and 0.0 for regions A and B respectively.

The various combinations of scattering ratios are shown later for WDD at this total cross section in table 7.4.

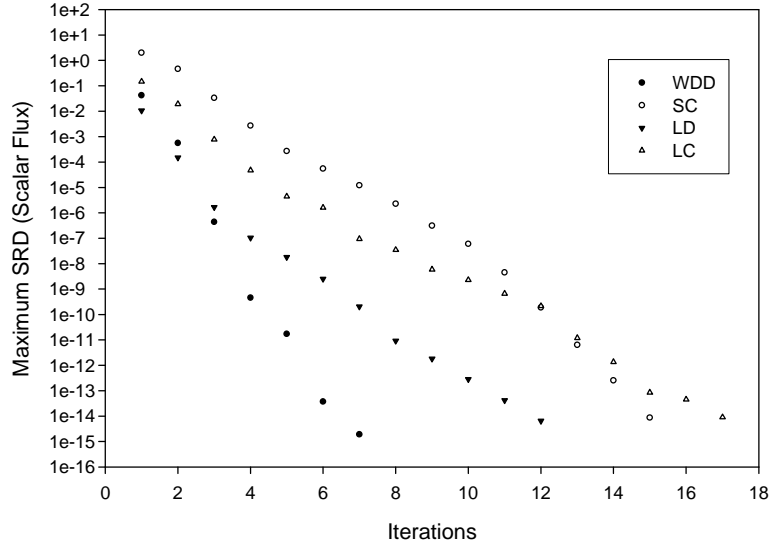


Figure 7.10. Convergence rates for different spatial methods versus iterations using  $S_6$  to the scattering ratio PHI problem. Total cross section is 10.0 and scattering ratios of 1.0 and 0.0 for regions A and B respectively.

### 1. Weighted Diamond Difference Performance

The various combinations of scattering ratios for regions A and B are shown in table 7.3 for a total cross section of 0.1. For combinations where both regions that are totally absorbing or with a scattering ratio of 0.0, the DI method converged in one iteration. As with the previous convergence rates, the values are determined by a linear regression of the linearized maximum SRD plots described in chapter six. In general, the convergence rates increase slightly for

higher scattering ratios, but the overall performance is good. For the other spatial methods, the convergence rates were similar.

Table 7.3. WDD results for scattering ratio PHI problem with total cross section  $\sigma = 0.1$  as scattering ratio varies.

	c Region A					
c Region B	0.0	0.2	0.4	0.6	0.8	1.0
0.0	0	0.0822	0.0772	0.0630	0.1501	0.1429
0.2	0.00002	0.0518	0.1104	0.0622	0.1338	0.1385
0.4	0.0656	0.0759	0.0624	0.1225	0.1666	0.1574
0.6	0.1051	0.0629	0.1464	0.1570	0.1831	0.1957
0.8	0.0780	0.1335	0.1588	0.1660	0.1864	0.1892
1.0	0.1119	0.1585	0.1529	0.1449	0.1992	0.2953

The various combinations of scattering ratios for regions A and B are shown in table 7.4 for a total cross section of 1.0 and the DI method with WDD. Again, where both regions that are totally absorbing or with a scattering ratio of 0.0, the DI method converged in one iteration. Again, the convergence rates increase slightly for higher scattering ratios, but the overall performance is very good. The convergence rates are slightly better than the previous total cross section of 0.1 shown in table 7.3. Again, the other spatial methods had similar performance for this total cross section, the LD method is presented next.

Table 7.4. WDD results for scattering ratio PHI problem with total cross section  $\sigma = 1.0$ .

	c Region A					
c Region B	0.0	0.2	0.4	0.6	0.8	1.0
0.0	0	0.0161	0.0643	0.0681	0.0685	0.0657
0.2	0.00004	0.0203	0.0674	0.0643	0.0476	0.0659
0.4	0.0499	0.0506	0.0532	0.0403	0.0439	0.0640
0.6	0.0344	0.0411	0.0348	0.0341	0.0457	0.0686
0.8	0.0280	0.0315	0.0413	0.0527	0.0542	0.0875
1.0	0.0499	0.0506	0.0595	0.0657	0.0587	0.1046

## 2. Linear Discontinuous Performance

The various combinations of scattering ratios for regions A and B are shown in table 7.5 for a total cross section of 1.0 and the DI method with LD. Again, where both regions that are totally absorbing, the DI method converged in one iteration.

Table 7.5. LD results for scattering ratio PHI problem with total cross section  $\sigma = 1.0$ . Shading indicates strictly positive solutions.

	c Region A					
c Region B	0.0	0.2	0.4	0.6	0.8	1.0
0.0	0	2.0E-06	0.0943	0.0049	0.0185	0.1489
0.2	9.8E-8	4.0E-06	0.0005	0.0858	0.0685	0.1518
0.4	5.1E-7	0.0003	0.0680	0.0906	0.0823	0.1548
0.6	0.0004	0.0772	0.1058	0.0691	0.0968	0.1332
0.8	0.1156	0.1009	0.0738	0.1005	0.1114	0.1773
1.0	0.0923	0.1057	0.1022	0.1427	0.1825	0.2571

The first moment methods, LD and LC, are not positive methods and can return negative values for certain problem values. A test was done to see if either the cell scalar flux or edge currents (and hence distributions) were negative during any iteration for the solutions presented in table 7.5. The results are shown in table 7.5, and the positive values are indicated by the shaded cells. The table shows that the LD method did indeed return negative values for most of the cases, where the scattering sources less than 0.8. However, for all the combinations in cross sections, the method was still able to converge in spite of the spatial method negative artifacts. The DI method is able to tolerate some negative values as demonstrated by this case.

The various combinations of scattering ratios for regions A and B from figure 7.10 are shown in table 7.6 for a total cross section of 10.0 and the DI method with WDD. In general, the convergence rates are constant across the range of scattering ratios. The overall convergence rates are fast for WDD and SC had similar performance. However, for this total cross section both the LD and LC spatial method did not converge for certain scattering ratios. The negative artifacts returned by these spatial methods prevented the DI method from working.



Table 7.6. WDD results for scattering ratio PHI problem with total cross section  $\sigma = 10.0$ .

	c Region A					
c Region B	0.0	0.2	0.4	0.6	0.8	1.0
0.0	0	5.9E-06	0.0067	0.0115	0.0079	0.0082
0.2	6.5E-6	2.3E-06	0.0063	0.0135	0.0143	0.0084
0.4	0.0070	0.0070	0.0195	0.0167	0.0151	0.0085
0.6	0.0126	0.0157	0.0162	0.0162	0.0153	0.0087
0.8	0.0139	0.0149	0.0148	0.0154	0.0168	0.0091
1.0	0.0077	0.0083	0.0080	0.0082	0.0085	0.0067

The scattering ratio periodic horizontal interface problem also demonstrated the robustness of the positive spatial methods for problems that have a difference in scattering ratio at cell boundaries. The positive methods performed well across the entire range of cross section combinations and different of total cross sections. This problem also highlighted the issue of how the DI method responds to the negative artifacts created by the first moment methods. The DI method is able to tolerate some negative values, but other cases will cause it to fail. An obvious approach, is to refine the mesh in an attempt to keep the first moment methods positive. Another commonly used approach is to impose a fix-up and set the negative values to zero. Both these approaches create issues for the rate of convergence. However, rather than address this issue,

it is more desirable to devise spatial methods that are strictly positive and not contain non-physical numerical artifacts.

## VIII. Conclusions and Recommendations

This research showed that the distribution iteration method is a practical alternative to current methods and suggests possibilities for new approaches to solving the discrete ordinates system of equations.

### A. Conclusions

My objectives have been achieved. The distribution iteration method was extended to 2-d Cartesian Geometry (objective 1) and demonstrated using multiple spatial and angular quadratures, including quadratures that correctly meet diffusion limits (objective 2). Unlike the synthetic acceleration methods, a different derivation is not required to change spatial methods, as this demonstrated. The global problem was recast as a finite-volume particle conservation formulation (objective 3) by using partial currents, rather than partial-range angular integrals of the directional flux, creating the global partial current problem. This change was not only shown to converge in fewer iterations, but also provides a clear methodology for the extension to higher dimensions. The global problem is defined in terms of only the spatial average of the two partial currents through each cell face. (Alternative schemes could include higher spatial moments and/or cell spatial moments as well, but this would increase the size of the global problem.) Thus, the method minimizes the

size of the global problem when applied to higher-order linear spatial quadratures (objective 4).

The distribution iteration method efficiently solved problems where the synthetic acceleration methods either failed or lost effectiveness; and testing on more challenging problems also demonstrated the success of the distribution iteration method (objective 5). Despite the comparisons with synthetic acceleration methods in this research, the distribution iteration method is not an acceleration technique.

PARDISO was evaluated (objective 6) and found to be extremely efficient throughout my testing. It required only a small fraction of the run time of the code. The red/black scheme maximizes opportunity for parallelization (objective 7a); while the sweep scheme enhances serial performance by requiring fewer cell calculations (objective 7b). The desirable properties of the method that constitute the goals for the research have been nearly fully achieved (objective 8):

*Robustness* – the method has been demonstrated for a broad range of cross sections and scattering ratios. Convergence was sometimes slow or divergent for some spatial quadratures but an inner loop with an adaptive number of sweeps per global solver call (1 to 10) offset this limitation. This is the one area that needs future work: finding a better sweep scheme for updating the angular distributions at cell faces.

*Flexibility* – Several spatial and angular quadratures were used. These changed the numbers in the matrices for the cell and global problems, but did not require changes to the algorithm (for given spatial moments carried).

*Parallelizability* – The global problem is solved by the PARDISO solver, which is commercially available for many parallel computing systems. The sweep method of improving angular distributions at cell faces has limited parallelizability, but the red/black alternative also demonstrated here is ideal for parallel computation.

*Extensibility* – the method could readily be extended to 3d. The algorithm design is unaffected, only changes in implementation (array dimensions, cell indexing and translation to sparse array data structure, etc.) are needed.

## **B. Recommendations**

The testing showed that a large portion of the code run time was for the matrix multiplications required in different steps. Additional time savings are likely by using optimized (vectorized) matrix multiplication routines and a more compact data structure within the code.

The sweeping scheme needs to converge faster for some challenging problems, such as the checkerboard problem. This might be achieved by tuning the number of sweeps per global solution, by applying a convergence accelerator to this inner iteration, or by trying variants on exactly how the sweeps are done.

The distribution iteration is not an accelerator for the source iteration. It may be improved by applying some acceleration scheme(s); this is an open question.

## Appendix A: Linear Discontinuous Equations in Slab Geometry

### Equation Section 1

In this section, the relations for the current representation of the linear discontinuous method in slab geometry are developed. As with the zeroth spatial moment methods, the usual representation found is in terms of the angular flux. The equations for the outgoing angular flux  $\psi^{right}$  in terms of the incoming angular flux  $\psi^{left}$ , scattering within the cell  $S^A$ ,  $S^X$  and emissions  $E^A$ , are previously derived and presented in the literature (8: 222-223). The linear discontinuous relation for the edge value is:

$$\psi^{Right} = \psi^A + \psi^X, \quad (\text{A.1})$$

This can be substituted into the zeroth and x moment cell balance equations:

$$\psi^{Right} - \psi^{Left} + \varepsilon\psi^A = S^A \frac{\Delta y}{\eta}, \quad (\text{A.2})$$

$$3(\psi^{Right} + \psi^{Left} - 2\psi^A) + \varepsilon\psi^X = S^X \frac{\Delta y}{\eta}, \quad (\text{A.3})$$

where the following relation is defined:

$$a = 6 + 4\varepsilon + \varepsilon^2, \quad (\text{A.4})$$

and

$$\varepsilon = \frac{\sigma\Delta x}{|\mu|}. \quad (\text{A.5})$$

The desired relations in the angular flux relation are found using equations (A.1) through (A.4):

$$\psi^{Right} = \frac{6-2\varepsilon}{a} \psi^{Left} + \frac{\Delta x(6+\varepsilon)}{a|\mu|} S^A + \frac{\Delta x \varepsilon}{a|\mu|} S^X + \frac{\Delta x(6+\varepsilon)}{a|\mu|} E^A, \quad (\text{A.6})$$

$$\psi^A = \frac{6+\varepsilon}{a} \psi^{Left} + \frac{\Delta x(3+\varepsilon)}{a|\mu|} S^A - \frac{\Delta x}{a|\mu|} S^X + \frac{\Delta x(3+\varepsilon)}{a|\mu|} E^A, \quad (\text{A.7})$$

and

$$\psi^A = \frac{-3\varepsilon}{a} \psi^{Left} + \frac{3\Delta x}{a|\mu|} S^A + \frac{\Delta x(1+\varepsilon)}{a|\mu|} S^X + \frac{3\Delta x}{a|\mu|} E^A. \quad (\text{A.8})$$

The definition for the current  $j^{Right} = |\mu| \psi^{Right}$  and similarly for the left, allows the transition from an angular flux to a current representation. The equations for the outgoing quantities are:

$$j^{Right} = \frac{6-2\varepsilon}{a} j^{Left} + \frac{\Delta x(6+\varepsilon)}{a} S^A + \frac{\Delta x \varepsilon}{a} S^X + \frac{\Delta x(6+\varepsilon)}{a} E^A, \quad (\text{A.9})$$

$$\psi^A = \frac{6+\varepsilon}{a|\mu|} j^{Left} + \frac{\Delta x(3+\varepsilon)}{a|\mu|} S^A - \frac{\Delta x}{a|\mu|} S^X + \frac{\Delta x(3+\varepsilon)}{a|\mu|} E^A, \quad (\text{A.10})$$

and

$$\psi^X = \frac{-3\varepsilon}{a|\mu|} j^{Left} + \frac{3\Delta x}{a|\mu|} S^A + \frac{\Delta x(1+\varepsilon)}{a|\mu|} S^X + \frac{3\Delta x}{a|\mu|} E^A. \quad (\text{A.11})$$

These are the relationships used in chapter 3.



## Appendix B: Zeroth Spatial Moment Methods Current Equations in XY-Geometry

### Equation Section 2

#### Step Characteristic Equations

In this section, the relations for the current representation of the step characteristic method are developed. The usual representation for the cell relations are in terms of the angular flux. In the scaled rectangular cell as shown in figure A.1, the equations for the outgoing angular fluxes  $\psi^{top}$  and  $\psi^{right}$  in terms of the incoming angular fluxes  $\psi^{bottom}$  and  $\psi^{left}$ , scattering within the cell  $S^A$ , and emissions  $E^A$ , are previously derived and presented in the literature (12: 21).

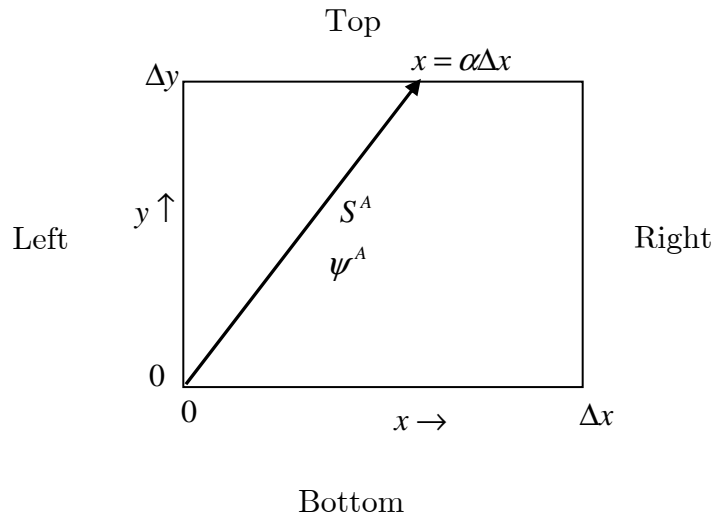


Figure B.1. Rectangular cell for zeroth spatial moment methods. Cell shows problem variables used for the discrete ordinates equations.

The angular flux relations for the cell shown in figure B.1 in the step characteristic spatial quadrature are:

$$\begin{aligned} \psi^{Top} = & \alpha M_0(\varepsilon_y) \psi^{Left} + (1-\alpha) e^{-\varepsilon_y} \psi^{Bottom} + \frac{\Delta y}{|\eta|} [(1-\alpha) M_0(\varepsilon_y) + \alpha M_1(\varepsilon_y)] S^A + \\ & \frac{\Delta y}{|\eta|} [(1-\alpha) M_0(\varepsilon_y) + \alpha M_1(\varepsilon_y)] E^A, \end{aligned} \quad (\text{B.1})$$

$$\psi^{Right} = M_0(\varepsilon_y) \psi^{Bottom} + \frac{\Delta y}{|\eta|} M_1(\varepsilon_y) S^A + \frac{\Delta y}{|\eta|} M_1(\varepsilon_y) E^A, \quad (\text{B.2})$$

$$\begin{aligned} \psi_A = & \alpha M_0(\varepsilon_y) \psi^{Left} + [(1-\alpha) M_0(\varepsilon_y) + \alpha M_1(\varepsilon_y)] \psi^{Bottom} + \\ & \frac{\Delta y}{|\eta|} [(1-\alpha) M_1(\varepsilon_y) + \alpha M_2(\varepsilon_y)] S^A + \frac{\Delta y}{|\eta|} [(1-\alpha) M_1(\varepsilon_y) + \alpha M_2(\varepsilon_y)] E^A. \end{aligned} \quad (\text{B.3})$$

Here  $\mu$  and  $\eta$  are the direction cosines along the x and y axis respectively from the angular quadrature,  $\varepsilon_y = \frac{\sigma \Delta y}{|\eta|}$  is the optical thickness in the y direction,

$\alpha = \frac{\varepsilon_y}{\varepsilon_x}$  is a parameter for the cell, and  $M_0(\varepsilon_y)$ ,  $M_1(\varepsilon_y)$ , and  $M_2(\varepsilon_y)$  are the

exponential moment functions (9: 27).

The definition for the currents,  $j^{Right} = |\mu| \psi^{Right}$  and  $j^{Top} = |\eta| \psi^{Top}$  and similarly for the left and bottom, allows the transition from angular fluxes to a current representation. The equations (B.1) through (B.3) in a current representation are:

$$\begin{aligned} j^{Top} = & \frac{|\eta|}{|\mu|} \alpha M_0(\varepsilon_y) j^{Left} + (1-\alpha) e^{-\varepsilon_y} j^{Bottom} + \Delta y [(1-\alpha) M_0(\varepsilon_y) + \alpha M_1(\varepsilon_y)] S^A + \\ & \Delta y [(1-\alpha) M_0(\varepsilon_y) + \alpha M_1(\varepsilon_y)] E^A, \end{aligned} \quad (\text{B.4})$$

$$j^{Right} = \frac{|\mu|}{|\eta|} M_0(\varepsilon_y) j^{Bottom} + \frac{|\mu| \Delta y}{|\eta|} M_1(\varepsilon_y) S^A + \frac{|\mu| \Delta y}{|\eta|} M_1(\varepsilon_y) E^A, \quad (\text{B.5})$$

$$\begin{aligned} \psi_A = & \frac{1}{|\mu|} \alpha M_0(\varepsilon_y) j^{Left} + \frac{1}{|\eta|} [(1-\alpha)M_0(\varepsilon_y) + \alpha M_1(\varepsilon_y)] j^{Bottom} + \\ & \frac{\Delta y}{|\eta|} [(1-\alpha)M_1(\varepsilon_y) + \alpha M_2(\varepsilon_y)] S^A + \frac{\Delta y}{|\eta|} [(1-\alpha)M_1(\varepsilon_y) + \alpha M_2(\varepsilon_y)] E^A. \end{aligned} \quad (\text{B.6})$$

These are the relations presented in chapter four.

### Weighted Diamond Difference Equations

In the rectangular cell as shown in figure B.1, the equations are again found for the outgoing angular fluxes,  $\psi^{top}$  and  $\psi^{right}$ , in terms of the incoming angular fluxes  $\psi^{bottom}$  and  $\psi^{left}$ , scattering within the cell  $S^A$ , and emissions  $E^A$ .

The WDD relations begin with the cell balance equation (3: 215):

$$\frac{|\mu|}{\Delta x} (\psi^{Right} - \psi^{Left}) + \frac{|\eta|}{\Delta y} (\psi^{Top} - \psi^{Bottom}) + \sigma \psi^A = S^A + E^A, \quad (\text{B.7})$$

with the weighted diamond difference assumption

$$\psi^A = \left( \frac{1 + \alpha^x}{2} \right) \psi^{Right} + \left( \frac{1 - \alpha^x}{2} \right) \psi^{Left}, \quad (\text{B.8})$$

and

$$\psi^A = \left( \frac{1 + \alpha^y}{2} \right) \psi^{Top} + \left( \frac{1 - \alpha^y}{2} \right) \psi^{Bottom}. \quad (\text{B.9})$$

The weights,  $\alpha^x$  and  $\alpha^y$ , change the relations from a diamond difference to step spatial quadrature using the following relations:

$$\alpha^x = \coth\left(\frac{\varepsilon_x}{2}\right) - \frac{2}{\varepsilon_x}, \quad (\text{B.10})$$

$$\alpha^y = \coth\left(\frac{\varepsilon_y}{2}\right) - \frac{2}{\varepsilon_y}. \quad (\text{B.11})$$

Again,  $\mu$  and  $\eta$  are the direction cosines along the x and y axis respectively from

the angular quadrature,  $\varepsilon_y = \frac{\sigma\Delta y}{|\eta|}$  is the optical thickness in the y direction,

and  $\varepsilon_x = \frac{\sigma\Delta x}{|\mu|}$  is the optical thickness in the x direction. These relations are

numerically ill conditioned for optically thin or thick cells, but may be

equivalently expressed using exponential moment functions (9: 27) as

$$\alpha^x = 2\rho(\varepsilon_x), \quad (\text{B.12})$$

where:

$$\rho(\varepsilon_x) = \frac{M_1(\varepsilon_x)}{M_0(\varepsilon_x)}, \quad (\text{B.13})$$

and similarly for the y component. A new notation for the weights can be

written as:

$$\delta_{In}^x = \frac{1-2\rho(\varepsilon_x)}{2}, \quad (\text{B.14})$$

$$\delta_{Out}^x = \frac{1+2\rho(\varepsilon_x)}{2}. \quad (\text{B.15})$$

The definition for the currents  $j^{Right} = |\mu|\psi^{Right}$  and  $j^{Top} = |\eta|\psi^{Top}$  allows the relations in equations (B.7) through (B.9) to be changed to:

$$j^{Top} = \frac{|\eta|\psi^A - \delta_{In}^y j^{Bottom}}{\delta_{Out}^y}, \quad (\text{B.16})$$

$$j^{Right} = \frac{|\mu|\psi^A - \delta_{In}^x j^{Left}}{\delta_{Out}^x}, \quad (\text{B.17})$$

$$\frac{j^{Right}}{|\mu|\varepsilon_x} + \frac{j^{Top}}{|\eta|\varepsilon_y} + \psi^A = \frac{E^A}{\sigma} + \frac{S^A}{\sigma} + \frac{j^{Left}}{|\mu|\varepsilon_x} + \frac{j^{Bottom}}{|\eta|\varepsilon_y}. \quad (\text{B.18})$$

These relations can then be solved in terms of the outgoing variables as shown in chapter four.

## Appendix C: First Spatial Moment Methods Derivation in XY-Geometry

### Equation Section 3

This appendix contains the complete derivation for the first spatial moment method presented in chapter four in a general form. Starting with the current equations using sub-matrices the cell face equations are:

$$\begin{aligned} \vec{j}_{Out}^R = & \mathbf{K}_{OI}^{RL} \vec{j}_{In}^L + \mathbf{K}_{OI}^{RR} \vec{j}_{In}^R + \mathbf{K}_{OI}^{RT} \vec{j}_{In}^T + \mathbf{K}_{OI}^{RB} \vec{j}_{In}^B + \mathbf{K}_{O\theta}^{RL} \vec{\theta}_{In}^L + \mathbf{K}_{O\theta}^{RR} \vec{\theta}_{In}^R \\ & + \mathbf{K}_{O\theta}^{RT} \vec{\theta}_{In}^T + \mathbf{K}_{O\theta}^{RB} \vec{\theta}_{In}^B + \mathbf{K}_{OSA}^R \vec{S}^A + \mathbf{K}_{OSX}^R \vec{S}^X + \mathbf{K}_{OSY}^R \vec{S}^Y + \mathbf{K}_{OEA}^R \vec{E}^A, \end{aligned} \quad (C.1)$$

$$\begin{aligned} \vec{j}_{Out}^L = & \mathbf{K}_{OI}^{LL} \vec{j}_{In}^L + \mathbf{K}_{OI}^{LR} \vec{j}_{In}^R + \mathbf{K}_{OI}^{LT} \vec{j}_{In}^T + \mathbf{K}_{OI}^{LB} \vec{j}_{In}^B + \mathbf{K}_{O\theta}^{LL} \vec{\theta}_{In}^L + \mathbf{K}_{O\theta}^{LR} \vec{\theta}_{In}^R \\ & + \mathbf{K}_{O\theta}^{LT} \vec{\theta}_{In}^T + \mathbf{K}_{O\theta}^{LB} \vec{\theta}_{In}^B + \mathbf{K}_{OSA}^L \vec{S}^A + \mathbf{K}_{OSX}^L \vec{S}^X + \mathbf{K}_{OSY}^L \vec{S}^Y + \mathbf{K}_{OEA}^L \vec{E}^A, \end{aligned} \quad (C.2)$$

$$\begin{aligned} \vec{j}_{Out}^T = & \mathbf{K}_{OI}^{TL} \vec{j}_{In}^L + \mathbf{K}_{OI}^{TR} \vec{j}_{In}^R + \mathbf{K}_{OI}^{TT} \vec{j}_{In}^T + \mathbf{K}_{OI}^{TB} \vec{j}_{In}^B + \mathbf{K}_{O\theta}^{TL} \vec{\theta}_{In}^L + \mathbf{K}_{O\theta}^{TR} \vec{\theta}_{In}^R \\ & + \mathbf{K}_{O\theta}^{TT} \vec{\theta}_{In}^T + \mathbf{K}_{O\theta}^{TB} \vec{\theta}_{In}^B + \mathbf{K}_{OSA}^T \vec{S}^A + \mathbf{K}_{OSX}^T \vec{S}^X + \mathbf{K}_{OSY}^T \vec{S}^Y + \mathbf{K}_{OEA}^T \vec{E}^A, \end{aligned} \quad (C.3)$$

and

$$\begin{aligned} \vec{j}_{Out}^B = & \mathbf{K}_{OI}^{BL} \vec{j}_{In}^L + \mathbf{K}_{OI}^{BR} \vec{j}_{In}^R + \mathbf{K}_{OI}^{BT} \vec{j}_{In}^T + \mathbf{K}_{OI}^{BB} \vec{j}_{In}^B + \mathbf{K}_{O\theta}^{BL} \vec{\theta}_{In}^L + \mathbf{K}_{O\theta}^{BR} \vec{\theta}_{In}^R \\ & + \mathbf{K}_{O\theta}^{BT} \vec{\theta}_{In}^T + \mathbf{K}_{O\theta}^{BB} \vec{\theta}_{In}^B + \mathbf{K}_{OSA}^B \vec{S}^A + \mathbf{K}_{OSX}^B \vec{S}^X + \mathbf{K}_{OSY}^B \vec{S}^Y + \mathbf{K}_{OEA}^B \vec{E}^A. \end{aligned} \quad (C.4)$$

In addition to the outgoing currents, the outgoing edge distributions are:

$$\begin{aligned} \vec{\theta}_{Out}^R = & \mathbf{K}_{\theta I}^{RL} \vec{j}_{In}^L + \mathbf{K}_{\theta I}^{RR} \vec{j}_{In}^R + \mathbf{K}_{\theta I}^{RT} \vec{j}_{In}^T + \mathbf{K}_{\theta I}^{RB} \vec{j}_{In}^B + \mathbf{K}_{\theta\theta}^{RL} \vec{\theta}_{In}^L + \mathbf{K}_{\theta\theta}^{RR} \vec{\theta}_{In}^R \\ & + \mathbf{K}_{\theta\theta}^{RT} \vec{\theta}_{In}^T + \mathbf{K}_{\theta\theta}^{RB} \vec{\theta}_{In}^B + \mathbf{K}_{\theta SA}^R \vec{S}^A + \mathbf{K}_{\theta SX}^R \vec{S}^X + \mathbf{K}_{\theta SY}^R \vec{S}^Y + \mathbf{K}_{\theta EA}^R \vec{E}^A, \end{aligned} \quad (C.5)$$

$$\begin{aligned} \vec{\theta}_{Out}^L = & \mathbf{K}_{\theta I}^{LL} \vec{j}_{In}^L + \mathbf{K}_{\theta I}^{LR} \vec{j}_{In}^R + \mathbf{K}_{\theta I}^{LT} \vec{j}_{In}^T + \mathbf{K}_{\theta I}^{LB} \vec{j}_{In}^B + \mathbf{K}_{\theta\theta}^{LL} \vec{\theta}_{In}^L + \mathbf{K}_{\theta\theta}^{LR} \vec{\theta}_{In}^R \\ & + \mathbf{K}_{\theta\theta}^{LT} \vec{\theta}_{In}^T + \mathbf{K}_{\theta\theta}^{LB} \vec{\theta}_{In}^B + \mathbf{K}_{\theta SA}^L \vec{S}^A + \mathbf{K}_{\theta SX}^L \vec{S}^X + \mathbf{K}_{\theta SY}^L \vec{S}^Y + \mathbf{K}_{\theta EA}^L \vec{E}^A, \end{aligned} \quad (C.6)$$

$$\begin{aligned} \vec{\theta}_{Out}^T = & \mathbf{K}_{\theta I}^{TL} \vec{j}_{In}^L + \mathbf{K}_{\theta I}^{TR} \vec{j}_{In}^R + \mathbf{K}_{\theta I}^{TT} \vec{j}_{In}^T + \mathbf{K}_{\theta I}^{TB} \vec{j}_{In}^B + \mathbf{K}_{\theta\theta}^{TL} \vec{\theta}_{In}^L + \mathbf{K}_{\theta\theta}^{TR} \vec{\theta}_{In}^R \\ & + \mathbf{K}_{\theta\theta}^{TT} \vec{\theta}_{In}^T + \mathbf{K}_{\theta\theta}^{TB} \vec{\theta}_{In}^B + \mathbf{K}_{\theta SA}^T \vec{S}^A + \mathbf{K}_{\theta SX}^T \vec{S}^X + \mathbf{K}_{\theta SY}^T \vec{S}^Y + \mathbf{K}_{\theta EA}^T \vec{E}^A, \end{aligned} \quad (C.7)$$

and

$$\begin{aligned}\bar{\theta}_{Out}^B &= \mathbf{K}_{\theta I}^{BL} \bar{j}_{In}^L + \mathbf{K}_{\theta I}^{BR} \bar{j}_{In}^R + \mathbf{K}_{\theta I}^{BT} \bar{j}_{In}^T + \mathbf{K}_{\theta I}^{BB} \bar{j}_{In}^B + \mathbf{K}_{\theta\theta}^{BL} \bar{\theta}_{In}^L + \mathbf{K}_{\theta\theta}^{BR} \bar{\theta}_{In}^R \\ &+ \mathbf{K}_{\theta\theta}^{BT} \bar{\theta}_{In}^T + \mathbf{K}_{\theta\theta}^{BB} \bar{\theta}_{In}^B + \mathbf{K}_{\theta SA}^B \bar{S}^A + \mathbf{K}_{\theta SX}^B \bar{S}^X + \mathbf{K}_{\theta SY}^B \bar{S}^Y + \mathbf{K}_{\theta EA}^B \bar{E}^A.\end{aligned}\quad (C.8)$$

The cell values are:

$$\begin{aligned}\bar{\psi}^A &= \mathbf{K}_{AI}^L \bar{j}_{In}^L + \mathbf{K}_{AI}^R \bar{j}_{In}^R + \mathbf{K}_{AI}^T \bar{j}_{In}^T + \mathbf{K}_{AI}^B \bar{j}_{In}^B + \mathbf{K}_{A\theta}^L \bar{\theta}_{In}^L + \mathbf{K}_{A\theta}^R \bar{\theta}_{In}^R \\ &+ \mathbf{K}_{A\theta}^T \bar{\theta}_{In}^T + \mathbf{K}_{A\theta}^B \bar{\theta}_{In}^B + \mathbf{K}_{ASA} \bar{S}^A + \mathbf{K}_{ASX} \bar{S}^X + \mathbf{K}_{ASY} \bar{S}^Y + \mathbf{K}_{AEA} \bar{E}^A,\end{aligned}\quad (C.9)$$

$$\begin{aligned}\bar{\psi}^X &= \mathbf{K}_{XI}^L \bar{j}_{In}^L + \mathbf{K}_{XI}^R \bar{j}_{In}^R + \mathbf{K}_{XI}^T \bar{j}_{In}^T + \mathbf{K}_{XI}^B \bar{j}_{In}^B + \mathbf{K}_{X\theta}^L \bar{\theta}_{In}^L + \mathbf{K}_{X\theta}^R \bar{\theta}_{In}^R \\ &+ \mathbf{K}_{X\theta}^T \bar{\theta}_{In}^T + \mathbf{K}_{X\theta}^B \bar{\theta}_{In}^B + \mathbf{K}_{XSA} \bar{S}^A + \mathbf{K}_{XSX} \bar{S}^X + \mathbf{K}_{XSY} \bar{S}^Y + \mathbf{K}_{XEA} \bar{E}^A,\end{aligned}\quad (C.10)$$

$$\begin{aligned}\bar{\psi}^Y &= \mathbf{K}_{YI}^L \bar{j}_{In}^L + \mathbf{K}_{YI}^R \bar{j}_{In}^R + \mathbf{K}_{YI}^T \bar{j}_{In}^T + \mathbf{K}_{YI}^B \bar{j}_{In}^B + \mathbf{K}_{Y\theta}^L \bar{\theta}_{In}^L + \mathbf{K}_{Y\theta}^R \bar{\theta}_{In}^R \\ &+ \mathbf{K}_{Y\theta}^T \bar{\theta}_{In}^T + \mathbf{K}_{Y\theta}^B \bar{\theta}_{In}^B + \mathbf{K}_{YSA} \bar{S}^A + \mathbf{K}_{YSX} \bar{S}^X + \mathbf{K}_{YSY} \bar{S}^Y + \mathbf{K}_{YEA} \bar{E}^A,\end{aligned}\quad (C.11)$$

$$\bar{S}^A = \sum_S \bar{\psi}^A, \quad (C.12)$$

$$\bar{S}^X = \sum_S \bar{\psi}^X, \quad (C.13)$$

and 
$$\bar{S}^Y = \sum_S \bar{\psi}^Y. \quad (C.14)$$

Equations (C.12) can be substituted in equation (C.9) to eliminate the average scattering source which gives.

$$\begin{aligned}\bar{\psi}^A &= (\mathbf{I} - \mathbf{K}_{ASA} \sum_S)^{-1} [\mathbf{K}_{AI}^L \bar{j}_{In}^L + \mathbf{K}_{AI}^R \bar{j}_{In}^R + \mathbf{K}_{AI}^T \bar{j}_{In}^T + \mathbf{K}_{AI}^B \bar{j}_{In}^B + \mathbf{K}_{A\theta}^L \bar{\theta}_{In}^L + \mathbf{K}_{A\theta}^R \bar{\theta}_{In}^R \\ &+ \mathbf{K}_{A\theta}^T \bar{\theta}_{In}^T + \mathbf{K}_{A\theta}^B \bar{\theta}_{In}^B + \mathbf{K}_{ASX} \bar{S}^X + \mathbf{K}_{ASY} \bar{S}^Y + \mathbf{K}_{AEA} \bar{E}^A].\end{aligned}\quad (C.15)$$

Letting  $\mathbf{L}_A = (\mathbf{I} - \mathbf{K}_{ASA} \sum_S)^{-1}$  equation (C.15) with (C.13) can be substituted in equation (C.10) to eliminate the x moment scattering sources. This gives:

$$\begin{aligned}
\bar{\psi}^X = & (\mathbf{I} - (\mathbf{K}_{X SX} + \mathbf{K}_{X SA} \mathbf{L}_A \mathbf{K}_{ASX})) \Sigma_S^{-1} [(\mathbf{K}_{XI}^L + \mathbf{K}_{X SA} \Sigma_S \mathbf{L}_A \mathbf{K}_{AI}^L) \bar{j}_{In}^L + \\
& (\mathbf{K}_{XI}^R + \mathbf{K}_{X SA} \Sigma_S \mathbf{L}_A \mathbf{K}_{AI}^R) \bar{j}_{In}^R + (\mathbf{K}_{XI}^T + \mathbf{K}_{X SA} \Sigma_S \mathbf{L}_A \mathbf{K}_{AI}^T) \bar{j}_{In}^T + \\
& (\mathbf{K}_{XI}^B + \mathbf{K}_{X SA} \Sigma_S \mathbf{L}_A \mathbf{K}_{AI}^B) \bar{j}_{In}^B + (\mathbf{K}_{X\theta}^L + \mathbf{K}_{X SA} \Sigma_S \mathbf{L}_A \mathbf{K}_{A\theta}^L) \bar{\theta}_{In}^L + \\
& (\mathbf{K}_{X\theta}^R + \mathbf{K}_{X SA} \Sigma_S \mathbf{L}_A \mathbf{K}_{A\theta}^R) \bar{\theta}_{In}^R + (\mathbf{K}_{X\theta}^T + \mathbf{K}_{X SA} \Sigma_S \mathbf{L}_A \mathbf{K}_{A\theta}^T) \bar{\theta}_{In}^T + \\
& (\mathbf{K}_{X\theta}^B + \mathbf{K}_{X SA} \Sigma_S \mathbf{L}_A \mathbf{K}_{A\theta}^B) \bar{\theta}_{In}^B + (\mathbf{K}_{XSY} + \mathbf{K}_{X SA} \Sigma_S \mathbf{L}_A \mathbf{K}_{ASY}) \bar{S}^Y + \\
& (K_{XEA} + K_{X SA} \Sigma_S \mathbf{L}_A K_{AEA}) \bar{E}^A]. \tag{C.16}
\end{aligned}$$

Letting  $\mathbf{L}_x = (\mathbf{I} - (\mathbf{K}_{x SX} + \mathbf{K}_{x SA} \mathbf{L}_A \mathbf{K}_{ASX})) \Sigma_S^{-1}$  both the average and x moment angular flux, equations (C.15) and (C.16), are substituted into the y moment of the angular flux, equation (C.11), with equation (C.14) to eliminate the y moment scattering source. This gives:

$$\begin{aligned}
\bar{\psi}^Y = & (\mathbf{I} - (\mathbf{K}_{YSY} + \mathbf{K}_{Y SA} \Sigma_S \mathbf{L}_A (\mathbf{K}_{ASY} + \mathbf{K}_{ASX} \Sigma_S \mathbf{L}_X \mathbf{K}_{XSY})) + \\
& \mathbf{K}_{YSX} \Sigma_S \mathbf{L}_X (\mathbf{K}_{XSY} + \mathbf{K}_{X SA} \Sigma_S \mathbf{L}_A \mathbf{K}_{ASY})) \Sigma_S^{-1} \\
& [(\mathbf{K}_{YI}^L + \mathbf{K}_{Y SA} \Sigma_S \mathbf{L}_A (\mathbf{K}_{AI}^L + \mathbf{K}_{ASX} \Sigma_S \mathbf{L}_X \mathbf{K}_{XI}^L) + \mathbf{K}_{YSX} \Sigma_S \mathbf{L}_X (\mathbf{K}_{XI}^L + \mathbf{K}_{X SA} \Sigma_S \mathbf{L}_A \mathbf{K}_{AI}^L)) \bar{j}_{In}^L + \\
& (\mathbf{K}_{YI}^R + \mathbf{K}_{Y SA} \Sigma_S \mathbf{L}_A (\mathbf{K}_{AI}^R + \mathbf{K}_{ASX} \Sigma_S \mathbf{L}_X \mathbf{K}_{XI}^R) + \mathbf{K}_{YSX} \Sigma_S \mathbf{L}_X (\mathbf{K}_{XI}^R + \mathbf{K}_{X SA} \Sigma_S \mathbf{L}_A \mathbf{K}_{AI}^R)) \bar{j}_{In}^R + \\
& (\mathbf{K}_{YI}^T + \mathbf{K}_{Y SA} \Sigma_S \mathbf{L}_A (\mathbf{K}_{AI}^T + \mathbf{K}_{ASX} \Sigma_S \mathbf{L}_X \mathbf{K}_{XI}^T) + \mathbf{K}_{YSX} \Sigma_S \mathbf{L}_X (\mathbf{K}_{XI}^T + \mathbf{K}_{X SA} \Sigma_S \mathbf{L}_A \mathbf{K}_{AI}^T)) \bar{j}_{In}^T + \\
& (\mathbf{K}_{YI}^B + \mathbf{K}_{Y SA} \Sigma_S \mathbf{L}_A (\mathbf{K}_{AI}^B + \mathbf{K}_{ASX} \Sigma_S \mathbf{L}_X \mathbf{K}_{XI}^B) + \mathbf{K}_{YSX} \Sigma_S \mathbf{L}_X (\mathbf{K}_{XI}^B + \mathbf{K}_{X SA} \Sigma_S \mathbf{L}_A \mathbf{K}_{AI}^B)) \bar{j}_{In}^B + \\
& (\mathbf{K}_{Y\theta}^L + \mathbf{K}_{Y SA} \Sigma_S \mathbf{L}_A (\mathbf{K}_{A\theta}^L + \mathbf{K}_{ASX} \Sigma_S \mathbf{L}_X \mathbf{K}_{X\theta}^L) + \mathbf{K}_{YSX} \Sigma_S \mathbf{L}_X (\mathbf{K}_{X\theta}^L + \mathbf{K}_{X SA} \Sigma_S \mathbf{L}_A \mathbf{K}_{A\theta}^L)) \bar{\theta}_{In}^L + \\
& (\mathbf{K}_{Y\theta}^R + \mathbf{K}_{Y SA} \Sigma_S \mathbf{L}_A (\mathbf{K}_{A\theta}^R + \mathbf{K}_{ASX} \Sigma_S \mathbf{L}_X \mathbf{K}_{X\theta}^R) + \mathbf{K}_{YSX} \Sigma_S \mathbf{L}_X (\mathbf{K}_{X\theta}^R + \mathbf{K}_{X SA} \Sigma_S \mathbf{L}_A \mathbf{K}_{A\theta}^R)) \bar{\theta}_{In}^R + \\
& (\mathbf{K}_{Y\theta}^T + \mathbf{K}_{Y SA} \Sigma_S \mathbf{L}_A (\mathbf{K}_{A\theta}^T + \mathbf{K}_{ASX} \Sigma_S \mathbf{L}_X \mathbf{K}_{X\theta}^T) + \mathbf{K}_{YSX} \Sigma_S \mathbf{L}_X (\mathbf{K}_{X\theta}^T + \mathbf{K}_{X SA} \Sigma_S \mathbf{L}_A \mathbf{K}_{A\theta}^T)) \bar{\theta}_{In}^T + \\
& (\mathbf{K}_{Y\theta}^B + \mathbf{K}_{Y SA} \Sigma_S \mathbf{L}_A (\mathbf{K}_{A\theta}^B + \mathbf{K}_{ASX} \Sigma_S \mathbf{L}_X \mathbf{K}_{X\theta}^B) + \mathbf{K}_{YSX} \Sigma_S \mathbf{L}_X (\mathbf{K}_{X\theta}^B + \mathbf{K}_{X SA} \Sigma_S \mathbf{L}_A \mathbf{K}_{A\theta}^B)) \bar{\theta}_{In}^B + \\
& (\mathbf{K}_{YEA} + \mathbf{K}_{Y SA} \Sigma_S \mathbf{L}_A (\mathbf{K}_{AEA} + \mathbf{K}_{ASX} \Sigma_S \mathbf{L}_X \mathbf{K}_{XEA})) + \\
& \mathbf{K}_{YSX} \Sigma_S \mathbf{L}_X (\mathbf{K}_{XEA} + \mathbf{K}_{X SA} \Sigma_S \mathbf{L}_A \mathbf{K}_{AEA}) \bar{E}^A]. \tag{C.17}
\end{aligned}$$



Let:

$$\begin{aligned} \mathbf{L}_Y = & (\mathbf{I} - (\mathbf{K}_{YSY} + \mathbf{K}_{YSA} \sum_S \mathbf{L}_A (\mathbf{K}_{ASY} + \mathbf{K}_{ASX} \sum_S \mathbf{L}_X \mathbf{K}_{XSY})) \\ & + \mathbf{K}_{YSX} \sum_S \mathbf{L}_X (\mathbf{K}_{XSY} + \mathbf{K}_{XSA} \sum_S \mathbf{L}_A \mathbf{K}_{ASY})) \Sigma_S)^{-1} \end{aligned}$$

and writing the following for the first term in equation (C.17):

$$\begin{aligned} \mathbf{m}_{YI}^L = & \mathbf{L}_Y (\mathbf{K}_{YI}^L + \mathbf{K}_{YSA} \sum_S \mathbf{L}_A (\mathbf{K}_{AI}^L + \mathbf{K}_{ASX} \sum_S \mathbf{L}_X \mathbf{K}_{XAI}^L) + \\ & \mathbf{K}_{YSX} \sum_S \mathbf{L}_X (\mathbf{K}_{XI}^L + \mathbf{K}_{XSA} \sum_S \mathbf{L}_A \mathbf{K}_{AI}^L)). \end{aligned}$$

This same convention is followed for the remaining terms and allows the updated equation:

$$\begin{aligned} \bar{\psi}_Y = & \mathbf{m}_{YI}^L \bar{j}_{In}^L + \mathbf{m}_{YI}^R \bar{j}_{In}^R + \mathbf{m}_{YI}^T \bar{j}_{In}^T + \mathbf{m}_{YI}^B \bar{j}_{In}^B + \mathbf{m}_{Y\theta}^L \bar{\theta}_{In}^L + \mathbf{m}_{Y\theta}^R \bar{\theta}_{In}^R \\ & + \mathbf{m}_{Y\theta}^T \bar{\theta}_{In}^T + \mathbf{m}_{Y\theta}^B \bar{\theta}_{In}^B + \mathbf{m}_{YEA} \bar{E}^A. \end{aligned} \quad (\text{C.18})$$

Equation (C.18) is substituted into equation (C.16) to eliminate the y moment of the angular flux:

$$\begin{aligned} \bar{\psi}^X = & \mathbf{L}_X [(\mathbf{K}_{XI}^L + \mathbf{K}_{XSA} \sum_S \mathbf{L}_A \mathbf{K}_{AI}^L + (\mathbf{K}_{XSY} + \mathbf{K}_{XSA} \sum_S \mathbf{L}_A \mathbf{K}_{ASY})) \Sigma_S \mathbf{m}_{YI}^L] \bar{j}_{In}^L + \\ & (\mathbf{K}_{XI}^R + \mathbf{K}_{XSA} \sum_S \mathbf{L}_A \mathbf{K}_{AI}^R + (\mathbf{K}_{XSY} + \mathbf{K}_{XSA} \sum_S \mathbf{L}_A \mathbf{K}_{ASY})) \Sigma_S \mathbf{m}_{YI}^R] \bar{j}_{In}^R + \\ & (\mathbf{K}_{XI}^T + \mathbf{K}_{XSA} \sum_S \mathbf{L}_A \mathbf{K}_{AI}^T + (\mathbf{K}_{XSY} + \mathbf{K}_{XSA} \sum_S \mathbf{L}_A \mathbf{K}_{ASY})) \Sigma_S \mathbf{m}_{YI}^T] \bar{j}_{In}^T + \\ & (\mathbf{K}_{XI}^B + \mathbf{K}_{XSA} \sum_S \mathbf{L}_A \mathbf{K}_{AI}^B + (\mathbf{K}_{XSY} + \mathbf{K}_{XSA} \sum_S \mathbf{L}_A \mathbf{K}_{ASY})) \Sigma_S \mathbf{m}_{YI}^B] \bar{j}_{In}^B + \\ & (\mathbf{K}_{X\theta}^L + \mathbf{K}_{XSA} \sum_S \mathbf{L}_A \mathbf{K}_{A\theta}^L + (\mathbf{K}_{XSY} + \mathbf{K}_{XSA} \sum_S \mathbf{L}_A \mathbf{K}_{ASY})) \Sigma_S \mathbf{m}_{Y\theta}^L] \bar{\theta}_{In}^L + \\ & (\mathbf{K}_{X\theta}^R + \mathbf{K}_{XSA} \sum_S \mathbf{L}_A \mathbf{K}_{A\theta}^R + (\mathbf{K}_{XSY} + \mathbf{K}_{XSA} \sum_S \mathbf{L}_A \mathbf{K}_{ASY})) \Sigma_S \mathbf{m}_{Y\theta}^R] \bar{\theta}_{In}^R + \\ & (\mathbf{K}_{X\theta}^T + \mathbf{K}_{XSA} \sum_S \mathbf{L}_A \mathbf{K}_{A\theta}^T + (\mathbf{K}_{XSY} + \mathbf{K}_{XSA} \sum_S \mathbf{L}_A \mathbf{K}_{ASY})) \Sigma_S \mathbf{m}_{Y\theta}^T] \bar{\theta}_{In}^T + \\ & (\mathbf{K}_{X\theta}^B + \mathbf{K}_{XSA} \sum_S \mathbf{L}_A \mathbf{K}_{A\theta}^B + (\mathbf{K}_{XSY} + \mathbf{K}_{XSA} \sum_S \mathbf{L}_A \mathbf{K}_{ASY})) \Sigma_S \mathbf{m}_{Y\theta}^B] \bar{\theta}_{In}^B + \\ & (\mathbf{K}_{XEA} + \mathbf{K}_{XSA} \sum_S \mathbf{L}_A \mathbf{K}_{AEA} + (\mathbf{K}_{XSY} + \mathbf{K}_{XSA} \sum_S \mathbf{L}_A \mathbf{K}_{ASY})) \Sigma_S \mathbf{m}_{YEA} \bar{E}^A]. \end{aligned} \quad (\text{C.19})$$

Let:

$\mathbf{m}_{XI}^L = \mathbf{L}_X (\mathbf{K}_{XI}^L + \mathbf{K}_{XSA} \sum_S \mathbf{L}_A \mathbf{K}_{AI}^L + (\mathbf{K}_{XSY} + \mathbf{K}_{XSA} \sum_S \mathbf{L}_A \mathbf{K}_{ASY}) \sum_S \mathbf{m}_{YI}^L)$  and follow

the convention is for the remaining terms. This allows equation (C.19) to be

written:

$$\begin{aligned} \bar{\psi}^X = & \mathbf{m}_{XI}^L \bar{j}_{In}^L + \mathbf{m}_{XI}^R \bar{j}_{In}^R + \mathbf{m}_{XI}^T \bar{j}_{In}^T + \mathbf{m}_{XI}^B \bar{j}_{In}^B + \mathbf{m}_{X\theta}^L \bar{\theta}_{In}^L + \mathbf{m}_{X\theta}^R \bar{\theta}_{In}^R \\ & + \mathbf{m}_{X\theta}^T \bar{\theta}_{In}^T + \mathbf{m}_{X\theta}^B \bar{\theta}_{In}^B + \mathbf{m}_{XEA} \bar{E}^A. \end{aligned} \quad (\text{C.20})$$

Both equations (C.18) and (C.20) can be substituted into back into equation

(C.15) to eliminate the higher order scattering moments. The average angular

flux is:

$$\begin{aligned} \bar{\psi}^A = & (\mathbf{L}_A \mathbf{K}_{AI}^L + \mathbf{K}_{ASX} \sum_S \mathbf{m}_{XI}^L + \mathbf{K}_{ASY} \sum_S \mathbf{m}_{YI}^L) \bar{j}_{In}^L + \\ & (\mathbf{L}_A \mathbf{K}_{AI}^R + \mathbf{K}_{ASX} \sum_S \mathbf{m}_{XI}^R + \mathbf{K}_{ASY} \sum_S \mathbf{m}_{YI}^R) \bar{j}_{In}^R + \\ & (\mathbf{L}_A \mathbf{K}_{AI}^T + \mathbf{K}_{ASX} \sum_S \mathbf{m}_{XI}^T + \mathbf{K}_{ASY} \sum_S \mathbf{m}_{YI}^T) \bar{j}_{In}^T + \\ & (\mathbf{L}_A \mathbf{K}_{AI}^B + \mathbf{K}_{ASX} \sum_S \mathbf{m}_{XI}^B + \mathbf{K}_{ASY} \sum_S \mathbf{m}_{YI}^B) \bar{j}_{In}^B + \\ & (\mathbf{L}_A \mathbf{K}_{A\theta}^L + \mathbf{K}_{ASX} \sum_S \mathbf{m}_{X\theta}^L + \mathbf{K}_{ASY} \sum_S \mathbf{m}_{Y\theta}^L) \bar{\theta}_{In}^L + \\ & (\mathbf{L}_A \mathbf{K}_{A\theta}^R + \mathbf{K}_{ASX} \sum_S \mathbf{m}_{X\theta}^R + \mathbf{K}_{ASY} \sum_S \mathbf{m}_{Y\theta}^R) \bar{\theta}_{In}^R + \\ & (\mathbf{L}_A \mathbf{K}_{A\theta}^T + \mathbf{K}_{ASX} \sum_S \mathbf{m}_{X\theta}^T + \mathbf{K}_{ASY} \sum_S \mathbf{m}_{Y\theta}^T) \bar{\theta}_{In}^T + \\ & (\mathbf{L}_A \mathbf{K}_{A\theta}^B + \mathbf{K}_{ASX} \sum_S \mathbf{m}_{X\theta}^B + \mathbf{K}_{ASY} \sum_S \mathbf{m}_{Y\theta}^B) \bar{\theta}_{In}^B \\ & (\mathbf{L}_A \mathbf{K}_{AEA} + \mathbf{K}_{ASX} \sum_S \mathbf{m}_{XEA} + \mathbf{K}_{ASY} \sum_S \mathbf{m}_{YEA}) \bar{E}^A. \end{aligned} \quad (\text{C.21})$$

Let  $m_{AI}^L = (\mathbf{L}_A \mathbf{K}_{AI}^L + \mathbf{K}_{ASX} \sum_S \mathbf{m}_{XI}^L + \mathbf{K}_{ASY} \sum_S \mathbf{m}_{YI}^L)$ , and follow the same

convention for the remaining terms. The average angular flux is:

$$\begin{aligned} \bar{\psi}^A = & \mathbf{m}_{AI}^L \bar{j}_{In}^L + \mathbf{m}_{AI}^R \bar{j}_{In}^R + \mathbf{m}_{AI}^T \bar{j}_{In}^T + \mathbf{m}_{AI}^B \bar{j}_{In}^B + \mathbf{m}_{A\theta}^L \bar{\theta}_{In}^L + \mathbf{m}_{A\theta}^R \bar{\theta}_{In}^R \\ & + \mathbf{m}_{A\theta}^T \bar{\theta}_{In}^T + \mathbf{m}_{A\theta}^B \bar{\theta}_{In}^B + \mathbf{m}_{AEA} \bar{E}^A. \end{aligned} \quad (\text{C.22})$$

Now equations (C.22), (C.20) and (C.18) with equations (C.12) through (C.14)

can be substituted into equation (C.1) to eliminate the scattering sources. This

gives:

$$\begin{aligned}
\vec{J}_{Out}^R &= (\mathbf{K}_{OI}^{RL} + \mathbf{K}_{OSA}^R \sum_S \mathbf{m}_{AI}^L + \mathbf{K}_{OSX}^R \sum_S \mathbf{m}_{XI}^L + \mathbf{K}_{OSY}^R \sum_S \mathbf{m}_{YI}^L) \vec{J}_{In}^L + \\
&(\mathbf{K}_{OI}^{RR} + \mathbf{K}_{OSA}^R \sum_S \mathbf{m}_{AI}^R + \mathbf{K}_{OSX}^R \sum_S \mathbf{m}_{XI}^R + \mathbf{K}_{OSY}^R \sum_S \mathbf{m}_{YI}^R) \vec{J}_{In}^R + \\
&(\mathbf{K}_{OI}^{RT} + \mathbf{K}_{OSA}^R \sum_S \mathbf{m}_{AI}^T + \mathbf{K}_{OSX}^R \sum_S \mathbf{m}_{XI}^T + \mathbf{K}_{OSY}^R \sum_S \mathbf{m}_{YI}^T) \vec{J}_{In}^T + \\
&(\mathbf{K}_{OI}^{RB} + \mathbf{K}_{OSA}^R \sum_S \mathbf{m}_{AI}^B + \mathbf{K}_{OSX}^R \sum_S \mathbf{m}_{XI}^B + \mathbf{K}_{OSY}^R \sum_S \mathbf{m}_{YI}^B) \vec{J}_{In}^B + \\
&(\mathbf{K}_{O\theta}^{RL} + \mathbf{K}_{OSA}^R \sum_S \mathbf{m}_{A\theta}^L + \mathbf{K}_{OSX}^R \sum_S \mathbf{m}_{X\theta}^L + \mathbf{K}_{OSY}^R \sum_S \mathbf{m}_{Y\theta}^L) \vec{\theta}_{In}^L + \\
&(\mathbf{K}_{O\theta}^{RR} + \mathbf{K}_{OSA}^R \sum_S \mathbf{m}_{A\theta}^R + \mathbf{K}_{OSX}^R \sum_S \mathbf{m}_{X\theta}^R + \mathbf{K}_{OSY}^R \sum_S \mathbf{m}_{Y\theta}^R) \vec{\theta}_{In}^R + \\
&(\mathbf{K}_{O\theta}^{RT} + \mathbf{K}_{OSA}^R \sum_S \mathbf{m}_{A\theta}^T + \mathbf{K}_{OSX}^R \sum_S \mathbf{m}_{X\theta}^T + \mathbf{K}_{OSY}^R \sum_S \mathbf{m}_{Y\theta}^T) \vec{\theta}_{In}^T + \\
&(\mathbf{K}_{O\theta}^{RB} + \mathbf{K}_{OSA}^R \sum_S \mathbf{m}_{A\theta}^B + \mathbf{K}_{OSX}^R \sum_S \mathbf{m}_{X\theta}^B + \mathbf{K}_{OSY}^R \sum_S \mathbf{m}_{Y\theta}^B) \vec{\theta}_{In}^B + \\
&(\mathbf{K}_{OEA}^R + \mathbf{K}_{OSA}^R \sum_S \mathbf{m}_{AEA} + \mathbf{K}_{OSX}^R \sum_S \mathbf{m}_{XEA} + \mathbf{K}_{OSY}^R \sum_S \mathbf{m}_{YEA}) \vec{E}^A.
\end{aligned} \tag{C.23}$$

Let  $\mathbf{m}_{OI}^{RL} = (\mathbf{K}_{OI}^{RL} + \mathbf{K}_{OSA}^R \sum_S \mathbf{m}_{AI}^L + \mathbf{K}_{OSX}^R \sum_S \mathbf{m}_{XI}^L + \mathbf{K}_{OSY}^R \sum_S \mathbf{m}_{YI}^L)$  and use the same convention for the remaining terms in equation (C.23). The same process used to produce equation (C.23) is applied to equations (C.2) through (C.8). The result is the equations for the sub-matrices presented in chapter four:

$$\begin{aligned}
\vec{J}_{Out}^R &= \mathbf{m}_{OI}^{RL} \vec{J}_{In}^L + \mathbf{m}_{OI}^{RR} \vec{J}_{In}^R + \mathbf{m}_{OI}^{RT} \vec{J}_{In}^T + \mathbf{m}_{OI}^{RB} \vec{J}_{In}^B + \mathbf{m}_{O\theta}^{RL} \vec{\theta}_{In}^L + \mathbf{m}_{O\theta}^{RR} \vec{\theta}_{In}^R \\
&+ \mathbf{m}_{O\theta}^{RT} \vec{\theta}_{In}^T + \mathbf{m}_{O\theta}^{RB} \vec{\theta}_{In}^B + \mathbf{m}_{OEA}^R \vec{E}^A,
\end{aligned} \tag{C.24}$$

$$\begin{aligned}
\vec{J}_{Out}^L &= \mathbf{m}_{OI}^{LL} \vec{J}_{In}^L + \mathbf{m}_{OI}^{LR} \vec{J}_{In}^R + \mathbf{m}_{OI}^{LT} \vec{J}_{In}^T + \mathbf{m}_{OI}^{LB} \vec{J}_{In}^B + \mathbf{m}_{O\theta}^{LL} \vec{\theta}_{In}^L + \mathbf{m}_{O\theta}^{LR} \vec{\theta}_{In}^R \\
&+ \mathbf{m}_{O\theta}^{LT} \vec{\theta}_{In}^T + \mathbf{m}_{O\theta}^{LB} \vec{\theta}_{In}^B + \mathbf{m}_{OEA}^L \vec{E}^A,
\end{aligned} \tag{C.25}$$

$$\begin{aligned}
\vec{J}_{Out}^T &= \mathbf{m}_{OI}^{TL} \vec{J}_{In}^L + \mathbf{m}_{OI}^{TR} \vec{J}_{In}^R + \mathbf{m}_{OI}^{TT} \vec{J}_{In}^T + \mathbf{m}_{OI}^{TB} \vec{J}_{In}^B + \mathbf{m}_{O\theta}^{TL} \vec{\theta}_{In}^L + \mathbf{m}_{O\theta}^{TR} \vec{\theta}_{In}^R \\
&+ \mathbf{m}_{O\theta}^{TT} \vec{\theta}_{In}^T + \mathbf{m}_{O\theta}^{TB} \vec{\theta}_{In}^B + \mathbf{m}_{OEA}^T \vec{E}^A,
\end{aligned} \tag{C.26}$$

$$\begin{aligned} \vec{J}_{Out}^B &= \mathbf{m}_{OI}^{BL} \vec{J}_{In}^L + \mathbf{m}_{OI}^{BR} \vec{J}_{In}^R + \mathbf{m}_{OI}^{BT} \vec{J}_{In}^T + \mathbf{m}_{OI}^{BB} \vec{J}_{In}^B + \mathbf{m}_{O\theta}^{BL} \vec{\theta}_{In}^L + \mathbf{m}_{O\theta}^{BR} \vec{\theta}_{In}^R \\ &\quad + \mathbf{m}_{O\theta}^{BT} \vec{\theta}_{In}^T + \mathbf{m}_{O\theta}^{BB} \vec{\theta}_{In}^B + \mathbf{m}_{OEA}^B \vec{E}^A, \end{aligned} \quad (C.27)$$

$$\begin{aligned} \vec{\theta}_{Out}^R &= \mathbf{m}_{\theta I}^{RL} \vec{J}_{In}^L + \mathbf{m}_{\theta I}^{RR} \vec{J}_{In}^R + \mathbf{m}_{\theta I}^{RT} \vec{J}_{In}^T + \mathbf{m}_{\theta I}^{RB} \vec{J}_{In}^B + \mathbf{m}_{\theta\theta}^{RL} \vec{\theta}_{In}^L + \mathbf{m}_{\theta\theta}^{RR} \vec{\theta}_{In}^R \\ &\quad + \mathbf{m}_{\theta\theta}^{RT} \vec{\theta}_{In}^T + \mathbf{m}_{\theta\theta}^{RB} \vec{\theta}_{In}^B + \mathbf{m}_{\theta EA}^R \vec{E}^A, \end{aligned} \quad (C.28)$$

$$\begin{aligned} \vec{\theta}_{Out}^L &= \mathbf{m}_{\theta I}^{LL} \vec{J}_{In}^L + \mathbf{m}_{\theta I}^{LR} \vec{J}_{In}^R + \mathbf{m}_{\theta I}^{LT} \vec{J}_{In}^T + \mathbf{m}_{\theta I}^{LB} \vec{J}_{In}^B + \mathbf{m}_{\theta\theta}^{LL} \vec{\theta}_{In}^L + \mathbf{m}_{\theta\theta}^{LR} \vec{\theta}_{In}^R \\ &\quad + \mathbf{m}_{\theta\theta}^{LT} \vec{\theta}_{In}^T + \mathbf{m}_{\theta\theta}^{LB} \vec{\theta}_{In}^B + \mathbf{m}_{\theta EA}^L \vec{E}^A, \end{aligned} \quad (C.29)$$

$$\begin{aligned} \vec{\theta}_{Out}^T &= \mathbf{m}_{\theta I}^{TL} \vec{J}_{In}^L + \mathbf{m}_{\theta I}^{TR} \vec{J}_{In}^R + \mathbf{m}_{\theta I}^{TT} \vec{J}_{In}^T + \mathbf{m}_{\theta I}^{TB} \vec{J}_{In}^B + \mathbf{m}_{\theta\theta}^{TL} \vec{\theta}_{In}^L + \mathbf{m}_{\theta\theta}^{TR} \vec{\theta}_{In}^R \\ &\quad + \mathbf{m}_{\theta\theta}^{TT} \vec{\theta}_{In}^T + \mathbf{m}_{\theta\theta}^{TB} \vec{\theta}_{In}^B + \mathbf{m}_{\theta EA}^T \vec{E}^A, \end{aligned} \quad (C.30)$$

and

$$\begin{aligned} \vec{\theta}_{Out}^B &= \mathbf{m}_{\theta I}^{BL} \vec{J}_{In}^L + \mathbf{m}_{\theta I}^{BR} \vec{J}_{In}^R + \mathbf{m}_{\theta I}^{BT} \vec{J}_{In}^T + \mathbf{m}_{\theta I}^{BB} \vec{J}_{In}^B + \mathbf{m}_{\theta\theta}^{BL} \vec{\theta}_{In}^L + \mathbf{m}_{\theta\theta}^{BR} \vec{\theta}_{In}^R \\ &\quad + \mathbf{m}_{\theta\theta}^{BT} \vec{\theta}_{In}^T + \mathbf{m}_{\theta\theta}^{BB} \vec{\theta}_{In}^B + \mathbf{m}_{\theta EA}^B \vec{E}^A. \end{aligned} \quad (C.31)$$

## Appendix D: First Spatial Moment Methods Current equations in XY-Geometry

### Equation Section 4

#### Linear Characteristic Equations

In this section, the relations for the current representation of the linear characteristic method are developed. As with the zeroth spatial moment methods, the usual representation found is in terms of the angular flux. In the rectangular cell as shown in figure D.1, the equations for the outgoing angular fluxes and edge spatial moments  $\psi^{top}$ ,  $\psi^{right}$ ,  $\theta^{top}$  and  $\theta^{right}$  in terms of the incoming angular fluxes and edge spatial moments  $\psi^{bottom}$ ,  $\psi^{left}$ ,  $\theta^{bottom}$  and  $\theta^{left}$ , scattering within the cell  $S^A$ ,  $S^X$  and  $S^Y$ , and emissions,  $E^A$ , are previously derived and presented in the literature. (12: 23)

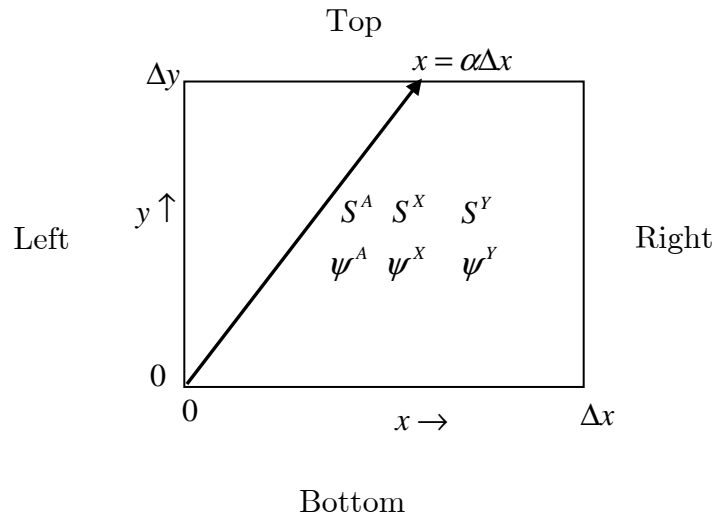


Figure D.1. Rectangular cell for first spatial moment methods. Cell shows problem variables used for solving the discrete ordinates equations.

For the rectangular cell as shown in figure D.1, the equations for the outgoing angular fluxes in terms of the incoming angular fluxes and edge distributions, scattering within the cell and emissions are:

$$\begin{aligned}
\psi^{Top} = & \alpha M_0(\varepsilon_y) \psi^{Left} + (1-\alpha) e^{-\varepsilon_y} \psi^{Bottom} + \\
& \alpha [2M_1(\varepsilon_y) - M_0(\varepsilon_y)] \theta^{Left} - \alpha (1-\alpha) e^{-\varepsilon_y} \theta^{Bottom} + \\
& \frac{\Delta y}{|\eta|} [(1-\alpha) M_0(\varepsilon_y) + \alpha M_1(\varepsilon_y)] S^A + \\
& \frac{\Delta y}{|\eta|} \alpha [-(1-\alpha) M_0(\varepsilon_y) + (1-2\alpha) M_1(\varepsilon_y) + \alpha M_2(\varepsilon_y)] S^X + \\
& \frac{\Delta y}{|\eta|} [-(1-\alpha) M_0(\varepsilon_y) + (2-3\alpha) M_1(\varepsilon_y) + \alpha M_2(\varepsilon_y)] S^Y + \\
& \frac{\Delta y}{|\eta|} [(1-\alpha) M_0(\varepsilon_y) + \alpha M_1(\varepsilon_y)] E^A,
\end{aligned} \tag{D.1}$$

$$\begin{aligned}
\psi^{Right} = & M_0(\varepsilon_y) \psi^{Bottom} + [(1-2\alpha) M_0(\varepsilon_y) + 2\alpha M_1(\varepsilon_y)] \theta^{Bottom} + \\
& \frac{\Delta y}{|\eta|} M_1(\varepsilon_y) S^A + \\
& \frac{\Delta y}{|\eta|} [(1-2\alpha) M_1(\varepsilon_y) + 2\alpha M_2(\varepsilon_y)] S^X + \\
& \frac{\Delta y}{|\eta|} [M_2(\varepsilon_y) - M_1(\varepsilon_y)] S^Y + \frac{\Delta y}{|\eta|} M_1(\varepsilon_y) E^A,
\end{aligned} \tag{D.2}$$

$$\begin{aligned}
\theta^{Top} = & 3\alpha[(2\alpha-1)M_0(\varepsilon_y) - 2\alpha M_1(\varepsilon_y)]\psi^{Left} + 3\alpha(1-\alpha)e^{-\varepsilon_y}\psi^{Bottom} + \\
& 3\alpha[(1-2\alpha)M_0(\varepsilon_y) + (6\alpha-2)M_1(\varepsilon_y) - 4\alpha M_2(\varepsilon_y)]\theta^{Left} + (1-3\alpha+2\alpha^2)e^{-\varepsilon_y}\theta^{Bottom} + \\
& \frac{\Delta y}{|\eta|} 3\alpha[(1-\alpha)M_0(\varepsilon_y) + (2\alpha-1)M_1(\varepsilon_y) - \alpha M_2(\varepsilon_y)]S^A + \\
& \frac{\Delta y}{|\eta|} [(1-3\alpha+2\alpha^3)M_0(\varepsilon_y) + (3\alpha-6\alpha^3)M_1(\varepsilon_y) + 6\alpha^3 M_2(\varepsilon_y) - 2\alpha^3 M_3(\varepsilon_y)]S^X + \quad (D.3) \\
& \frac{\Delta y}{|\eta|} 3\alpha[-(1-\alpha)M_0(\varepsilon_y) + (3-4\alpha)M_1(\varepsilon_y) - (2-5\alpha)M_2(\varepsilon_y) - 2\alpha M_3(\varepsilon_y)]S^Y + \\
& \frac{\Delta y}{|\eta|} [(1-\alpha)M_0(\varepsilon_y) + \alpha M_1(\varepsilon_y)]E^A,
\end{aligned}$$

$$\begin{aligned}
\theta^{Right} = & 3[M_0(\varepsilon_y) - 2M_1(\varepsilon_y)]\psi^{Bottom} + \\
& 3[(1-2\alpha)M_0(\varepsilon_y) + (6\alpha-2)M_1(\varepsilon_y) - 4\alpha M_2(\varepsilon_y)]\theta^{Bottom} + \\
& \frac{\Delta y}{|\eta|} 3[M_1(\varepsilon_y) - M_2(\varepsilon_y)]S^A + \\
& \frac{\Delta y}{|\eta|} 3[(1-2\alpha)M_1(\varepsilon_y) - (1-4\alpha)M_2(\varepsilon_y) - 2\alpha M_3(\varepsilon_y)]S^X + \quad (D.4) \\
& \frac{\Delta y}{|\eta|} [-3M_1(\varepsilon_y) + 6M_2(\varepsilon_y) - 2M_3(\varepsilon_y)]S^Y + \\
& \frac{\Delta y}{|\eta|} 3[M_1(\varepsilon_y) - M_2(\varepsilon_y)]E^A,
\end{aligned}$$

$$\begin{aligned}
\psi^A = & \alpha M_1(\varepsilon_y)\psi^{Left} + [(1-\alpha)M_0(\varepsilon_y) + \alpha M_1(\varepsilon_y)]\psi^{Bottom} + \\
& \alpha[M_2(\varepsilon_y) - M_1(\varepsilon_y)]\theta^{Left} + \alpha[-(1-\alpha)M_0(\varepsilon_y) + (1-2\alpha)M_1(\varepsilon_y) + \alpha M_2(\varepsilon_y)]\theta^{Bottom} + \\
& \frac{\Delta y}{|\eta|} [(1-\alpha)M_1(\varepsilon_y) + \alpha M_2(\varepsilon_y)]S^A + \\
& \frac{\Delta y}{|\eta|} \alpha[-(1-\alpha)M_1(\varepsilon_y) + (1-2\alpha)M_2(\varepsilon_y) + \alpha M_3(\varepsilon_y)]S^X + \quad (D.5) \\
& \frac{\Delta y}{|\eta|} [-(1-\alpha)M_1(\varepsilon_y) + (1-2\alpha)M_2(\varepsilon_y) + \alpha M_3(\varepsilon_y)]S^Y + \\
& \frac{\Delta y}{|\eta|} [(1-\alpha)M_1(\varepsilon_y) + \alpha M_2(\varepsilon_y)]E^A,
\end{aligned}$$

$$\begin{aligned}
\psi^X &= 3\alpha[(2\alpha-1)M_1(\varepsilon_y)-2\alpha M_2(\varepsilon_y)]\psi^{Left} + \\
& 3\alpha[(1-\alpha)M_0(\varepsilon_y)+(2\alpha-1)M_1(\varepsilon_y)-\alpha M_2(\varepsilon_y)]\psi^{Bottom} + \\
& 3\alpha[(1-2\alpha)M_1(\varepsilon_y)-(4\alpha-1)M_2(\varepsilon_y)-2\alpha M_3(\varepsilon_y)]\theta^{Left} + \\
& [(1-3\alpha+2\alpha^3)M_0(\varepsilon_y)+(3\alpha-6\alpha^3)M_1(\varepsilon_y)+6\alpha^3 M_2(\varepsilon_y)-2\alpha^3 M_3(\varepsilon_y)]\theta^{Bottom} + \\
& \frac{\Delta y}{|\eta|} 3\alpha[(1-\alpha)M_1(\varepsilon_y)+(2\alpha-1)M_2(\varepsilon_y)-\alpha M_3(\varepsilon_y)]S^A + \\
& \frac{\Delta y}{|\eta|} [(1-3\alpha+2\alpha^3)M_1(\varepsilon_y)+(3\alpha-6\alpha^3)M_2(\varepsilon_y)+6\alpha^3 M_3(\varepsilon_y)-2\alpha^3 M_4(\varepsilon_y)]S^X + \\
& \frac{\Delta y}{|\eta|} 3\alpha[-(1-\alpha)M_1(\varepsilon_y)+(2-3\alpha)M_2(\varepsilon_y)-(1-3\alpha)M_3(\varepsilon_y)-\alpha M_4(\varepsilon_y)]S^Y + \\
& \frac{\Delta y}{|\eta|} 3\alpha[(1-\alpha)M_1(\varepsilon_y)+(2\alpha-1)M_2(\varepsilon_y)-\alpha M_3(\varepsilon_y)]E^A,
\end{aligned} \tag{D.6}$$

$$\begin{aligned}
\psi^Y &= 3\alpha[M_1(\varepsilon_y)-M_2(\varepsilon_y)]\psi^{Left} + \\
& 3[(1-\alpha)M_0(\varepsilon_y)+(3\alpha-2)M_1(\varepsilon_y)-2\alpha M_2(\varepsilon_y)]\psi^{Bottom} + \\
& \alpha[-3M_0(\varepsilon_y)+6M_1(\varepsilon_y)-2M_2(\varepsilon_y)]\theta^{Left} + \\
& 3\alpha[-(1-\alpha)M_0(\varepsilon_y)+(3-4\alpha)M_1(\varepsilon_y)+(5\alpha-2)M_2(\varepsilon_y)-2\alpha M_3(\varepsilon_y)]\theta^{Bottom} + \\
& \frac{\Delta y}{|\eta|} 3[(1-\alpha)M_1(\varepsilon_y)+(2\alpha-1)M_2(\varepsilon_y)-\alpha M_3(\varepsilon_y)]S^A + \\
& \frac{\Delta y}{|\eta|} 3\alpha[-(1-\alpha)M_1(\varepsilon_y)+(2-3\alpha)M_2(\varepsilon_y)-(1-3\alpha)M_3(\varepsilon_y)-\alpha M_4(\varepsilon_y)]S^X + \\
& \frac{\Delta y}{|\eta|} [-3(1-\alpha)M_1(\varepsilon_y)+(6-9\alpha)M_2(\varepsilon_y)-(2-8\alpha)M_3(\varepsilon_y)-2\alpha M_4(\varepsilon_y)]S^Y + \\
& \frac{\Delta y}{|\eta|} 3[(1-\alpha)M_1(\varepsilon_y)+(2\alpha-1)M_2(\varepsilon_y)-\alpha M_3(\varepsilon_y)]E^A.
\end{aligned} \tag{D.7}$$

For these relations,  $\mu$  and  $\eta$  are the direction cosines along the x and y axis respectively from the angular quadrature,  $\varepsilon_y = \frac{\sigma\Delta y}{|\eta|}$  is the optical thickness in



the y direction,  $\alpha = \frac{\varepsilon_y}{\varepsilon_x}$  is a parameter for the cell, and  $M_0(\varepsilon_y)$ ,  $M_1(\varepsilon_y)$ ,  $M_2(\varepsilon_y)$ ,

$M_3(\varepsilon_y)$ , and  $M_4(\varepsilon_y)$  are the exponential moment functions (11: 27).

The definition for the currents  $j^{Right} = |\mu|\psi^{Right}$ , and  $j^{Top} = |\eta|\psi^{Top}$  and similarly for the left and bottom, allows the transition from angular fluxes to a current representation. For the first spatial moment methods however, the edge spatial moments must also be transformed, as they now represent the spatial moment of the current, not the angular flux. This is done in the same manner as the currents  $\theta^{Right} = |\mu|\theta^{Right}$  and  $\theta^{Top} = |\eta|\theta^{Top}$ , although the notation is the same for both. The equations (D.1) through (D.7) in a current representation are:

$$\begin{aligned}
j^{Top} &= \frac{\eta}{\mu} \alpha M_0(\varepsilon_y) j^{Left} + (1-\alpha) e^{-\varepsilon_y} j^{Bottom} + \\
&\frac{\eta}{\mu} \alpha [2M_1(\varepsilon_y) - M_0(\varepsilon_y)] \theta^{Left} - \alpha (1-\alpha) e^{-\varepsilon_y} \theta^{Bottom} + \\
&\Delta y [(1-\alpha) M_0(\varepsilon_y) + \alpha M_1(\varepsilon_y)] S^A + \\
&\Delta y \alpha [-(1-\alpha) M_0(\varepsilon_y) + (1-2\alpha) M_1(\varepsilon_y) + \alpha M_2(\varepsilon_y)] S^X + \\
&\Delta y [-(1-\alpha) M_0(\varepsilon_y) + (2-3\alpha) M_1(\varepsilon_y) + \alpha M_2(\varepsilon_y)] S^Y + \\
&\Delta y [(1-\alpha) M_0(\varepsilon_y) + \alpha M_1(\varepsilon_y)] E^A,
\end{aligned} \tag{D.8}$$

$$\begin{aligned}
j^{Right} &= \frac{\mu}{\eta} M_0(\varepsilon_y) j^{Bottom} + \frac{\mu}{\eta} [(1-2\alpha) M_0(\varepsilon_y) + 2\alpha M_1(\varepsilon_y)] \theta^{Bottom} + \\
&\frac{\mu \Delta y}{\eta} M_1(\varepsilon_y) S^A + \\
&\frac{\mu \Delta y}{\eta} [(1-2\alpha) M_1(\varepsilon_y) + 2\alpha M_2(\varepsilon_y)] S^X + \\
&\frac{\mu \Delta y}{\eta} [M_2(\varepsilon_y) - M_1(\varepsilon_y)] S^Y + \frac{\mu \Delta y}{\eta} M_1(\varepsilon_y) E^A,
\end{aligned} \tag{D.9}$$

$$\begin{aligned}
\theta^{Top} = & \frac{\eta}{\mu} 3\alpha[(2\alpha-1)M_0(\varepsilon_y) - 2\alpha M_1(\varepsilon_y)]j^{Left} + 3\alpha(1-\alpha)e^{-\varepsilon_y} j^{Bottom} + \\
& \frac{\eta}{\mu} 3\alpha[(1-2\alpha)M_0(\varepsilon_y) + (6\alpha-2)M_1(\varepsilon_y) - 4\alpha M_2(\varepsilon_y)]\theta^{Left} + \\
& (1-3\alpha+2\alpha^2)e^{-\varepsilon_y} \theta^{Bottom} + \\
& \Delta y 3\alpha[(1-\alpha)M_0(\varepsilon_y) + (2\alpha-1)M_1(\varepsilon_y) - \alpha M_2(\varepsilon_y)]S^A + \\
& \Delta y [(1-3\alpha+2\alpha^3)M_0(\varepsilon_y) + (3\alpha-6\alpha^3)M_1(\varepsilon_y) + 6\alpha^3 M_2(\varepsilon_y) - 2\alpha^3 M_3(\varepsilon_y)]S^X + \\
& \Delta y 3\alpha[-(1-\alpha)M_0(\varepsilon_y) + (3-4\alpha)M_1(\varepsilon_y) - (2-5\alpha)M_2(\varepsilon_y) - 2\alpha M_3(\varepsilon_y)]S^Y + \\
& \Delta y [(1-\alpha)M_0(\varepsilon_y) + \alpha M_1(\varepsilon_y)]E^A,
\end{aligned} \tag{D.10}$$

$$\begin{aligned}
\theta^{Right} = & \frac{\mu}{\eta} 3[M_0(\varepsilon_y) - 2M_1(\varepsilon_y)]j^{Bottom} + \\
& \frac{\mu}{\eta} 3[(1-2\alpha)M_0(\varepsilon_y) + (6\alpha-2)M_1(\varepsilon_y) - 4\alpha M_2(\varepsilon_y)]\theta^{Bottom} + \\
& \frac{\mu \Delta y}{\eta} 3[M_1(\varepsilon_y) - M_2(\varepsilon_y)]S^A + \\
& \frac{\mu \Delta y}{\eta} 3[(1-2\alpha)M_1(\varepsilon_y) - (1-4\alpha)M_2(\varepsilon_y) - 2\alpha M_3(\varepsilon_y)]S^X + \\
& \frac{\mu \Delta y}{\eta} [-3M_1(\varepsilon_y) + 6M_2(\varepsilon_y) - 2M_3(\varepsilon_y)]S^Y + \\
& \frac{\mu \Delta y}{\eta} 3[M_1(\varepsilon_y) - M_2(\varepsilon_y)]E^A,
\end{aligned} \tag{D.11}$$

$$\begin{aligned}
\psi^A = & \frac{1}{\mu} \alpha M_1(\varepsilon_y) j^{Left} + \frac{1}{\eta} [(1-\alpha)M_0(\varepsilon_y) + \alpha M_1(\varepsilon_y)] j^{Bottom} + \\
& \frac{1}{\mu} \alpha [M_2(\varepsilon_y) - M_1(\varepsilon_y)] \theta^{Left} + \\
& \frac{\alpha}{\eta} [-(1-\alpha)M_0(\varepsilon_y) + (1-2\alpha)M_1(\varepsilon_y) + \alpha M_2(\varepsilon_y)] \theta^{Bottom} + \\
& \frac{\Delta y}{\eta} [(1-\alpha)M_1(\varepsilon_y) + \alpha M_2(\varepsilon_y)] S^A + \\
& \frac{\Delta y \alpha}{\eta} [-(1-\alpha)M_1(\varepsilon_y) + (1-2\alpha)M_2(\varepsilon_y) + \alpha M_3(\varepsilon_y)] S^X + \\
& \frac{\Delta y}{\eta} [-(1-\alpha)M_1(\varepsilon_y) + (1-2\alpha)M_2(\varepsilon_y) + \alpha M_3(\varepsilon_y)] S^Y + \\
& \frac{\Delta y}{\eta} [(1-\alpha)M_1(\varepsilon_y) + \alpha M_2(\varepsilon_y)] E^A,
\end{aligned} \tag{D.12}$$

$$\begin{aligned}
\psi^X = & \frac{1}{\mu} 3\alpha [(2\alpha-1)M_1(\varepsilon_y) - 2\alpha M_2(\varepsilon_y)] j^{Left} + \\
& \frac{1}{\eta} 3\alpha [(1-\alpha)M_0(\varepsilon_y) + (2\alpha-1)M_1(\varepsilon_y) - \alpha M_2(\varepsilon_y)] j^{Bottom} + \\
& \frac{1}{\mu} 3\alpha [(1-2\alpha)M_1(\varepsilon_y) - (4\alpha-1)M_2(\varepsilon_y) - 2\alpha M_3(\varepsilon_y)] \theta^{Left} + \\
& \frac{1}{\eta} [(1-3\alpha+2\alpha^3)M_0(\varepsilon_y) + (3\alpha-6\alpha^3)M_1(\varepsilon_y) + \\
& 6\alpha^3 M_2(\varepsilon_y) - 2\alpha^3 M_3(\varepsilon_y)] \theta^{Bottom} + \\
& \frac{\Delta y 3\alpha}{\eta} [(1-\alpha)M_1(\varepsilon_y) + (2\alpha-1)M_2(\varepsilon_y) - \alpha M_3(\varepsilon_y)] S^A + \\
& \frac{\Delta y}{\eta} [(1-3\alpha+2\alpha^3)M_1(\varepsilon_y) + (3\alpha-6\alpha^3)M_2(\varepsilon_y) + 6\alpha^3 M_3(\varepsilon_y) - 2\alpha^3 M_4(\varepsilon_y)] S^X + \\
& \frac{\Delta y 3\alpha}{\eta} [-(1-\alpha)M_1(\varepsilon_y) + (2-3\alpha)M_2(\varepsilon_y) - (1-3\alpha)M_3(\varepsilon_y) - \alpha M_4(\varepsilon_y)] S^Y + \\
& \frac{\Delta y 3\alpha}{\eta} [(1-\alpha)M_1(\varepsilon_y) + (2\alpha-1)M_2(\varepsilon_y) - \alpha M_3(\varepsilon_y)] E^A,
\end{aligned} \tag{D.13}$$

$$\begin{aligned}
\psi^Y &= \frac{3\alpha}{\mu} [M_1(\varepsilon_y) - M_2(\varepsilon_y)] j^{Left} + \\
&\frac{3}{\eta} [(1-\alpha)M_0(\varepsilon_y) + (3\alpha-2)M_1(\varepsilon_y) - 2\alpha M_2(\varepsilon_y)] j^{Bottom} + \\
&\frac{1}{\mu} \alpha [-3M_0(\varepsilon_y) + 6M_1(\varepsilon_y) - 2M_2(\varepsilon_y)] \theta^{Left} + \\
&\frac{3\alpha}{\eta} [-(1-\alpha)M_0(\varepsilon_y) + (3-4\alpha)M_1(\varepsilon_y) + (5\alpha-2)M_2(\varepsilon_y) - 2\alpha M_3(\varepsilon_y)] \theta^{Bottom} + \\
&\frac{\Delta y^3}{\eta} [(1-\alpha)M_1(\varepsilon_y) + (2\alpha-1)M_2(\varepsilon_y) - \alpha M_3(\varepsilon_y)] S^A + \\
&\frac{\Delta y^3 \alpha}{\eta} [-(1-\alpha)M_1(\varepsilon_y) + (2-3\alpha)M_2(\varepsilon_y) - (1-3\alpha)M_3(\varepsilon_y) - \alpha M_4(\varepsilon_y)] S^X + \\
&\frac{\Delta y}{\eta} [-3(1-\alpha)M_1(\varepsilon_y) + (6-9\alpha)M_2(\varepsilon_y) - (2-8\alpha)M_3(\varepsilon_y) - 2\alpha M_4(\varepsilon_y)] S^Y + \\
&\frac{\Delta y^3}{\eta} [(1-\alpha)M_1(\varepsilon_y) + (2\alpha-1)M_2(\varepsilon_y) - \alpha M_3(\varepsilon_y)] E^A.
\end{aligned} \tag{D.14}$$

These are the relations used in chapter four for substitution into the first spatial moment method.

### Linear Discontinuous Equations

In this section, the relations for the current representation of the linear discontinuous method are developed. As with the zeroth spatial moment methods, the usual representation found is in terms of the angular flux. In the rectangular cell as shown in figure D.1, the equations for the outgoing angular fluxes and edge spatial moments  $\psi^{top}$ ,  $\psi^{right}$ ,  $\theta^{top}$  and  $\theta^{right}$  in terms of the incoming angular fluxes and edge spatial moments  $\psi^{bottom}$ ,  $\psi^{left}$ ,  $\theta^{bottom}$  and  $\theta^{left}$ , scattering within the cell  $S^A$ ,  $S^X$ ,  $S^Y$ , and emissions  $E^A$ , are previously

derived and presented in the literature (4: 289-290). The linear discontinuous relations for the edge values are:

$$\psi^{Right} = \psi^A + \psi^X, \quad (D.15)$$

$$\psi^{Top} = \psi^A + \psi^Y, \quad (D.16)$$

$$\theta^{Right} = \psi^Y, \quad (D.17)$$

and

$$\theta^{Top} = \psi^X. \quad (D.18)$$

These can be substituted into the zeroth, x and y moment cell balance equations:

$$\alpha(\psi^{Right} - \psi^{Left}) + (\psi^{Top} - \psi^{Bottom}) + \varepsilon_y \psi^A = S^A \frac{\Delta y}{\eta}, \quad (D.19)$$

$$3\alpha(\psi^{Right} + \psi^{Left} - 2\psi_A) + (\theta^{Top} - \theta^{Bottom}) + \varepsilon_y \psi^X = S^X \frac{\Delta y}{\eta}, \quad (D.20)$$

$$3(\psi^{Top} + \psi^{Bottom} - 2\psi_A) + \alpha(\theta^{Right} - \theta^{Left}) + \varepsilon_y \psi^Y = S^Y \frac{\Delta y}{\eta}, \quad (D.21)$$

where the following relations are defined:

$$\begin{aligned} a &= 1 + \alpha + \varepsilon_y + \frac{3}{4 + \varepsilon_y} + \frac{3\alpha^2}{1 + 3\alpha + \varepsilon_y}, \\ b &= 4 + \varepsilon_y, \\ c &= 1 + 3\alpha + \varepsilon_y. \end{aligned} \quad (D.22)$$

After some algebra, the cell values are:

$$\psi^A = \frac{\frac{\Delta y}{|\eta|} S^A + \psi^{Bottom} + \alpha \psi^{Left} + \frac{3\psi^{Bottom} - \theta^{Left} - \frac{\Delta y}{|\eta|} S^Y}{b} + \frac{\alpha(3\psi^{Left} - \theta^{Bottom} - \frac{\Delta y}{|\eta|} S^X)}{c}}{a} \quad (D.23)$$

$$\psi^X = \frac{\frac{\Delta y}{|\eta|} S^X + \theta^{Bottom} + 3\alpha(\psi^A - \psi^{Left})}{c}, \quad (D.24)$$

and

$$\psi^Y = \frac{\frac{\Delta y}{|\eta|} S^Y + \theta^{Left} + 3(\psi^A - \psi^{Bottom})}{b}. \quad (D.25)$$

The desired relations in the angular flux relation are found using equations (D.15) through (D.18) with equations (D.23) through (D.25):

$$\begin{aligned} \psi^{Top} = & \left[ \frac{(3+b)\alpha}{ab} + \frac{3(3+b)\alpha}{abc} \right] \psi^{Left} + \frac{(9+6b-3ab+b^2)}{ab^2} \psi^{Bottom} + \frac{(-3+(a-1)b)}{ab^2} \theta^{Left} - \\ & \frac{\alpha(b+3)}{abc} \theta^{Bottom} + \frac{\Delta y(b+3)}{ab|\eta|} S^A - \frac{\Delta y\alpha(b+3)}{abc|\eta|} S^X + \frac{\Delta y(-3+(a-1)b)}{ab^2|\eta|} S^Y + \\ & \frac{\Delta y(b+3)}{ab|\eta|} E^A, \end{aligned} \quad (D.26)$$

$$\begin{aligned} \psi^{Right} = & \left[ \frac{3\alpha(c-ac+3\alpha)}{ac^2} + \frac{\alpha(c+3\alpha)}{ac} \right] \psi^{Left} + \frac{(3+b)(c+3\alpha)}{abc} \psi^{Bottom} - \frac{(c+3\alpha)}{abc} \theta^{Left} + \\ & \frac{(ac-\alpha(c+3\alpha))}{ac^2} \theta^{Bottom} + \frac{\Delta y(c+3\alpha)}{ac|\eta|} S^A + \frac{\Delta y(ac-\alpha(c+3\alpha))}{ac^2|\eta|} S^X - \\ & \frac{\Delta y(c+3\alpha)\mu}{abc|\eta|} S^Y + \frac{\Delta y(c+3\alpha)}{ac|\eta|} E^A, \end{aligned} \quad (D.27)$$

$$\begin{aligned} \theta^{Top} = & \left[ \frac{3\alpha^2}{ac} - \frac{3\alpha(ac-3\alpha)}{ac^2} \right] \psi^{Left} + \frac{3(3+b)\alpha}{abc} \psi^{Bottom} - \frac{3\alpha}{abc} \theta^{Left} + \frac{(ac-3\alpha^2)}{ac^2} \theta^{Bottom} + \\ & \frac{\Delta y 3\alpha}{ac|\eta|} S^A + \frac{\Delta y(ac-3\alpha^2)}{ac^2|\eta|} S^X - \frac{\Delta y 3\alpha}{abc|\eta|} S^Y + \frac{\Delta y 3\alpha}{ac|\eta|} E^A, \end{aligned} \quad (D.28)$$

$$\begin{aligned} \theta^{Right} = & \left[ \frac{3\alpha}{ab} + \frac{9\alpha}{abc} \right] \psi^{Left} + \frac{9+3B-3ab}{ab^2} \psi^{Bottom} + \frac{(-3+ab)}{ab^2} \theta^{Left} - \\ & \frac{3\alpha}{abc} \theta^{Bottom} + \frac{3\Delta y}{ab|\eta|} S^A - \frac{3\Delta y\alpha}{abc|\eta|} S^X + \frac{\Delta y(ab-3)}{ab^2|\eta|} S^Y + \frac{3\Delta y}{ab|\eta|} E^A, \end{aligned} \quad (D.29)$$

$$\begin{aligned} \psi^A = & \left[ \frac{\alpha}{a} + \frac{3\alpha}{ac} \right] \psi^{Left} + \frac{(3+b)}{ab} \psi^{Bottom} - \frac{1}{ab} \theta^{Left} - \frac{\alpha}{ac} \theta^{Bottom} + \\ & \frac{\Delta y}{a|\eta|} S^A - \frac{\Delta y \alpha}{ac|\eta|} S^X - \frac{\Delta y}{ab|\eta|} S^Y + \frac{\Delta y}{a|\eta|} E^A, \end{aligned} \quad (D.30)$$

$$\begin{aligned} \psi^X = & \left[ \frac{3\alpha^2}{ac} - \frac{3\alpha(ac-3\alpha)}{ac^2} \right] \psi^{Left} + \frac{3(3+b)\alpha}{abc} \psi^{Bottom} - \\ & \frac{3\alpha}{abc} \theta^{Left} + \frac{(ac-3\alpha^2)}{ac^2} \theta^{Bottom} + \\ & \frac{\Delta y 3\alpha}{ac|\eta|} S^A + \frac{\Delta y(ac-3\alpha^2)}{ac^2|\eta|} S^X - \frac{\Delta y 3\alpha}{abc|\eta|} S^Y + \frac{\Delta y 3\alpha}{ac|\eta|} E^A, \end{aligned} \quad (D.31)$$

$$\begin{aligned} \psi^Y = & \left[ \frac{3\alpha}{ab} + \frac{9\alpha}{abc} \right] \psi^{Left} + \frac{(9+3b-3ab)}{ab^2} \psi^{Bottom} + \frac{(-3+ab)}{ab^2} \theta^{Left} - \frac{3\alpha}{abc} \theta^{Bottom} + \\ & \frac{\Delta y 3}{ab|\eta|} S^A - \frac{\Delta y 3\alpha}{abc|\eta|} S^X + \frac{\Delta y(ab-3)}{ab^2|\eta|} S^Y + \frac{\Delta y 3\alpha}{ac|\eta|} E^A. \end{aligned} \quad (D.32)$$

The definition for the currents  $j^{Right} = |\mu| \psi^{Right}$ , and  $j^{Top} = |\eta| \psi^{Top}$  and similarly for the left and bottom, allows the transition from an angular flux to a current representation. As with the LC method, the edge spatial moments must also be transformed, as they now represent the spatial moment of the current, not the angular flux. This is done in the same manner as the currents  $\theta^{Right} = |\mu| \theta^{Right}$ , and  $\theta^{Top} = |\eta| \theta^{Top}$  although the notation is the same for both. The equations for the outgoing quantities are:

$$\begin{aligned} j^{Top} = & \frac{(3+b)(3+c)\alpha\eta}{abc|\mu|} j^{Left} + \frac{(9+6b-3ab+b^2)}{ab^2} j^{Bottom} + \frac{(-3+(a-1)b)\eta}{ab^2|\mu|} \theta^{Left} - \\ & \frac{\alpha(b+3)}{abc} \theta^{Bottom} + \frac{\Delta y(b+3)}{ab} S^A - \frac{\Delta y \alpha(b+3)}{abc} S^X + \frac{\Delta y(-3+(a-1)b)}{ab^2} S^Y + \\ & \frac{\Delta y(b+3)}{ab} E^A, \end{aligned} \quad (D.33)$$

$$\begin{aligned}
j^{Right} &= \frac{\alpha(c^2 + 9\alpha + c(3 - 3a + 3\alpha))}{ac^2} j^{Left} + \frac{(3+b)(c+3\alpha)|\mu|}{abc|\eta|} j^{Bottom} - \frac{(c+3\alpha)}{abc} \theta^{Left} + \\
&\frac{(ac - \alpha(c+3\alpha))|\mu|}{ac^2|\eta|} \theta^{Bottom} + \frac{\Delta y(c+3\alpha)|\mu|}{ac|\eta|} S^A + \frac{\Delta y(ac - \alpha(c+3\alpha))\mu}{ac^2\eta} S^X - \\
&\frac{\Delta y(c+3\alpha)|\mu|}{abc|\eta|} S^Y + \frac{\Delta y(c+3\alpha)|\mu|}{ac|\eta|} E^A, \tag{D.34}
\end{aligned}$$

$$\begin{aligned}
\theta^{Top} &= \frac{3\alpha(-ac + (3+c)\alpha)|\eta|}{ac^2|\mu|} j^{Left} + \frac{3(3+b)\alpha}{abc} j^{Bottom} - \\
&\frac{3\alpha|\eta|}{abc|\mu|} \theta^{Left} + \frac{(ac - 3\alpha^2)}{ac^2} \theta^{Bottom} + \\
&\frac{\Delta y 3\alpha}{ac} S^A + \frac{\Delta y(ac - 3\alpha^2)}{ac^2} S^X - \frac{\Delta y 3\alpha}{abc} S^Y + \frac{\Delta y 3\alpha}{ac} E^A, \tag{D.35}
\end{aligned}$$

$$\begin{aligned}
\theta^{Right} &= \frac{3\alpha(3+c)}{abc} j^{Left} - \frac{3(-3 + (a-1)b)|\mu|}{ab^2|\eta|} j^{Bottom} + \frac{(-3+ab)}{ab^2} \theta^{Left} - \\
&\frac{3\alpha|\mu|}{abc|\eta|} \theta^{Bottom} + \frac{3\Delta y|\mu|}{ab|\eta|} S^A - \frac{3\Delta y\alpha|\mu|}{abc|\eta|} S^X + \\
&\frac{\Delta y(ab-3)|\mu|}{ab^2|\eta|} S^Y + \frac{3\Delta y|\mu|}{ab|\eta|} E^A, \tag{D.36}
\end{aligned}$$

$$\begin{aligned}
\psi^A &= \frac{\alpha(3+c)}{ac|\mu|} j^{Left} + \frac{(3+b)}{ab|\eta|} j^{Bottom} - \frac{1}{ab|\mu|} \theta^{Left} - \frac{\alpha}{ac|\eta|} \theta^{Bottom} + \\
&\frac{\Delta y}{a|\eta|} S^A - \frac{\Delta y\alpha}{ac|\eta|} S^X - \frac{\Delta y}{ab|\eta|} S^Y + \frac{\Delta y}{a|\eta|} E^A, \tag{D.37}
\end{aligned}$$

$$\begin{aligned}
\psi^X &= \frac{3\alpha(-ac + (3+c)\alpha)}{ac^2|\mu|} j^{Left} + \frac{3(3+b)\alpha}{abc|\eta|} j^{Bottom} - \\
&\frac{3\alpha}{abc|\mu|} \theta^{Left} + \frac{(ac - 3\alpha^2)}{ac^2|\eta|} \theta^{Bottom} + \\
&\frac{\Delta y 3\alpha}{ac|\eta|} S^A + \frac{\Delta y(ac - 3\alpha^2)}{ac^2|\eta|} S^X - \frac{\Delta y 3\alpha}{abc|\eta|} S^Y + \frac{\Delta y 3\alpha}{ac|\eta|} E^A, \tag{D.38}
\end{aligned}$$



$$\begin{aligned}
\psi^Y = & \frac{3\alpha(3+c)}{abc|\mu|} j^{Left} + \frac{(9+3b-3ab)}{ab^2|\eta|} j^{Bottom} + \frac{(-3+ab)}{ab^2|\mu|} \theta^{Left} - \frac{3\alpha}{abc|\eta|} \theta^{Bottom} + \\
& \frac{\Delta y 3}{ab|\eta|} S^A - \frac{\Delta y 3\alpha}{abc|\eta|} S^X + \frac{\Delta y(ab-3)}{ab^2|\eta|} S^Y + \frac{\Delta y 3\alpha}{ac|\eta|} E^A.
\end{aligned} \tag{D.39}$$

These are the relationships used in chapter four.

## Appendix E: First Spatial Moment Methods Derivation in Slab Geometry

### Equation Section 5

This appendix contains the complete derivation for the first spatial moment method presented in chapter three in a general form. The first spatial moment methods need several additional equations to account for the contribution to the flux from the first moment of the scattering source. The relations described for the zeroth spatial moment methods in chapter three become:

$$\vec{\psi}^{out} = \mathbf{K}_{OI} \vec{\psi}^{in} + \mathbf{K}_{OSA} \bar{S}^A + \mathbf{K}_{OSX} \bar{S}^X + \mathbf{K}_{OEA} \bar{E}^A, \quad (\text{E.1})$$

$$\vec{\psi}^A = \mathbf{K}_{AI} \vec{\psi}^{in} + \mathbf{K}_{ASA} \bar{S}^A + \mathbf{K}_{ASX} \bar{S}^X + \mathbf{K}_{AEA} \bar{E}^A, \quad (\text{E.2})$$

$$\vec{\psi}^X = \mathbf{K}_{XI} \vec{\psi}^{in} + \mathbf{K}_{XSA} \bar{S}^A + \mathbf{K}_{XSX} \bar{S}^X + \mathbf{K}_{XEA} \bar{E}^A, \quad (\text{E.3})$$

$$\bar{S}^A = \sum_S \vec{\psi}^A, \quad (\text{E.4})$$

and

$$\bar{S}^X = \sum_S \vec{\psi}^X. \quad (\text{E.5})$$

Again,  $\mathbf{K}_{OI}$ ,  $\mathbf{K}_{OSA}$ ,  $\mathbf{K}_{OEA}$ ,  $\mathbf{K}_{AI}$ ,  $\mathbf{K}_{ASA}$ ,  $\mathbf{K}_{ASX}$ ,  $\mathbf{K}_{AEA}$ ,  $\mathbf{K}_{XI}$ ,  $\mathbf{K}_{XSA}$ ,  $\mathbf{K}_{XSX}$ , and  $\mathbf{K}_{XEA}$  represent diagonal matrices of transport coefficients that define the relations of the inputs of a cell to the calculated quantity. For example  $\mathbf{K}_{XI}$  represents the contribution to the first moment flux from the incoming flux and  $\sum_S$  is the scattering matrix described in chapter three. These matrices are the sub-matrices used in the general derivation shown in chapter three.

Equations (E.4) can be substituted into equation (E.2) to eliminate the average scatter:

$$\vec{\psi}^A = (\mathbf{I} - \mathbf{K}_{ASA} \Sigma_S)^{-1} [\mathbf{K}_{AI} \vec{\psi}^{in} + \mathbf{K}_{ASX} \vec{S}^X + \mathbf{K}_{AEA} \vec{E}^A]. \quad (\text{E.6})$$

As a shorthand notation, let  $\mathbf{L}_A = (\mathbf{I} - \mathbf{K}_{ASA} \Sigma_S)^{-1}$ . This result can be substituted into equation (E.3) with (E.5) to eliminate both the x moment of scatter and the average scatter:

$$\begin{aligned} \vec{\psi}^X = & (\mathbf{I} - (\mathbf{K}_{XSX} \Sigma_S + \mathbf{K}_{ASX} \Sigma_S \mathbf{L}_A \mathbf{K}_{ASX} \Sigma_S))^{-1} \times \\ & [(\mathbf{K}_{XI} + \mathbf{K}_{ASX} \Sigma_S \mathbf{L}_A \mathbf{K}_{AI}) \vec{\psi}^{in} + \\ & (\mathbf{K}_{XEA} + \mathbf{K}_{ASX} \Sigma_S \mathbf{L}_A \mathbf{K}_{AEA}) \vec{E}^A]. \end{aligned} \quad (\text{E.7})$$

Let:

$$\mathbf{L}_X = (\mathbf{I} - (\mathbf{K}_{XSX} \Sigma_S + \mathbf{K}_{ASX} \Sigma_S \mathbf{L}_A \mathbf{K}_{ASX} \Sigma_S))^{-1}, \quad (\text{E.8})$$

$$\mathbf{m}_{XI} = (\mathbf{K}_{XI} + \mathbf{K}_{ASX} \Sigma_S \mathbf{L}_A \mathbf{K}_{AI}), \quad (\text{E.9})$$

and

$$\mathbf{m}_{XEA} = (\mathbf{K}_{XEA} + \mathbf{K}_{ASX} \Sigma_S \mathbf{L}_A \mathbf{K}_{AEA}), \quad (\text{E.10})$$

are used for equation (E.7). Equation (E.7) is now substituted back into equation (E.6) to eliminate the x moment of scatter:

$$\begin{aligned} \vec{\psi}^A = & \mathbf{L}_A [(\mathbf{K}_{AI} + \mathbf{K}_{ASX} \Sigma_S \mathbf{L}_X \mathbf{m}_{XI}) \vec{\psi}^{in} + \\ & (\mathbf{K}_{AEA} + \mathbf{K}_{ASX} \Sigma_S \mathbf{L}_X \mathbf{m}_{XEA}) \vec{E}^A]. \end{aligned} \quad (\text{E.11})$$

Let:

$$\mathbf{m}_{AI} = (\mathbf{K}_{AI} + \mathbf{K}_{ASX} \Sigma_S \mathbf{L}_X \mathbf{m}_{XI}), \quad (\text{E.12})$$

and

$$\mathbf{m}_{AEA} = (\mathbf{K}_{AEA} + \mathbf{K}_{ASX} \sum_S \mathbf{L}_X \mathbf{m}_{XEA}), \quad (\text{E.13})$$

are used for equation (E.11). Both equations (E.7) and (E.11) can be substituted in equation (E.1) to eliminate the scattering terms. This gives the outgoing detailed flow for a cell in terms of the incoming detailed flow and emissions in a cell:

$$\begin{aligned} \bar{\psi}^{out} = & (\mathbf{K}_{OI} + \mathbf{K}_{OSA} \sum_S \mathbf{L}_A \mathbf{m}_{AI} + \mathbf{K}_{OSX} \sum_S \mathbf{L}_X \mathbf{m}_{XI}) \bar{\psi}^{in} \\ & + (\mathbf{K}_{OEA} + \mathbf{K}_{OSA} \sum_S \mathbf{L}_A \mathbf{m}_{AEA} + \mathbf{K}_{OSX} \sum_S \mathbf{L}_X \mathbf{m}_{XEA}) \bar{E}^A. \end{aligned} \quad (\text{E.14})$$

## Bibliography

1. Abu-Shumays, I. K., "Compatible Product Angular Quadrature for Neutron Transport in x-y Geometry," *Nuclear Science and Engineering: 64:299-316*,(1977).
2. Adams, Marvin L. and Edward W Larsen. "Fast Iterative Methods for Discrete-Ordinates Particle Transport Calculations," *Nuclear Science and Engineering:40:3-149* (2002).
3. Azmy, Y.Y., "Unconditionally Stable and Robust Adjacent-Cell Diffusive Preconditioning of Weighted-Difference Particle Transport Methods is Impossible," *Journal of Computational Physics: 182:213-233* (2002)
4. Borgers, C, E.W. Larson, and M. L. Adams, "The Asymptotic Diffusion Limit of A linear Discontinuous Discretization of a Two-Dimensional Linear Transport Equation," *Journal of Computational Physics: 98:285-300* (1992)
5. Chang, Jae, and Marvin Adams, "Analysis of Transport Synthetic Acceleration For Highly Heterogeneous Problems", Conference Paper from Nuclear Mathematical and Computational Sciences: A Century in Review, A Century Anew. 1/16-16/16. Gatlinburg, Tennessee, April 6-11, 2003, on CD-ROM, American Nuclear Society, Lagrange Park, IL (2003).

6. *Compaq Extended Math Library Reference Guide..* Houston TX: Compaq Computer Corporation, January 2001.
7. Kincaid, David and Ward Cheney, *Numerical Analysis: Mathematics of Scientific Computing*, 3<sup>rd</sup> Edition. Pacific Grove, California: Brooks/Cole Thompson Learning, 2002.
8. Larson, E.W., and J. E. Morel, "Asymptotic Solutions of Numerical Transport Problems in optically Thick, Diffusive Regimes II," *Journal of Computational Physics: 83:212-236 (1989)*
9. Lewis, W. F. and Miller, Elmer E. *Computational Methods of Neutron Transport*. Illinois: American Nuclear Society, 1993.
10. Mathews, Kirk A., "Discrete Elements Method of Neutral Particle Transport", PhD Dissertation, Air Force Institute of Technology, Wright-Patterson Air Force Base, OH (1983).
11. Mathews, Kirk A., Glen Sjoden and Bryon Minor. "Exponential Characteristic Spatial Quadrature for Discrete Ordinates Radiation Transport in Slab Geometry," *Nuclear Science and Engineering: 118:27-32 (1994)*.
12. Miller, Dennis J., "Linear Characteristic Spatial Quadrature for Discrete Ordinates Neutral Particle Transport on Arbitrary Triangles", PhD Dissertation, Air Force Institute of Technology, Wright-Patterson Air Force Base, OH (1993).

13. Morel, J. E., J.E Dendy, and, T. A.Wareing, “Diffusion-Accelerated Solution of the Two-Dimensional Sn Equations with Bilinear-Discontinuous Differencing,” *Nuclear Science and Engineering: 115:304-319*,(1993).
14. Suriano, Mark A, “Short and independent characteristic methods for discrete ordinates radiation transport with 2D and 3D regular cartesian meshes”, PhD Dissertation, Air Force Institute of Technology, Wright-Patterson Air Force Base, OH (2001).
15. Wager, Nicholas J., “A Rapidly-Converging Alternative to Source Iteration for Solving the Discrete Ordinates Radiation Transport Equations in Slab Geometry”, PhD Dissertation, Air Force Institute of Technology, Wright-Patterson Air Force Base, OH (2004).
16. Wareing, T. A, W.F. Walters, and J. E. Morel, “Diffusion-Accelerated Solution of the Two-Dimensional X-Y Sn Equations with Linear-Bilinear Nodal Differencing,” *Nuclear Science and Engineering: 115:304-319*,(1993).
17. Warsa, J.S., Wareing, T. A., and J. E. Morel, “On the Degraded Effectiveness of Diffusion Synthetic Acceleration for Multidimensional SN Calculations in the Presence of Material discontinuities”, Conference Paper from Nuclear Mathematical and Computational Sciences: A Century in Review, A Century Anew. 1/17-16/17. Gatlinburg, Tennessee, April 6-11, 2003, on CD-ROM, American Nuclear Society, Lagrange Park, IL (2003)

**REPORT DOCUMENTATION PAGE**

*Form Approved  
OMB No. 074-0188*

The public reporting burden for this collection of information is estimated to average 1 hour per response, including the time for reviewing instructions, searching existing data sources, gathering and maintaining the data needed, and completing and reviewing the collection of information. Send comments regarding this burden estimate or any other aspect of the collection of information, including suggestions for reducing this burden to Department of Defense, Washington Headquarters Services, Directorate for Information Operations and Reports (0704-0188), 1215 Jefferson Davis Highway, Suite 1204, Arlington, VA 22202-4302. Respondents should be aware that notwithstanding any other provision of law, no person shall be subject to a penalty for failing to comply with a collection of information if it does not display a currently valid OMB control number.

**PLEASE DO NOT RETURN YOUR FORM TO THE ABOVE ADDRESS.**

<b>1. REPORT DATE (DD-MM-YYYY)</b> 15-08-2008		<b>2. REPORT TYPE</b> Ph D. Dissertation		<b>3. DATES COVERED (From – To)</b> Sep 2002 – Sep 2008	
<b>4. TITLE AND SUBTITLE</b>  Distribution Iteration: A Robust Alternative to Source Iteration for Solving the Discrete Ordinates Radiation Transport Equations In Slab and XY - Geometries				<b>5a. CONTRACT NUMBER</b>	
				<b>5b. GRANT NUMBER</b>	
				<b>5c. PROGRAM ELEMENT NUMBER</b>	
<b>6. AUTHOR(S)</b>  Prins, Nicholas, J., LTC, US Army				<b>5d. PROJECT NUMBER</b>	
				<b>5e. TASK NUMBER</b>	
				<b>5f. WORK UNIT NUMBER</b>	
<b>7. PERFORMING ORGANIZATION NAMES(S) AND ADDRESS(S)</b> Air Force Institute of Technology Graduate School of Engineering and Management (AFIT/EN) 2950 Hobson Way, Building 640 WPAFB OH 45433-7765				<b>8. PERFORMING ORGANIZATION REPORT NUMBER</b>  AFIT/DS/ENP/08-S04	
<b>9. SPONSORING/MONITORING AGENCY NAME(S) AND ADDRESS(ES)</b> Intentionally Left Blank				<b>10. SPONSOR/MONITOR'S ACRONYM(S)</b>	
				<b>11. SPONSOR/MONITOR'S REPORT NUMBER(S)</b>	
<b>12. DISTRIBUTION/AVAILABILITY STATEMENT</b> APPROVED FOR PUBLIC RELEASE; DISTRIBUTION UNLIMITED.					
<b>13. SUPPLEMENTARY NOTES</b>					
<b>14. ABSTRACT</b> The discrete ordinates method is widely used to solve the Boltzmann transport equation for neutral particle transport for many engineering applications. Source iteration is used to solve the discrete ordinates system of equations, but can be slow to converge in highly scattering problems. Synthetic acceleration techniques have been developed to address this shortcoming; however, recent research has shown synthetic acceleration to lose effectiveness or diverge for certain problems. LTC Wager introduced an alternative to source iteration and demonstrated it in slab geometry. Here the method is further developed, enhancing efficiency in various ways, and demonstrated in XY-geometry as well as slab geometry. It is shown to be efficient even for those problems for which diffusion-synthetic and transport-synthetic accelerations fail or are ineffective. The method has significant advantages for massively-parallel implementations.					
<b>15. SUBJECT TERMS</b> Radiation Transport, Boltzmann Transport Equation, Discrete Ordinates, Rapidly Converging					
<b>16. SECURITY CLASSIFICATION OF: UNCLASSIFIED</b>		<b>17. LIMITATION OF ABSTRACT</b>  UU	<b>18. NUMBER OF PAGES</b>  214	<b>19a. NAME OF RESPONSIBLE PERSON</b> Kirk A Mathews, Professor,(ENP)	
<b>REPORT</b> U	<b>ABSTRACT</b> U			<b>c. THIS PAGE</b> U	<b>19b. TELEPHONE NUMBER (Include area code)</b> (937) 255-3636, ext 4508; e-mail: Kirk.Mathews@afit.edu